Veröffentlichung

MeteoSchweiz
MétéoSuisse
MeteoSvizzera
MeteoSvizra
MeteoSwiss

Autor
Simon C. Scherrer

73 Interannual climate variability in the European and Alpine region

Veröffentlichung

MeteoSchweiz

Nummer: 73

ISSN: 1422-1381

Autor
Simon C. Scherrer

Interannual climate variability in the European and Alpine region

Contents

Abstract

The present PhD dissertation examines climate variability in the European and Alpine regions. Measurements from the high-density climatological snow-, precipitation- and temperature networks are used to analyze local climate variability. Large-scale climate data sets are explored to characterise the continental-scale climate and to elucidate the connection between local and large-scale climate variability. The main purpose of the thesis is to improve our knowledge of variability in the climate system. Possible implications from ongoing and future climate change are also discussed. The main body of the thesis is composed of five publications in peer-reviewed journals.

Chapters 2 and 3 investigate variability and trends in Swiss Alpine snow pack and the links to local climate variability and large-scale circulation. In the late 20th century, significant decreases in snow days have been observed for low-altitude stations. Simple statistical modelling shows that these trends can be mainly attributed to increases in temperature. The seasonal mean precipitation influence on trends is small. The North Atlantic Oscillation (NAO), as the major mode of large scale circulation variability over Europe, is found to be important in explaining the observed snow day trends, but not in explaining the large interannual snow day variability. The latter is primarily related to a flow anomaly pattern centred over south-eastern Europe – resembling the so called Euro-Atlantic atmospheric blocking pattern.

Swiss snow pack variability can be decomposed into three well separated patterns of variability. The leading pattern shows comparatively small geographical variations explaining roughly 50% of total interannual variability. The second pattern distinguishes between the northern and southern slope of the Alps. It explains about 15% of total variability. The third pattern shows large loadings in the lowlands, explains approximately 8% of total variability, and is height dependent. It is shown that the relation to temperature and precipitation depends on the specific snow parameter considered. Variability in seasonally averaged snow parameters that are determined by the conditions during snow accumulation only (e.g. new snow sums) is primarily related to local precipitation variability. Variability in parameters that are influenced by accumulation and ablation processes (e.g. average snow height and snow days) is related more to temperature or both temperature and precipitation variability.

In Chapter 4, three new two-dimensional atmospheric blocking indicators are used to analyse the statistical relationship between the leading climate patterns of mid-tropospheric flow and atmospheric blocking over the Euro-Atlantic region during winter. The results indicate that the blocking-NAO relation is not restricted to the North Atlantic region where blocking and the NAO are known to be out of phase. The positive NAO phase is characterised by an enhanced occurrence of blocking-type high-pressure systems over the European

mainland. An extension to the second to fourth pattern of mid-tropospheric flow variability reveals that the clearest separation between positive (negative) phases and blocking (no-blocking) situations is found for the second and third pattern and is associated with changes from zonal to ridge-like flow.

Chapters 5 and 6 investigate problems with standard variables of climate monitoring in a nonstationary climate, and the question whether temperature variability has already changed or how it could change in the future. Beside observed temperature data, temperature projections from several climate models participating in the Intergovernmental Panel on Climate Change assessment are used to address this issue over continental Europe. It is shown that since 1990 the probability to observe a positive temperature anomaly with respect to the 1961–1990 normal increased from 50% to about 80% for certain months of the year. This change is statistically significant for seven out of the twelve months. The strongest standardized temperature changes in mean are found for the summer season, both in observations and climate models, whereas observed temperatures in fall do not show any trends. Very similar results are found throughout continental Europe. Estimates for variability changes in recent observations show a weak increase (decrease) in summer (winter), but these changes are not statistically significant at the 90% level. For the 21st century all climate scenario runs suggest large relative increases in mean for all seasons with maximum amplitude in summer. Although changes in relative variability vary substantially between the models, there is a tendency for increasing (decreasing) variability in future summers (winters).

Zusammenfassung

Die vorliegende Doktorarbeit untersucht Aspekte der Klimavariabilität in Europa und in den Alpen. Klimatologische Schnee-, Niederschlags- und Temperaturmessungen des hochaufgelösten Beobachtungsnetzes werden benutzt um die lokale Klimavariabilität zu untersuchen. Grossskalige Klimadatensätze werden analysiert, um das kontinentalskalige Klima zu charakterisieren sowie die Beziehung zwischen lokaler und grossräumiger Klimavariabilität herauszuarbeiten. Das Hauptziel dieser Arbeit ist unser Wissen über die Klimavariabilität im Klimasystem zu verbessern. Weiter werden heutige und mögliche zukünftige Auswirkungen von der sich bereits im Gange befindlichen Klimaänderung diskutiert. Der Hauptteil der Arbeit besteht aus fünf Publikationen in begutachteten Zeitschriften.

Kapitel 2 und 3 untersuchen die Variabilität und Trends der alpinen Schweizer Schneedecke und deren Beziehung zur lokalen Klimavariabilität und grossskaligen Strömung. Gegen Ende des 20. Jahrhunderts wurden speziell an tiefliegenden Stationen signifikante Abnahmen der Schneetage beobachtet. Einfache statistische Modelle zeigen, dass diese Trends vorwiegend den zunehmenden Temperaturen zugeschrieben werden können. Der Einfluss saisonal gemittelter Niederschläge auf die Schneetagetrends ist klein. Die nordatlantische Oszillation (NAO), das wichtigste Muster der grossskaligen Zirkulation in Europa, ist wichtig um die beobachteten Trends in den Schneetagen zu erklären. Allerdings kann die NAO keinen grossen Anteil der Jahr zu Jahr Variabilität erklären. Letztere geht primär mit einem dynamischen Anomaliemuster einher, welches über Südosteuropa zentriert ist und dem so genannten Euro-Atlantischen atmosphärischen Blockingmuster ähnelt.

Die Schweizer Schneevariabilität kann in drei gut voneinander abgegrenzte Muster zerlegt werden. Das wichtigste Muster zeigt kleine geografische Unterschiede und erklärt ungefähr 50% der Jahr zu Jahr Variabilität. Das zweite Muster zeigt Unterschiede zwischen dem Alpennord- und Alpensüdhang auf. Es erklärt etwa 15% der Gesamtvariabilität. Das drittwichtigste Muster ist vor allem in tiefen Lagen mitbestimmend, erklärt rund 8% der Gesamtvariabilität und ist höhenabhängig. Die Beziehung des Schnees zu Temperatur und Niederschlag ist stark von der Art des Schneeparameters abhängig. Die Variabilität von saisonal gemittelten Schneeparametern, die nur von den meteorologischen Bedingungen während der Schneeakkumulation abhängen (z.B. Neuschneesummen), korreliert sehr gut mit saisonal gemitteltem Niederschlag. Die Variabilität von Grössen, die von Schneeakkumulation und Ablation bestimmt werden (z.B. Schneehöhe und Schneetage), korrelieren gut mit saisonaler Temperatur oder der Kombination von Temperatur und Niederschlag.

In Kapitel 4 der Arbeit werden drei neue zweidimensionale atmosphärische Blockingindikatoren benutzt, um die statische Beziehung zwischen den wichtigsten Klimadruckmustern und atmosphärischem Blocking im Euro-Atlantischen Raum im Winter zu untersuchen. Die Resultate zeigen, dass sich die NAO-Blocking Beziehung nicht auf die nordatlan-

tische Region beschränkt, wo bekannt ist, dass Blocking und die NAO ausser Phase sind. Positive NAO Phasen gehen mit einer erhöhten Anzahl an blockingähnlichen stabilen Hochdrucklagen über dem Europäischen Festland einher. Die Erweiterung der Analyse auf das zweite bis vierte Muster der mitteltropospärischen Strömungsvariabilität zeigt die klarste Trennung zwischen positiven (negativen) blockierten (nicht blockierten) Phasen und dem zweiten und dritten Muster, welche sich beide durch einen Wechsel von zonaler zu blockierter Strömung auszeichnen.

Kapitel 5 und 6 untersuchen Probleme im Zusammenhang mit Standardvariablen der Klimaüberwachung im nichtstationären Klima. Es wird der Frage nachgegangen, ob die Temperaturvariabilität in den Beobachtungen schon zugenommen hat, bzw. sich in Zukunft verändern könnte. Neben gemessenen Stationsdaten werden dazu auch Temperaturszenarien von mehreren am "Intergovernmental Panel on Climate Change" Prozess teilnehmenden globalen Zirkulationsmodellen verwendet. Es zeigt sich, dass seit 1990 die Wahrscheinlichkeit einer positiven Temperaturanomalie, berechnet auf Basis der 1961–1990 Normalwerte, in einigen Monaten des Jahres von 50% auf gegen 80% angestiegen ist. Diese Änderung ist statistisch signifikant für sieben der zwölf Monate. Sowohl in den Beobachtungen, wie auch in den Modellen, wird der stärkste standardisierte Temperaturanstieg im Sommer gefunden. Im Herbst gibt es keine klaren Trends. Sehr ähnliche Resultate werden für Kontinentaleuropa gefunden. Schätzungen für Änderungen der Variabilität in den letzten Jahrzehnten zeigen eine schwache Zunahme (Abnahme) im Sommer (Winter), die allerdings auf dem 90% Niveau nicht signifikant sind. Für das 21. Jahrhundert zeigen alle Klimaszenarien für alle Jahreszeiten grosse relative Zunahmen im Mittel. Die stärkste Zunahme wird für den Sommer gefunden. Obwohl die relative Variabilität von Modell zu Modell stark schwankt, gibt es eine Tendenz für zunehmende (abnehmende) Temperaturvariabilität in zukünftigen Sommern (Wintern).

Chapter 1

Introduction

1.1 Motivation

In recent years climate change or more accentuated global warming has gained substantial attention in the media and on the political agenda. In terms of global mean surface temperature, the 1990s has been the warmest decade, at least since the beginning of instrumental measurements (Houghton et al., 2001, p. 156). In central Europe eight of the ten warmest years of the 1851–2004 temperature record have been observed from 1989–2003 (Scherrer et al., 2006a, chapter 5). In the Alpine region the temperature increases observed have been twice or three times as large as the global average figures (Philipona et al., 2004; Begert et al., 2005). Climate model simulations show that most of the observed trend can only be explained when the anthropogenic influence (primarily greenhouse gas emissions) are taken into account (Houghton et al., 2001). For the 21st century the third Intergovernmental Panel on Climate Change (IPCC) assessment report suggests changes in mean that are several times larger than those caused by natural variability in the past millennium.

Climate is more than mean temperatures and climate change more than as a steady increase in the mean temperature. For an appropriate assessment of the possible impacts of climate change it is useful to establish the term climate itself. Public perception tends to confuse weather with climate or the ozone whole problematic with climate change (Bostrom et al., 1994). This confusion is enhanced by the media where the term *"climate"* is often misleadingly used. For example Hirstein (2005) argues in the *NZZ am Sonntag* that the climate does not exist: *"Es [das Klima] ist eine Fiktion, ein Werk des Menschen, der das komplizierte Wettergeschehen in einem Mittelwert bündeln will"* (engl.: it [the climate] is fiction, a creation of men, who bundles complex weather processes into a mean value). This understanding of climate lacks a key ingredient of every modern definition of the climate, namely VARIABILITY. The IPCC assessment report glossary defines climate as *"the statistical description in terms of the mean and variability of relevant quantities over a period of time (...)"*.

An appropriate knowledge and communication of natural variability is a key to a broad understanding of the climate system and implications of climate change. Mean changes need to be assessed relative to the intrinsic variability of the system. Taking variability into account also implies that extraordinary events may be part of natural fluctuations and not necessarily indicative for long-term climate changes (Rebetez, 1996). Although extreme weather and climatic events initiated several important acts at federal level in the history of Switzerland (Pfister, 1999), the perception of variability is distorted by human expectations and

highly biased long-term memories. A well known example is the often exaggerated expectation of white Christmas in central Europe (White, 1985; Rebetez, 1996). Simple statistical analysis shows that for most high populated regions the probability for white Christmas (snow height >0 cm) is only about 25-40%, depending on station altitude (Temperli, 2002).

The present study examines climate variability and trends in the European and Alpine region. Measurements from the high-density climatological snow, temperature and precipitation networks are used to analyze both local climate variability and how this variability is influenced by large-scale climate dynamics. The aim is to improve our knowledge of the climate system and to reveal possible implications related to climate change.

In the remainder of this introductory chapter, statistical concepts and methods used are shortly introduced. Afterwards a short review of the characteristics of climate variability in Europe and the European Alps is given, with a focus on temperature, precipitation and snow pack. Finally the aims of the thesis are defined and an outline is presented.

1.2   Statistical concepts

Studying the climate system is a difficult problem for several reasons. First the climate system is highly complex. Second the system is unique, so strict comparative studies are impossible. Third controlled experiments in the classical sense are equally out of reach except for idealised numerical experiments. Often used approaches to study the climate system are physically based climate models or statistical analysis techniques. According to Zwiers and von Storch (2004) statistics plays two main roles in climatology: *i)* it helps to quantify the effects of uncertainty both in terms of observation and measurement and in the understanding of the processes that govern climate variability and *ii)* it guides in constructing the knowledge of climate. Various techniques applied in climate science can be used to extract information from the data (descriptive methods, statistical estimation and testing).

1.2.1   Data treatment and statistical significance

Climate variables in the Alpine region can differ substantially from location to location due to various influences of the complex topography, geographical location and flow situation. In this study our interest is not primarily to know the value at station A or B, but rather whether the climate elements at station A and B react in the same manner to a large-scale forcing. Within this framework it is sufficient to compute the statistics using standardized variables (Wilks, 1995). As a consequence most of the data used in this thesis are standardized before further statistics are computed (see chapter texts for details).

Testing for statistical significance is a standard procedure in science. Several reasons complicate matters in climate sciences. Most time series possess a substantial autocorrelation (Katz, 1988; Wilks, 1997) and fields are often spatially correlated which can easily lead to multiplicity problems (Brown and Katz, 1991). Given these complications most standard techniques of statistical inference need to be used with care and some are even inappropriate. To circumvent several problems with standard tests statistical significance is often assessed using surrogate data with similar properties in conjunction with Monte-Carlo experiments or bootstrap techniques (Efron and Tibshirani, 1993; von Storch and Zwiers, 1999, chapters 5 and 6 of this thesis).

1.2.2   Probability distribution functions

Another fundamental problem in climate sciences is to reveal the mechanisms of the climate system having only a limited number of observations at hand. It is therefore inevitable to have a concept that can describe the climate systems' statistical nature, i.e. the distribution of the variables under consideration. A very helpful and often used qualitative concept to characterise a distribution is to look at the empirical histogram of the variable in question. However, its applicability for inference is limited. For more quantitative questions a theoretical probability distribution function (PDF) can be fitted to the observed data, which hopefully represents the "true" distribution of the data (e.g. Wilks, 1995). The fit needs several assumptions but allows statistical inference and therefore is of great interest and benefit for many climatological questions.

The PDF concept is widely used also in other branches of atmospheric sciences, e.g. in numerical weather prediction to verify probabilistic forecasting systems (cf. Scherrer et al., 2004a, not part of this thesis). It is a core concept for studies concerning the past and future changes of the climate (cf. Schär et al., 2004 and Chapter 6 of this thesis). To give an example, Figure 1.1 displays seasonal 2-m temperature in northern Switzerland for the instrumental period since 1864. Shown are histograms for the 1864(5)–1990 summer and winter period, rug plots and the fitted distributions assuming an underlying Gaussian distribution. Visual evaluation and statistical tests show that 2-m mean temperature is reasonably well Gaussian distributed for the full 140 years of observations. The sample of the last 15 years (1991–2005) is clearly shifted towards warmer temperatures, both in winter and summer (red lines in Figure 1.1).

The Gaussian assumption is used extensively in several chapters of this thesis. Problems arising with this concept in case of small sample sizes, decadal variability and nonstationarities will also be discussed (see Chapter 5).
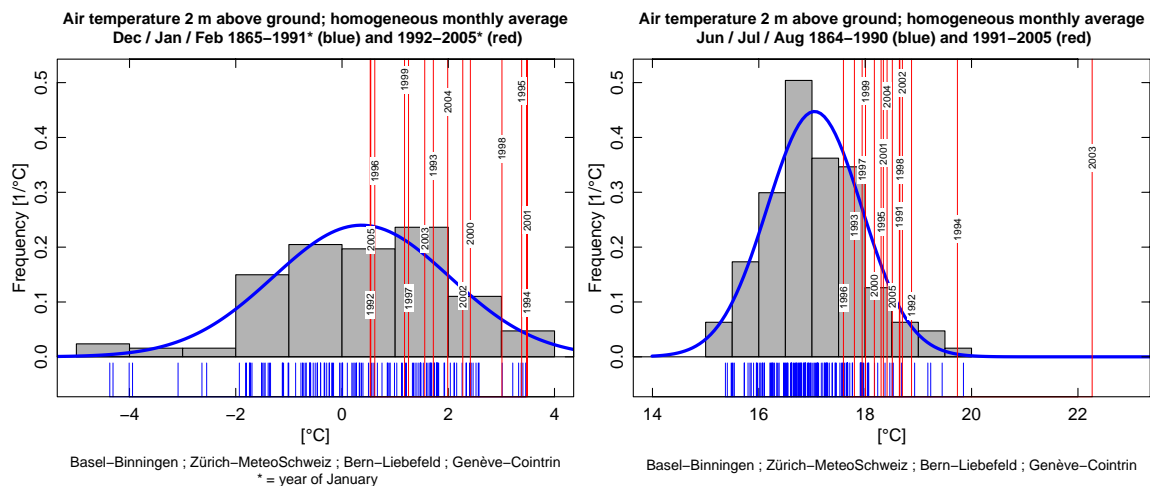
Figure 1.1: Histogram, fitted probability distribution function and rug plot for northern Switzerland (mean of the MeteoSwiss station series Basel-Binningen, Zürich-MeteoSchweiz, Bern-Liebefeld and Genève-Cointrin) winter (DJF) and summer (JJA) 2-m temperatures. Data period used for the grey frequency histograms, blue rug plot and Gaussian fit to the data (solid blue line) is 1864(5)–1990 for JJA (DJF). The values for the 1991 to 2005 DJF (JJA) period are labelled (in red). Units on the abscissa are in degrees centigrade.

1.2.3 Defining patterns of climate variability

The climate is a dynamical system with a large number of spatial degrees of freedom. To analyze such systems dimensionality needs to be reduced, but at the same time as much variability as possible should be retained. Many different methods such as principal component analysis (PCA), also called empirical orthogonal function (EOF) analysis, principal oscillation pattern (POP) analysis, cluster analysis (CA) or neural networks have been developed to identify recurrent large-scale patterns of variability (see von Storch and Zwiers (1999) for an overview).

One of the most often used methods in many fields of science and technology is PCA. The first applications of PCA to meteorological data goes back to the 1940s, 50s and 60s (e.g. Obukhov, 1947; Fukuoka, 1951; Lorenz, 1956; Obukhov, 1960; Kutzbach, 1967). Since then PCA has been applied to a wide range of time-space phenomena in meteorology and climatology (Preisendorfer, 1988; Jolliffe, 2002) for a review).

PCA determines a new orthogonal basis to the data with the constraint that the variance explained by the leading patterns is maximized. There exist several different methods to calculate PCA. In this thesis PCA is computed in spatial domain (S-mode) (Preisendorfer, 1988). For details concerning the definition and computation refer to Widmann (1996) or Peixoto and Oort (1992). The resulting optimized orthogonal basis (spatial loadings) called Empirical Orthogonal Functions (EOFs), can be interpreted as characteristic patterns of variability. The expansion coefficients of these patterns, the temporal scores, are called principal components (PCs) in this thesis.

A big advantage of classical PCA against other methods is that it is completely objective (no subjective decisions are needed). Unfortunately this does not imply that PCA patterns are physically meaningful (Cherry, 1997; Dommenget and Latif, 2002; Jolliffe, 2003; Stephenson et al., 2004). The patterns derived from PCA are thus merely climate patterns and not necessarily climate modes, using a well defined nomenclature. For more detailed information about the physical interpretation of PCA and often misleadingly used terms the reader is referred to Stephenson et al. (2004).

If the focus is on physical interpretation, rotating the basis set of eigenvectors may be preferential to using the orthogonal original (Horel, 1981; Richman, 1986). However, there is still no guarantee for physical meaningfulness (Jolliffe, 1987; 2003; Hannachi et al., 2006). If PCs are used as input for statistical models it may be better to use orthogonal time series. In this thesis classical PCA (without rotation) is used to determine patterns of large-scale (sea level pressure and geopotential) and local (temperature, precipitation and snow pack) climate variability.

There are several methods for deciding which PCA patterns to keep and which ones to discard (see Preisendorfer (1988) for a thorough review). Especially popular are the so called *rule N*, North's rule of thumb (North et al., 1982) or robustness tests using Monte Carlo approaches. In this thesis, North's rule of thumb is applied.

PCA with missing values

Classical PCA assumes that there are no missing values in the input data. In Chapter 3 of this study PCA is applied to a snow data set with a relatively small amount (~20%) of missing values. There exists no standard way to deal with missing values. Two methods used in

literature are *i)* filling in the missing data by some kind of interpolation method before application to PCA or *ii)* calculating the eigenvalues and eigenvectors of the correlation or covariance matrix using only available data (Kaplan et al., 1997; von Storch and Zwiers, 1999). Both approaches contain subjective components (choice of interpolation methods and parameters, levels of significance, etc…). In this thesis the fully objective approach recently developed in the field of oceanography by Beckers and Rixen (2003) is used. It allows to determine EOFs, PCs, optimal numbers of EOFs (also for data sets with no missing data), interpolated missing values and an error estimate in one procedure without subjective decisions. The basic idea of the method is as follows (for full details see their paper).

First all missing data points of the centred (or standardized) data matrix $\mathbf{X}$ are set to zero. Then the singular value decomposition (SVD) of this new matrix $\mathbf{X'}=\mathbf{UDV}^{\mathrm{T}}$ is used to get a first estimation of the EOFs ($\mathbf{U}$) and PCs ($\mathbf{V}$). The first guess of the interpolated value at a missing data point is then obtained by reconstructing the data matrix using only the first spatial EOF $\mathbf{U}_1$ ($\mathbf{X}_1'=\mathbf{U}_1\mathbf{D}_1\mathbf{V}_1$). The missing data points (set to zero above) are replaced by their new values $\mathbf{X}_1'$. The procedure is now repeated and the missing values updated always with only the first spatial EOF retained until convergence (resulting in a final $\mathbf{X}_1^{\mathrm{conv}}$). The above procedure is then again repeated but now with a second spatial EOF retained in the reconstruction process using the reconstructed matrix $\mathbf{X}_1^{\mathrm{conv}}$ as a starting point. This leads to new reconstructed $\mathbf{X}_2$s and after convergence to $\mathbf{X}_2^{\mathrm{conv}}$. Afterwards the whole process is repeated with 3…N EOFs retained in the reconstruction process always starting with the converged interpolation $\mathbf{X}_{N-1}^{\mathrm{conv}}$. The optimal number of EOFs retained (N^*) is determined using a cross validation procedure. A random set of valid data points (at least 30) is flagged as missing value to determine the interpolation error (e.g. root mean square error between reconstructed data and the original data) after every convergence of the reconstruction with N EOFs retained. The optimal number N^* is then defined as the N with the smallest interpolation error. Once N^* is defined the calculation of the PCA can be fine-tuned. The data set aside for the cross validation procedure are injected into the interpolation procedure starting with the optimal number N^* of EOFs retained.

1.2.4 The relation between large-scale and local variability

Several empirical techniques have been suggested to determine the interrelation between large-scale patterns and local climate variables. Especially popular among climate scientists are the widely used correlation analysis and compositing (Walker, 1909; Exner, 1913), the analysis of atmospheric teleconnections (Wallace and Gutzler, 1981; Glantz et al., 1991), singular value decomposition (SVD) analysis (Bretherton et al., 1992; Widmann, 1996; Venegas et al., 1997), canonical correlation analysis (CCA) (von Storch and Zwiers, 1999) or other multivariate techniques. Most of these methods have the strategy to identify the dominant patterns of the two parameters that tend to occur simultaneously or lagged. Junge and Stephenson (2003) noted that to quantify the importance of certain factors, descriptive methods may not suffice and statistical models need to be applied. A simple way is the use of stepwise multiple linear regression models to determine optimal models (R, 2005). In this thesis, both, descriptive methods and multiple linear regression models are used extensively.

1.3   Climate patterns and climate variability in Europe

Europe stretches from the subtropics over the temperate zone to the arctic zone. The western parts are in a maritime regime, whereas the eastern parts are highly continental. European climate variability is strongly influenced by the presence of the North-Atlantic Ocean and the characteristics of atmospheric dynamics in the mid-latitudes. Northern Europe experiences abnormally mild conditions compared with other regions at the same latitudes. Most sources say that the main reason behind this property is poleward advection of warm water from the tropics and subtropics (Hartmann, 1994; Broecker, 1997; Latif et al., 2000b). A recent study by Seager et al. (2003) showed that the deviations from zonal symmetry in winter are fundamentally caused by the atmospheric circulation interacting with the oceanic mixed layer. The characteristics of the atmospheric dynamics depend on the season.
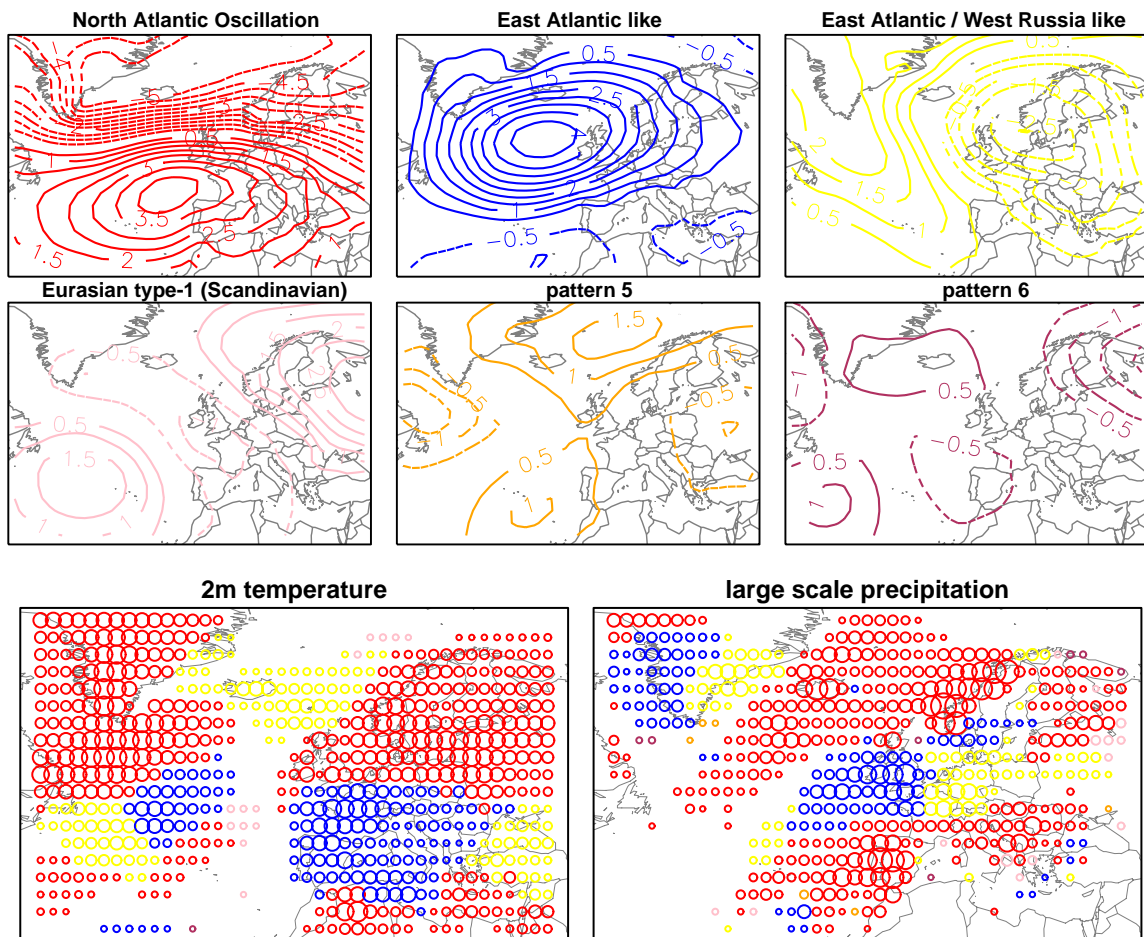
Figure 1.2: Top panels: Maps of the six leading sea level pressure climate patterns in the Euro-Atlantic region. Considered are DJF means in the period 1958–1999. North Atlantic Oscillation (red), East Atlantic like pattern (blue), East Atlantic/ West Russia like pattern (yellow), Eurasian type-1 (Scandinavian) like pattern (pink), pattern 5 (orange), pattern 6 (maroon). The geographical domain used is 60°W–40°E, 30°N–80°N. *Bottom panels:* The climate patterns explaining most of ERA-40 2-m temperature (left) and large-scale precipitation (right) variability in winter. The size of the circles is proportional to the explained variance. Blank regions: none of the first ten sea level pressure patterns is significantly related to the local variability on the 99% level.

In winter the synoptic systems are characterised by eastward moving sequences of low and high-pressure systems and their embedded frontal systems (Schwierz, 2001). This large winter synoptic activity is interlinked in a complex manner with quasi-stationary patterns, called the Icelandic low, the Azores high and the continental low and high-pressure systems (Wanner et al., 2000). In summer the quasi-stationary synoptic systems are still present albeit much weaker. The moving synoptic systems are normally further in the north and most parts of Europe are more influenced by local scale (thermally driven) processes.

The North Atlantic Oscillation (NAO) is the major mode of winter variability in the northern extratropics on the monthly to seasonal scale (Exner, 1913; Walker, 1924; van Loon and Rogers, 1978; Barnston and Livezey, 1987; Hurrell, 1995). The impact of the NAO on climate and ecosystem parameters in Northern and Southern Europe is well documented in the literature (see e.g. Appenzeller et al., 1998a; Marshall et al., 2001; Wanner et al., 2001; Hurrell et al., 2003). However, a large fraction of the observed variability remains unexplained in several regions. Depending on location and season other patterns are more important than the NAO. Examples are winter precipitation and extreme climatic events in central Europe (Widmann, 1996; Qian et al., 2000; Massacand and Davies, 2001a; Yiou and Nogaj, 2004).

The relevant European climate patterns are usually defined using a rotated or unrotated principal component analysis approach (Barnston and Livezey, 1987; Pavan et al., 2000a). The overall leading patterns in the Euro-Atlantic region are the North Atlantic Oscillation, the East Atlantic pattern, the East Atlantic/West Russia pattern and the Eurasian type-1 pattern also called Scandinavian pattern (pattern 1-4 in Figure 1.2). Figure 1.2 also illustrates which of these climate patterns explains most of the Euro-Atlantic seasonal mean 2-m winter temperature and large-scale precipitation at every 2.5°x2.5° grid point. The areas with the same leading climate pattern are clustering. Note that in some regions the same pattern explains most of seasonal temperature and precipitation variability (e.g. Norway), whereas in others temperature and precipitation variability is explained best by two different patterns (e.g. the Alps or the Iberian peninsula). Often also the "next most important" large-scale climate patterns explain large amounts of variability as will be shown in Section 1.4.5 and Chapters 2 and 3.

1.4 Climate variability in the European Alps

1.4.1 Topographical features, weather and climate processes

This section summarizes among other things some aspects of the review articles of Schär et al. (1998) and the chapter 2.2 in Wanner et al. (2000).

The European Alps are geologically spoken a relatively young and topographically complex western European mountain range (centre located roughly at 47°N and 10°E) with a west-east (north-south) dimension of approximately 800 (200) km (cf. Figure 1.3). The highest peaks are found in the western part (heights between 4000 and 4800 m asl). Typical north-south crossing passes are 2000–2500 m in the west and below 2000 m in the east.

The Alps are affected by a large number of different air masses from different directions. The major influences are maritime (predominantly wet and mild) air coming from the west (Atlantic region) and continental (predominantly dry and cold) air from the east (Eastern

Europe and Central Asia). The mountain range also acts as a barrier between the temperate zone in the north and the Mediterranean climate in the south.

The limited length of the Alpine mountain barrier, the "croissant-like" shape and the relatively large heights of the passes constitute the complex topography of the Alps. Diverse, distinct and sometimes rather small scale weather phenomena are created by the interaction of this highly complex topography with the manifold influences of different air masses coming from different directions. The high northern and southern mountain chains lead to shadowing effects for inner alpine valleys with pronounced consequences for the local climate, e.g. a lack of fog, more sunshine duration and considerably smaller amounts of precipitation (Frei and Schär, 1998; Kirchhofer, 2001).

Depending on the properties of the air masses moving towards the Alps the flow can split or surmount the mountain chain. An important example is flow from north-westerly direction with an embedded cold front impinging on the Alps. Several well studied typical phenomena associated with it are *(i)* Föhn on the northern slopes before the arrival of the front, *(ii)* flow split, slowing down, bending and deformation of the front (Steinacker, 1987; Egger and Hoinka, 1992), *(iii)* flow around the western and eastern slopes associated with several local wind systems like Mistral, Bora and Bise (Wanner and Furger, 1990) and *(iv)* lee cyclongenesis (Smith, 1984; Pichler and Steinacker, 1987; Schär, 2002).
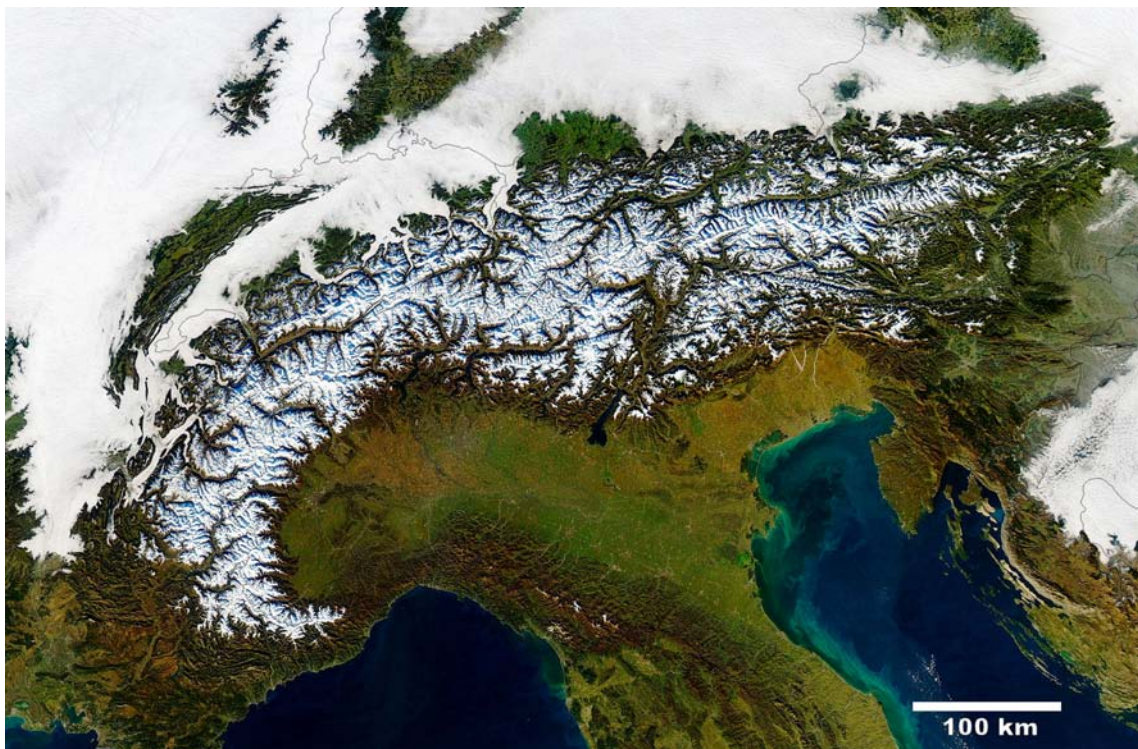
Figure 1.3: The European Alps as seen from the MODIS AQUA satellite on 11 December 2004 12:25 UTC. An approximate scale is given in the lower right corner. Picture freely available from MODIS Rapid Response Project at NASA/GSFC (`http://rapidfire.sci.gsfc.nasa.gov`).
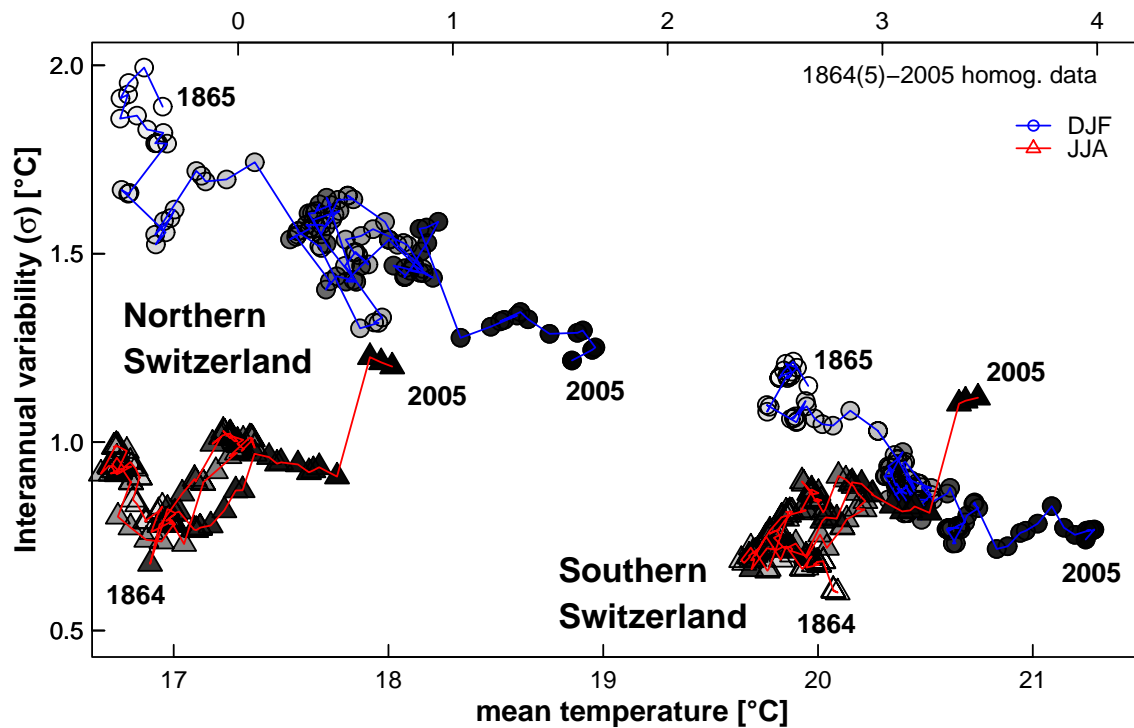
Figure 1.4: Changes in 2-m temperature mean and standard deviation for northern Switzerland (mean of the Basel-Binningen, Bern, Genève, Zürich) and southern Switzerland (Lugano). The time range considered is 1864/5–2005 for JJA (red)/ DJF (blue). 30-year running period results are shown. The greyscale of the circles indicates the 30-year period considered. The darker the shading, the more recent the 30-year window, i.e. the 1864/5-1893/4 circle is white, the 1976-2005 circle is black. All values are in Centigrade. The JJA (DJF) mean values are given on the lower (upper) axis.

Although it is clear that large-scale flow systems play a crucial role for the local weather and climate in the Alpine region it is difficult to construct an accurate and automated weather classification (Schüepp, 1979; Salvisberg, 1996; Wanner et al., 1998). The large-scale influences strongly depend on the season and are different for different parts of the Alps (Wanner et al., 1997; Böhm et al., 2001). In winter the Alpine weather is determined to a large degree by synoptic systems embedded in the westerlies bringing humidity to the Alpine slopes. These wet phases can be interrupted by longer blocking-like permanent high pressure phases (Beniston et al., 1994; Schär et al., 1998; Scherrer et al., 2006b).

Year-to-year variability is large and therefore it is possible that large parts of a season are either dominated by mild and wet air advection while others are rather cold and dry (Beniston, 1997). In summer pressure variability over the Alps is smaller and the local climate is determined to a substantial degree by regional scale processes like thermally driven mountain winds, instabilities and thunderstorms (Luterbacher et al., 2002; Leuenberger, 2005). The Azores High can extend to the Alpine region which is mostly associated with comparatively warm and dry conditions. The transitional seasons spring and autumn are characterised by a mix of both summer and winter features.

Table 1.1: Trend results for the Swiss 20th century daily precipitation statistics. Shown are only entries for indices and categories for which the trends for most stations in a region (and indices within a category) have the same sign. A plus (minus) indicates that the lower (upper) quartile of the trend values is larger (smaller) than zero. A bold sign denotes that at least one-third of the stations have a significant trend at the 95% level. MEA: Mean precipitation; FRE: Frequency of wet days (precipitation >1 mm); INT: Precipitation intensity (mean wet-day precipitation). Heavy precipitation: based on several indices defined in terms of threshold exceedances. Wet (dry) spells: based on several indices characteristic for the duration of consecutive wet- and dry-day sequences. N: northern Switzerland, E: eastern Switzerland, W: western Switzerland, S: southern Switzerland. Taken from Schmidli and Frei (2005).

Statistics	Winter				Spring				Summer				Autumn			
	N	E	W	S	N	E	W	S	N	E	W	S	N	E	W	S
MEA	+	+	**+**		+								+		+	+
FRE	+	+	+					−	−		−					−
INT	**+**	+	**+**		+			+					**+**	+	+	**+**
Heavy Precip	**+**	+	**+**		+			+					**+**	+	+	**+**
Wet spells	**+**	**+**	+								−		−			
Dry spells	−		−					+								+

1.4.2 Temperature observations

The near-surface temperature records in the Alpine region are among the longest and the measurement network among the densest in the world. The complex flow-topography interaction, the special geographic location of the Alps and recent climate change motivated several studies about interannual and longer-term temperature changes based on instrumental data (Auer et al., 2001; Böhm et al., 2001; Begert et al., 2005). These kinds of investigations need careful homogenization of the time series under consideration to correct for non-climatological shifts. Results show that beside large year-to-year variability also considerable decadal variability is found in the record (e.g. Böhm et al., 2001; Begert et al., 2005).

An illustrative way to determine changes in the temperature distribution is presented in Figure 1.4. Changes in mean and standard deviation are visualized using data batches of running 30-year periods. Shown are the 1864(5)–2005 values for summer (JJA) and winter (DJF) season in northern Switzerland and southern Switzerland separately (see legend of Figure 1.4 for a definition). Southern Switzerland temperatures are 2–3 °C higher than those in northern Switzerland for both winter and summer season. Changes in winter temperature are larger than those in summer temperature. Changes in northern Switzerland are larger than those in southern Switzerland. This is in agreement with previous studies for Switzerland (Bader and Bantle, 2004) and the Alpine region (Böhm et al., 2001). The trends are larger than those of the corresponding period on the hemispheric and global scale (Houghton et al., 2001; Jones and Moberg, 2003). In northern Switzerland seasonal variability is larger in winter than in summer. Winter and summer seasonal variability is very similar in southern Switzerland. There is a statistically significant negative trend in variability for both regions in winter. In summer no statistically significant trends can be found for the whole period. Note the strong increase in summer variability caused by the extreme value in 2003 (cf. also Schär et al., 2004).

1.4.3 Precipitation observations

Extreme precipitation events (in both liquid and frozen state) are one of the most important natural hazards in the Alpine region. The August 2005 flooding caused 6 fatalities and preliminary estimations of total damage are 1500–2500+ million Swiss Francs in Switzerland alone. Precipitation is also of importance for many economical applications (e.g. in the energy sector) and in conjunction with climate change (impacts, hazards, etc.). For a long time the Alpine precipitation climatology of Fliri (1974) was state of the art. Recently, efforts to collect the data across borders (Frei and Schär, 1998; Auer et al., 2005) made it possible to study high resolution precipitation variability in the whole Alps (Schmidli et al., 2001; Auer et al., 2005). These investigations show that Alpine precipitation is characterised by large interannual to decadal variability (Schmidli et al., 2002). Several works determined spatial variability of precipitation using cluster analysis (Baeriswyl and Rebetez, 1997) or principal component analysis (Widmann and Schär, 1997; Schmidli et al., 2002).

For northern Switzerland significant trends in mean precipitation are observed at most sites in winter and in some of the yearly series (Widmann and Schär, 1997; Bader and Bantle, 2004; Begert et al., 2005). Schmidli et al. (2002) find statistically significant positive trends for northern Switzerland and the south-western Alps in winter and negative trends in the southern and eastern Alps in autumn. This is in agreement with Schönwiese and Rapp (1997) and Auer and Böhm (1994) who report increases (decreases) in the western (eastern) parts of Austria. A recent study by Schmidli and Frei (2005) determined trends of heavy precipitation and dry and wet spells in Switzerland during the 20$^{\text{th}}$ century (see Table 1.1). In winter, statistically significant increases are found for all statistics related to precipitation strength and occurrence and all regions except southern Switzerland. In autumn, increases are found only for heavy precipitation, whereas precipitation frequency and spell-length show little changes. No significant trends are found in spring and summer.

1.4.4 Snow pack

Observations

Snow fall, the frozen form of precipitation, is a resource of great commercial (tourism, hydro-power) and social value for the Alpine region. It also bears considerable hazards such as avalanches (Abegg, 1996; Bürki, 2000; Laternser and Schneebeli, 2002). Given its significance it is no surprise that research areas related to snow (glaciology, hydrology, avalanche and permafrost research) have a long tradition in the Alpine region.

The first articles that tried to derive climatological relations in terms of snow lines were published in the 1940s and 1950s (Mörikofer, 1948; Zingg, 1951; 1954). In the 1970s and 80s national climate snow studies were conducted and the climatological relation between altitude and snow heights or snow duration improved (Schüepp et al., 1980; Witmer et al., 1986). Other studies determined the seasonal course and local characteristics of the snow pack in detail (Fliri, 1984; Lang and Rohrer, 1987). For a more complete overview of earlier studies on snow climatology the reader is referred to Laternser (2002) and references therein.

Interannual and decadal variability in Swiss Alpine snow is large (Rohrer et al., 1994; Beniston, 1997; Scherrer and Appenzeller, 2003). Long term snow trends in the Swiss Alps are similar for snow depth, the duration of continuous snow cover and the number of snowfall days. A gradual increase until the early 1980s is followed by a statistically significant

decrease towards the end of the century (Laternser and Schneebeli, 2003). Similar results have been found for other mountain regions of the world, e.g. in the north-western USA (Mote, 2003) and on the hemispheric scale (Brown, 2000).

There are a considerable number of analyses dealing with meteorological aspects associated with snow. An example is the variability in meteorological snow fall lines (Grebner, 1978; Steinacker, 1983; Rohrer, 1989). Climate sensitivity of snow cover has been studied in detail for Austria in Hantel et al. (2000) and for Switzerland in Wielke et al. (2004). Aspects of the relation between Alpine snow pack and large-scale climate with a focus on the NAO has been discussed in Beniston (1997).

Snow in a future climate

The sensitivity of the snow pack to climate change has been assessed in several different ways. Föhn (1990) bases his snow cover scenarios on climatological reasoning. Beniston et al. (2003a) use an empirical approach to develop a relation between precipitation, minimum temperature and snow-cover duration. Breiling and Charamza (1999) applied simple statistical models derived from the relation between observed snow pack, temperature and precipitation to climate change projections. Some studies used downscaled projected global circulation model output to drive conceptual or physically based snow models (Martin et al., 1994; Beniston et al., 2003b; Gyalistras et al., 2005). Several other studies used hydrological model approaches to estimate changes in snow pack (Ehrler, 1998; Verbunt et al., 2003; Jasper et al., 2004; Mote et al., 2005). In spite of projected increases in precipitation, all studies generally agree that the Alpine snow volume will decrease considerably with increasing climate change. The low lying regional losses seem to outweigh the possible increases at high elevations (Beniston et al., 2003b).

1.4.5   Influence of large-scale climate patterns

The Alpine region lies between the two poles of the leading mean sea level pressure pattern NAO (Hurrell, 1995; Jones et al., 2003). Alpine upper air trends (e.g. in total ozone in Arosa, Switzerland) have been shown to be considerably influenced by the NAO (Appenzeller et al., 2000). The total interannual variance explained by the NAO is rather small for temperature and precipitation at most stations and regions (Widmann and Schär, 1997; Schmidli et al., 2002). Figure 1.5 shows that large amounts of Swiss temperature and precipitation variance can be explained by large-scale sea level pressure patterns. Depending on the variable the Eastern Atlantic like pattern and the European-blocking like pattern explain a similar or even larger amount of total variance than the NAO. Higher order patterns explain relatively small amounts of variability.

Massacand and Davies (2001a) show that the third principal component of potential vorticity is highly correlated with monthly precipitation especially in January. Quadrelli et al. (2001a) present a significant relationship between the first two principal components of greater Alpine precipitation, the NAO and Euro-Atlantic blocking. Beniston and Jungo (2002) propose a relation with Swiss pressure, moisture and temperature when using highly smoothed time series. They find the strongest influences for extreme values and when the index is positive and high. It is unclear whether these differences are statistically significant. Beniston (1997) has shown that there exists a link between the persistent high surface pressure in fall and spring with low amounts of snow in the Alps.
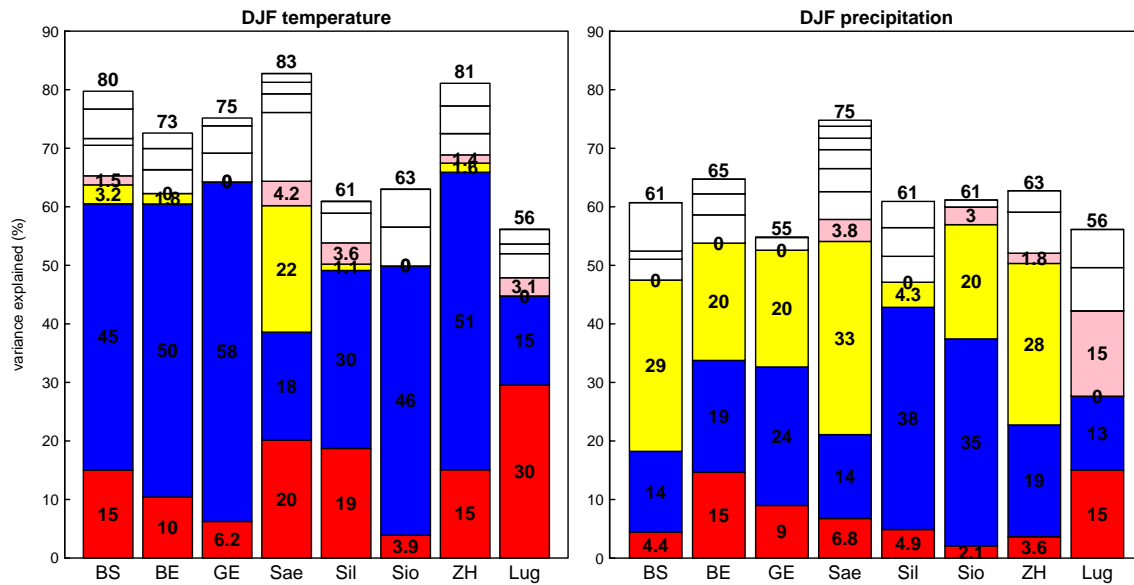
Figure 1.5: DJF 2-m temperature and precipitation variance explained at 8 Swiss stations using a multiple linear regression model with the first 10 large-scale sea level pressure patterns as predictors. From bottom to top of bars: North Atlantic Oscillation (red), Eastern Atlantic like pattern (blue), European-blocking like pattern (yellow), East Atlantic/ West Russia like pattern (pink), patterns 5–10 (white). Units are in percent of total variance; time range is 1958–1999. The domain for large-scale pressure patterns definition is 60°W–40°E, 30°N–80°N. Station abbreviations and topographical character: BS=Basel-Binningen (Mittelland), BE=Bern-Liebefeld (Mittelland), GE=Genève-Cointrain (Mittelland), Sae=Säntis (northern Alps, mountain top), Sil=Segl-Maria (Alps, Engadina), Sio=Sion (Alps, Valais), ZH=Zürich-MeteoSchweiz (Mittelland), Lug=Lugano (Ticino).

1.5 Aims and outline

The aim of this thesis is to contribute to a better understanding of interannual climate variability in the European and Alpine region. The focus is on the relation between large-scale dynamics (climate patterns, atmospheric blocking) and the variability of important local climate elements. High quality instrumental and reanalysis data are used to investigate the role of local and large-scale climate variability in understanding observed snow variability and trends. The relation between atmospheric blocking and climate patterns of variability is worked out. Further, problems are tackled arising with standard variables of climate monitoring in times of increasing anthropogenic climate change (nonstationary conditions). Finally, the question is addressed whether the characteristics of interannual variability have changed in the past and will change in a future climate.

Although the chapters of this thesis are thematically related, each chapter stands for itself and can be read completely independently. The first two chapters investigate snow pack in the Swiss Alps. The other three chapters focus on large-scale dynamics and temperature variability on a central European to continental scale.

Chapter 2 (published in GRL by Scherrer et al. (2004b)) focuses on the influence of local temperature and precipitation as well as large-scale climate flow patterns on trends in Swiss Alpine snow days. Simple statistical models linking local climate elements and large-scale climate patterns are applied to model snow day variability and trends.

Chapter 3 (manuscript submitted) extends the work reported in Chapter 2 in different ways. In contrast to Chapter 2 the focus is more on snow variability. The main modes of variability in Swiss Alpine snow pack are determined and the relation of large-scale climate patterns on local temperature, precipitation and snow pack is worked out in detail.

In Chapter 4 (Scherrer et al., 2006b) the statistical relation between atmospheric blocking and climate patterns is determined using three different two dimensional indices of atmospheric blocking of low and high complexity.

Chapter 5 (Scherrer et al., 2006a, in press, Int. J. Clim.) addresses the problems of the interpretation and communication of climate normals in the past, present and future. The problem is discussed from an applied (weather service) perspective using temperature anomalies as variables.

In Chapter 6 (published in GRL by Scherrer et al. (2005)) recent observations and global climate model IPCC scenario runs are used to elaborate the central European temperature distribution changes in the near past and present and changes projected by climate change simulations in the course of the 21st century.

Chapter 7 summarizes the main findings of the thesis and gives an outlook for possible future work and an overview of the remaining problems.

Chapter 2

Trends in Swiss Alpine snow days: The role of local- and large-scale climate variability

SIMON C. SCHERRER[1], CHRISTOF APPENZELLER[1] AND MARTIN LATERNSER[2]

[1] Climate Services, Federal Office of Meteorology and Climatology (MeteoSwiss), Zürich, Switzerland
[2] Swiss Federal Institute for Snow and Avalanche Research (SLF), Davos, Switzerland

ABSTRACT

Swiss Alpine snow cover is varying substantially on interannual to decadal time scales. In the late 20th century decreases in snow days (SD) have been observed for stations below 1300 m asl. A regression model is used in this work to quantify the importance of mean temperature and precipitation as well as large-scale climate variability in order to explain the observed trends. Both, local- and large-scale models account for a modest fraction of the observed seasonal variability. Results suggest that the recent decrease in low altitude snow cover can mainly be attributed to an increase in temperature. Differences are found for northern and southern Switzerland concerning the influence of large-scale climate patterns. In contrast to southern Alpine regions, northern Alpine interannual SD variability is almost unaffected by the North Atlantic Oscillation (NAO). Decadal trends, however, can be explained via temperature only by a model that includes the explanatory variable NAO.

2.1 Introduction

Snow is a resource of great commercial and social value for the Swiss Alpine region (tourism, drinking water reservoir, hydro-electricity) but it also bears considerable hazards (avalanches, road closures) (e.g. Elsasser and Messerli, 2001; Beniston et al., 2003b). However, the number of snow days (SD) varies substantially on interannual to decadal time scales. A decrease has been reported for low altitude stations in the late 1980s and 1990s (Laternser and Schneebeli, 2003). A similar decline in spring snow cover has been found for other

mountain regions of the world (Brown, 2000; Mote, 2003). For most stations the decline coincided with a significant increase in local temperature.

Several studies point out a pronounced impact of seasonal climate modes on snowpack in the Western USA (Cayan, 1996; McCabe and Dettinger, 2002). In the European region the North Atlantic Oscillation (NAO) is the leading climate mode of seasonal to decadal variability (Hurrell, 1995). However, since Switzerland is located between the poles of the NAO temperature impact, the NAO influence in the Alpine region is ambiguous. Large-scale upper air fields such as pressure and stratospheric ozone are rather strongly forced by the NAO variability (Beniston, 1997; Appenzeller et al., 2000). Surface and possibly smaller scale variables such as precipitation seem to be dominated by other modes on the seasonal to interannual time scale (Massacand and Davies, 2001a; Schmidli et al., 2002).

This work examines the influence of local seasonal mean temperature and precipitation as well as seasonal large-scale Euro-Atlantic climate patterns of sea level pressure (SLP) on Swiss Alpine midwinter snow day variability and trends.
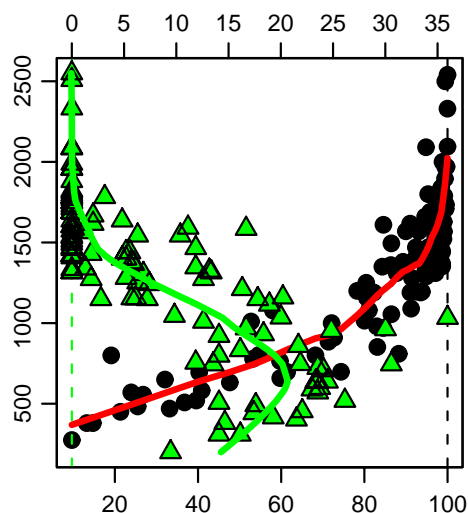
Figure 2.1: Variability and saturation of DJF Swiss snow days with respect to altitude (units: m). The green triangles show a robust estimation of the standard deviation expressed as the inter quartile range divided by 1.349 (upper horizontal axis, units: days). The median percentage of DJF days classified as snow days is depicted by black dots (lower horizontal axis). The thick lines are lowess (f = 0.3) smoothed curves to the corresponding data.

2.2 Data and methods

2.2.1 Snow and climate data

DJF SD have been calculated from a quality checked snow dataset covering the Swiss Alps and parts of the forelands described in detail by Laternser and Schneebeli (2003). A subset consisting of 110 almost complete and spatially almost uniformly distributed daily snow

height measurements ranging from 275 m to 2540 m asl and covering the period from 1958 to 1999 was used in this study. SD were defined as days with a snow height of more than 5 cm as suggested by Hantel et al. (2000). Local seasonal temperature and precipitation time series at the snow stations were derived from 67 (360) carefully homogenized monthly temperature (precipitation) observations (Begert et al., 2003). The interpolation to the snow station coordinates was achieved by linear fits to the station height using the 5 (10) nearest surrounding temperature (precipitation) stations as predictors. The DJF mean SLP fields were derived from the European reanalysis project (ERA–40) data set.

2.2.2 Statistical methods

Interannual to decadal scale trends were analyzed using ordinary least square 15-year running window trends. Standard principal component analysis was used to determine the leading SLP patterns (Wilks, 1995). The first principal component of the DJF SLP fields over the Euro-Atlantic region [80°W–60°E, 30°N–80°N] turned out to be virtually identical with a station based NAO index as defined by Hurrell (1995).

Standard linear regression analysis was used to quantify how well seasonal SD sums can be modelled *(i)* by taking local seasonal mean temperature (T) and mean precipitation (P) as explanatory variables and *(ii)* by taking large-scale climate patterns represented by the first 6 SLP principal components (PC's) as explanatory variables (cf. Junge and Stephenson, 2003). For the latter the local snow day anomaly ΔSD^k is thus modelled as

$$\Delta SD^k = \sum_{i=1}^{6} \alpha_i^k \cdot SLP_{PCi} + \varepsilon \qquad \text{(Eq.2.1)}$$

where α_i^k are the coefficients to be fitted, ε is an independent identically distributed error and k is the index of the stations considered. Optimal model sets were selected using a stepwise forward and backward selection procedure. Absolute model trends that can be attributed to T and P were determined following the method described by Mote (2003).

2.3 Results

2.3.1 Snow variability and trends

The number of SD is difficult to analyze in a statistical sense. Its variability in mean and standard deviation is large and highly dependent on altitude. In midwinter (DJF), SD saturation occurs for stations with heights above ~1300 m asl, indicating snow cover over the entire season (Figure 2.1). This inhomogeneity of the variability with altitude and our focus on low altitudes makes it reasonable to restrict the interpretation of the model results to altitudes below this saturation level.

The trends in Swiss SD are displayed in Figure 2.2 as time-height sections using a 15-year running window trends. No uniform trend is discernible over the whole period. Negative trends are observed at the beginning and at the end, positive trends in between. The most striking decline is found at the end of the observation period.
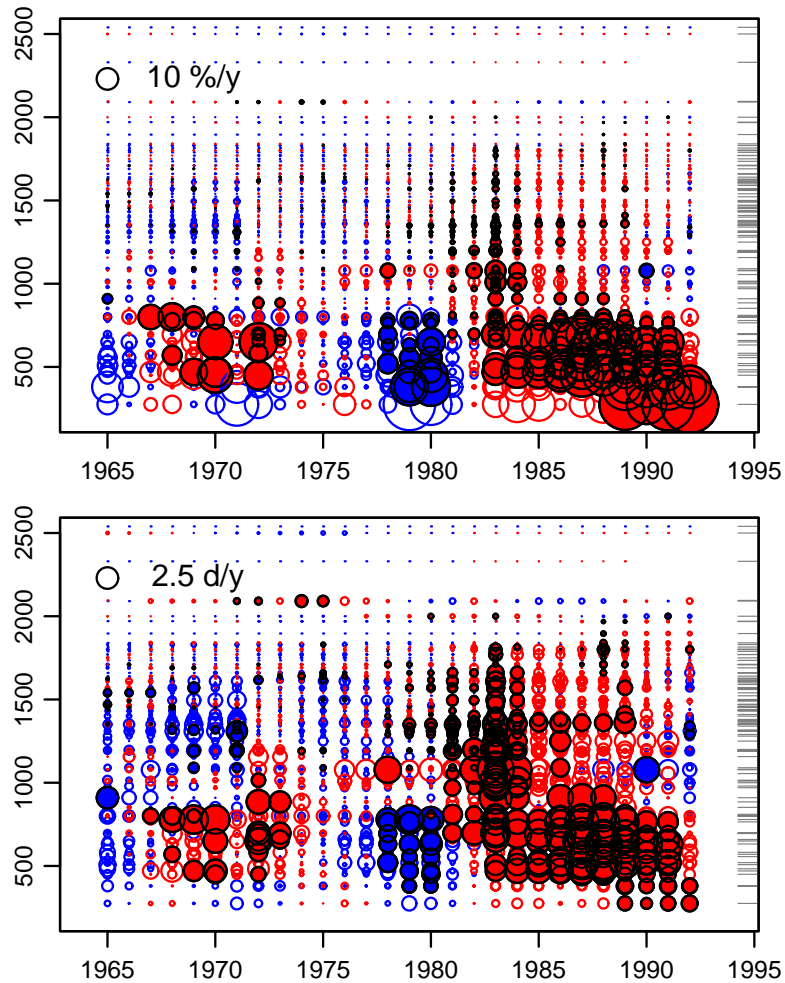
Figure 2.2: Time-height section of decadal Swiss snow day trends. Upper panel: relative 15-year running window trends (units:%/yr), lower panel: absolute 15-year running window trends (units: days/yr). Blue (red) circles show positive (negative) trends. Significant trends according to a two sided t-test on the 10% level are filled and have a black border. The height distribution of the snow stations is indicated by dashes on the right side. A scale for the circles is shown in both panels.

Relative trends are large for low and negligible for high stations (Figure 2.2 (top)). This low-high altitude dissimilarity is a direct consequence of the declining variability and the saturation with altitude (cf. Figure 2.1). The station height of maximum trends (~600 m) is of the same order as the current height of maximum sensitivity in Switzerland and Austria (Hantel et al., 2000). Absolute trends are less dependent on altitude, but the largest trends are again found for relatively low stations (Figure 2.2 (bottom)).

Although SD reveal considerable interannual to decadal variability, it is common to compute linear trends for the whole 42 yr time period considered. The corresponding relative observed trends are shown in Figure 2.3. The results are consistent with the decadal trend plots discussed above. Relative trends are negligible for stations above ~1300 m, whereas large negative trends are found for lower stations. Both northern and southern Swiss SD trends are similar with slightly smaller trends in the southern regions.

Table 2.1: Mean multiple R² for different kinds of linear snow day models applied to northern (NCH) and southern Switzerland (SCH) stations below 1000 m asl.

model type	predictors	multiple R^2 (%)	
		NCH	**SCH**
local	P_{only}	8	14
	T_{only}	35	23
	$T_{and}P$	45	35
large-scale	NAO_{only}	6	20
	SLP PC2–6	37	12
	NAO and SLP PC2–6	43	32
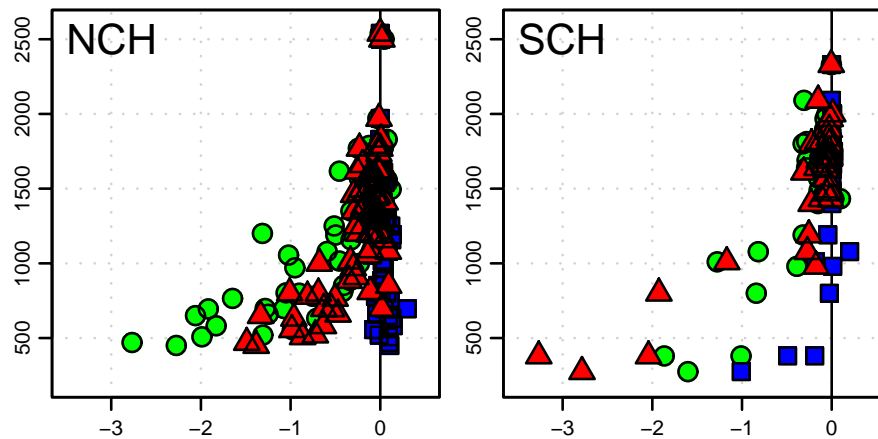
Figure 2.3: 1958–1999 observed and modelled linear snow day trends. Shown are relative trends (units:%/yr) for the observations (green circles), combined temperature and precipitation (red triangles) and precipitation only model (blue squares). Results for northern (NCH) and southern Switzerland (SCH) are shown in the left (right) panel.

The strong altitudinal dependence of trends is in general a typical sign of a T shift since relative changes in SD (similar as for snow water equivalent) are quite uniform with altitude for changes in P (Mote, 2003). A moderate shift in T on the other hand can change the fraction of P that falls as snow considerably. To test the above statement, local T and P models are constructed in the next section.

2.3.2 Local temperature and precipitation models

Earlier studies on climatological snow variability showed that to a first approximation local T and P have a large impact on local snow water equivalent (Mote, 2003).

Table 2.1 indicates that Swiss Alpine midwinter SD variability can be described with modest success using a statistical model that comprises seasonal local mean T and mean P as explanatory variables. For stations below 1000 m asl the explained variance is ~45%

(35%) for northern (southern) Switzerland. The T_{only} model results suggest that most of the explained variability is explained by mean T variability. This is no surprise since DJF mean T for these low regions are around 0 °C, where already small variations determine whether P falls as snow or rain. The influence of P is stronger for southern than for northern Switzerland, indicating that SD on the southern side of the Alps might also be P limited (cf. Table 2.1). The relatively moderate percentage of overall variability explained suggests that either temporal variability and/or other (local) effects in the sub-seasonal range which are lost by seasonally averaging play an important role.

The observed long-term trends can be modelled rather well using the above model (Figure 2.3). The combined T and P model explains more than 50% of the trend observed for northern Switzerland. The P_{only} model on the other hand is not able to reproduce any reasonable trends. This is a further indication, that the recent negative Swiss Alpine snow day trend is mainly T determined. It is consistent with the hypothesis discussed in the previous section and the results found for the Pacific Northwest region of the USA (Mote, 2003).

The absolute model trends that can be attributed to T and P are quantified in Figure 2.4. Although the fit considerably underestimates the trends for certain stations in analogy to the results found by Mote (2003), it reveals that the increasing trends in mean T explain almost all of the modelled decreasing snow day trends. The mean T contribution is particularly large for stations below 1000 m asl independent of region. The P related trends are in general very small, e.g. Figure 2.4 (left). A weak P related increase in SD is found for stations north of the Alpine mountain divide, whereas a weak P related decrease appears on the southern regions (Figure 2.4 (right)).
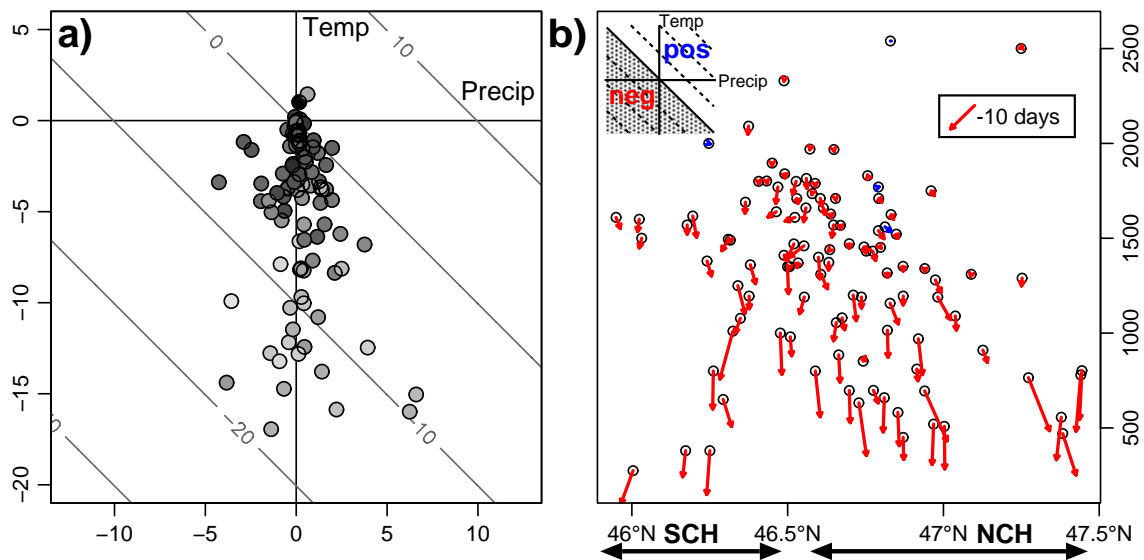
Figure 2.4: Snow day trends attributed to local mean temperature and precipitation based on the local snow day model (units: days/42yrs). (left) precipitation (x-direction) vs. temperature (y-direction) attributions. The greyscale of the points shows station altitude: the higher the station, the darker the points. Contour lines depict total (temperature plus precipitation) trends (units: days/42yrs). (right) Latitude (S-N) vs. altitude section. The trends attributed to precipitation (x-direction) and temperature (y-direction) are shown as pseudo vectors. Similar to the left panel the 135° line divides positive and negative combined trends (see inset in the upper left corner).

2.3.3   Large-scale influences on variability and trends

The variability in local variables discussed above is mainly related to larger-scale atmospheric flow variations (Beniston, 1997). For North America it was shown, that the influence of synoptic scale flow patterns as well as seasonal climate modes on local snow water equivalent is crucial (Dettinger and Cayan, 1995; Cayan, 1996; McCabe and Dettinger, 2002). Furthermore, large-scale climate modes such as the NAO are important in quantifying recent global change impacts (see e.g. Hurrell et al., 2003).

The snow day multiple R^2 of models with seasonal large-scale climate patterns (SLP PC's) as the only explanatory variables are similar to models that use local seasonal mean T and P (Table 2.1). Higher values (up to 70%) are again found for low stations. These numbers reflect that large-scale SLP patterns as a single variable are a fairly good predictor of low station SD variability.

They also suggest that the large-scale impact on local variables is not necessarily smaller for low than for high altitudes. The major reason is the vulnerability of snow on the 0 °C temperature threshold. Temperatures at higher stations are more often below 0 °C and therefore fallen snow persists without direct reaction on T variations.

By including and excluding the first PC of the seasonal SLP pattern into the model, the role of the NAO in explaining the observed Swiss SD variability can be quantified. For northern Switzerland the model without NAO has a multiple R^2 only marginally smaller than that of the full model (Table 2.1). For southern Switzerland the model without NAO loses more than half of the full model value R^2. Hence, the NAO alone plays a minor role in determining the interannual SD variability in northern Switzerland ($0 < R^2 < 20\%$, dependent on station height), whereas for southern Switzerland the NAO is the most important model component. This is in agreement with studies that found a pronounced NAO impact on precipitation in the regions influenced by Mediterranean climate (Quadrelli et al., 2001b).
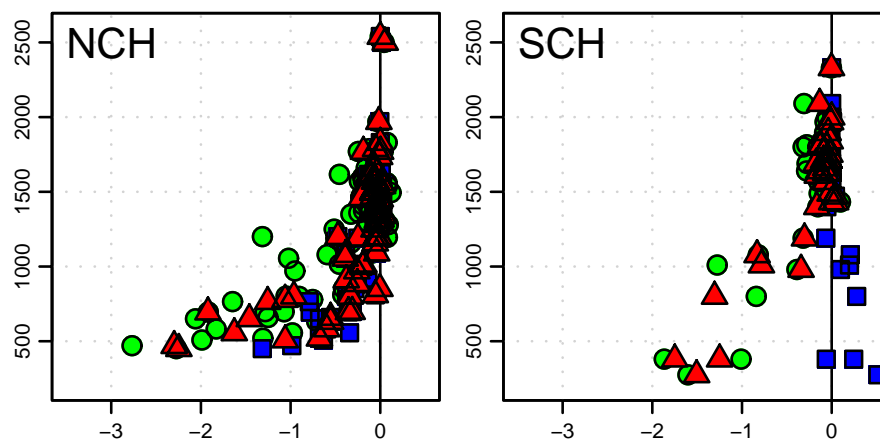

Figure 2.5: As Figure 2.4, but for large-scale climate pattern model trends. Shown are the results for the full (SLP PC1–6) model (red triangles) and the non NAO (SLP PC2–6) model (blue squares).

The NAO influence is enhanced substantially when longer term trends rather than inter-annual variability are investigated. The relative linear trends with respect to altitude are depicted in Figure 2.5 for the optimal full SLP PC as well as the optimal SLP model without NAO. The latter underestimates the trends considerably for northern Switzerland and fails completely to explain any trend for southern Swiss stations. The models including the NAO are able to model most of the observed trend, although there is still an underestimation for northern Switzerland.

To strengthen the hypothesis that the NAO variability can mainly explain decadal scale trends, the models were rerun and optimized for low and high pass filtered predictands and predictor fields. The low pass filter applied to the yearly time series was a five point triangular filter. High pass filtered values were constructed by subtracting the original from the low pass filtered data. For southern Switzerland, 88% of the stations include the NAO in both (low and high pass) optimal models. This suggests that the NAO not just explains trends but also considerable parts of interannual SD variability. Different results are found for the northern side of the Alpine mountain divide. A relatively small number of stations (35%) include the NAO as explanatory variable in the high pass filtered SD data. This again suggests that interannual SD variability is not primarily linked to NAO variability. The increase to 57% for the low pass filtered data corroborates the presumption that the NAO is important on decadal time scales.

2.4 Conclusions

In the late 20th century, Swiss midwinter Alpine snow cover showed a pronounced decrease at low altitude stations. Our statistical model results indicate that this decrease can mainly be attributed to an increase in seasonal mean temperature. Seasonal mean precipitation neither explains large amounts of variability nor affects recent trends in a substantial manner. Differences are found for the northern and southern parts of Switzerland concerning the influence of the NAO in explaining snow day variability. NAO related year-to-year variability is of minor importance for northern Switzerland but relevant for southern Switzerland. NAO related decadal variability was necessary for an adequate statistical description of decadal scale SD trends on both sides of the Alps but again with stronger impact on the southern side.

Finally, note that the late 20th century NAO trends might simply be natural decadal variability. However, if there is indeed a global change related trend to more frequent positive NAO index winters in the 21st century, as seen in some climate change model scenarios (e.g. Hurrell et al., 2003), our results indicate a stronger decrease in low altitude snow cover than expected from a global mean temperature increase alone.

Supplementary material

Map of the 110 total snow height stations
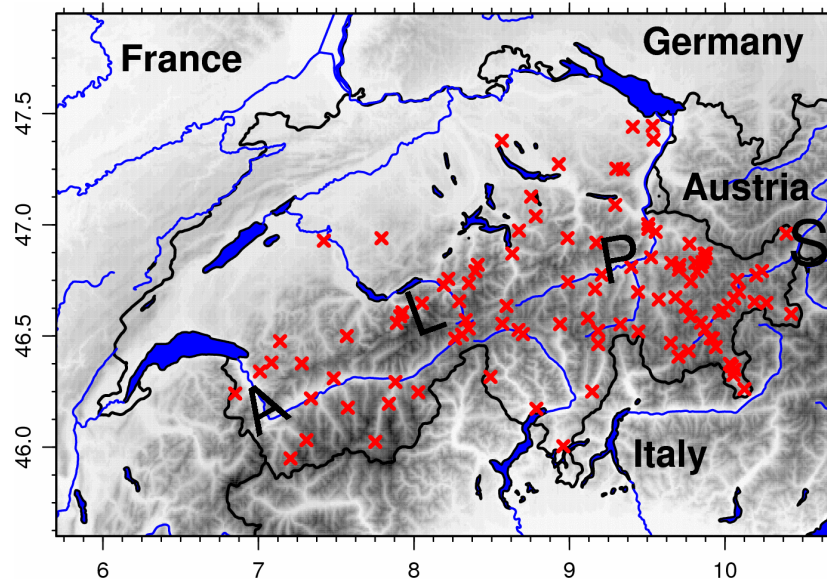
Figure 2.6: Map of the 110 total snow height stations considered in this study.

Frost day model

The temperature dependence of snow is not linear over the temperature range. To a first approximation snow accumulates for temperatures below 0 °C and melts above this threshold. Therefore it may be better to use cumulated seasonal frost days instead of averaged temperatures to model snow days. The corresponding results of using a model including frost days and precipitation are shown in Figure 2.7. The trends explained are only marginally different from the model using temperature averages (cf. Figure 2.8). A very similar conclusion is true for the amount of variability explained (cf. Table 2.1 and Table 2.2).

Table 2.2: Mean multiple R^2 for different kinds of linear snow day models applied to northern (NCH) and southern Switzerland (SCH) stations below 1000 m asl.

model type	predictors	multiple R^2 (%)	
		NCH	SCH
local	P_{only}	8	16
	FD_{only}	32	16
	FD and P	46	33
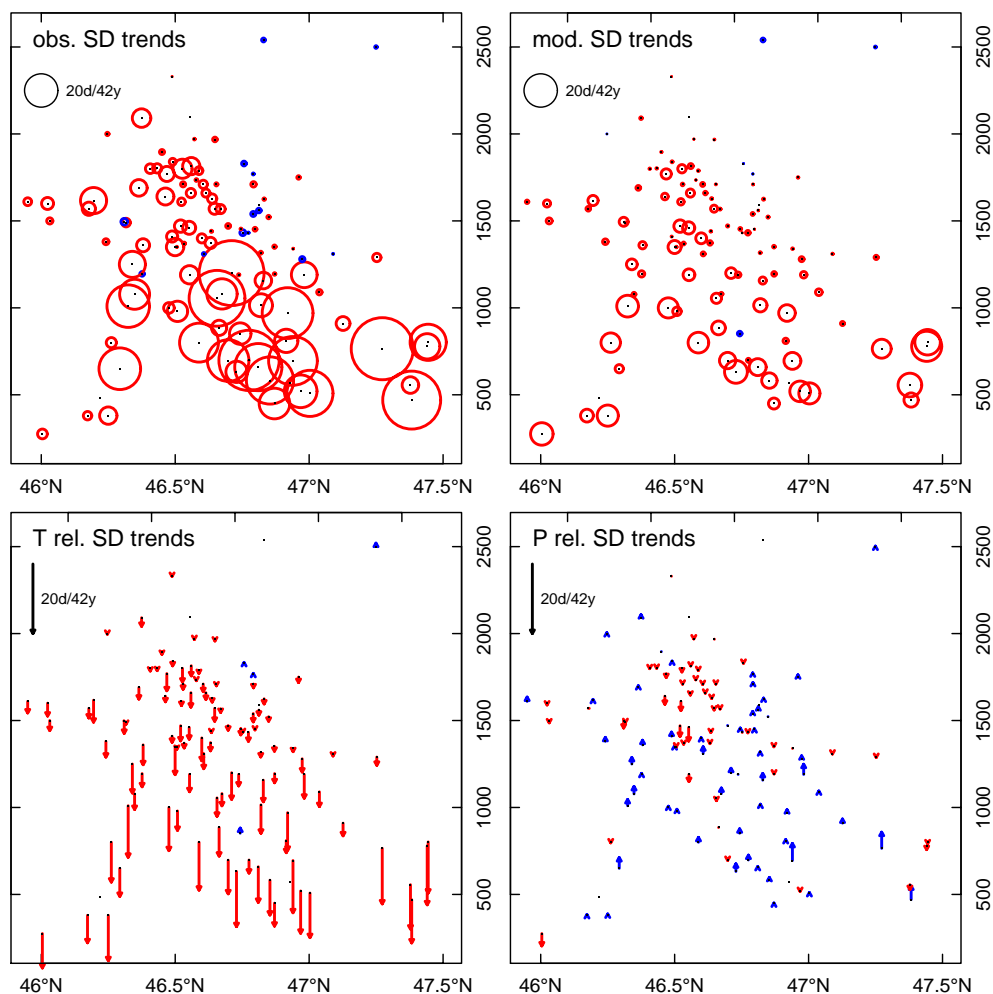
Figure 2.7: Observed and modelled snow day trends using the model of equation 2.1 but with frost days instead of temperature as predictor (upper panels). SD Trends explained by frost days and precipitation are shown in the lower panels.

Height dependence of temperature and precipitation impact

The precipitation-frost day model has been applied to snow days, snow height and new snow sums. The best results in terms of explained variability have been found for new snow sums. Figure 2.9 shows the variability explained as a function of altitude for precipitation alone (blue) and frost days alone (red) and together (right panel). It can be seen that the explained variance attributed to temperature is largest for low stations (in the order of 20–30%) and declines to almost zero for high stations. In contrast, the explained variance attributed to precipitation increases from around 20% for low stations to roughly 40–70% for high stations. This change of relevance from temperature to precipitation is physically plausible and was already mentioned in a more qualitative manner by several authors (e.g. Breiling and Charamza, 1999; Beniston et al., 2003a; Beniston et al., 2003b; Gyalistras et al., 2005).
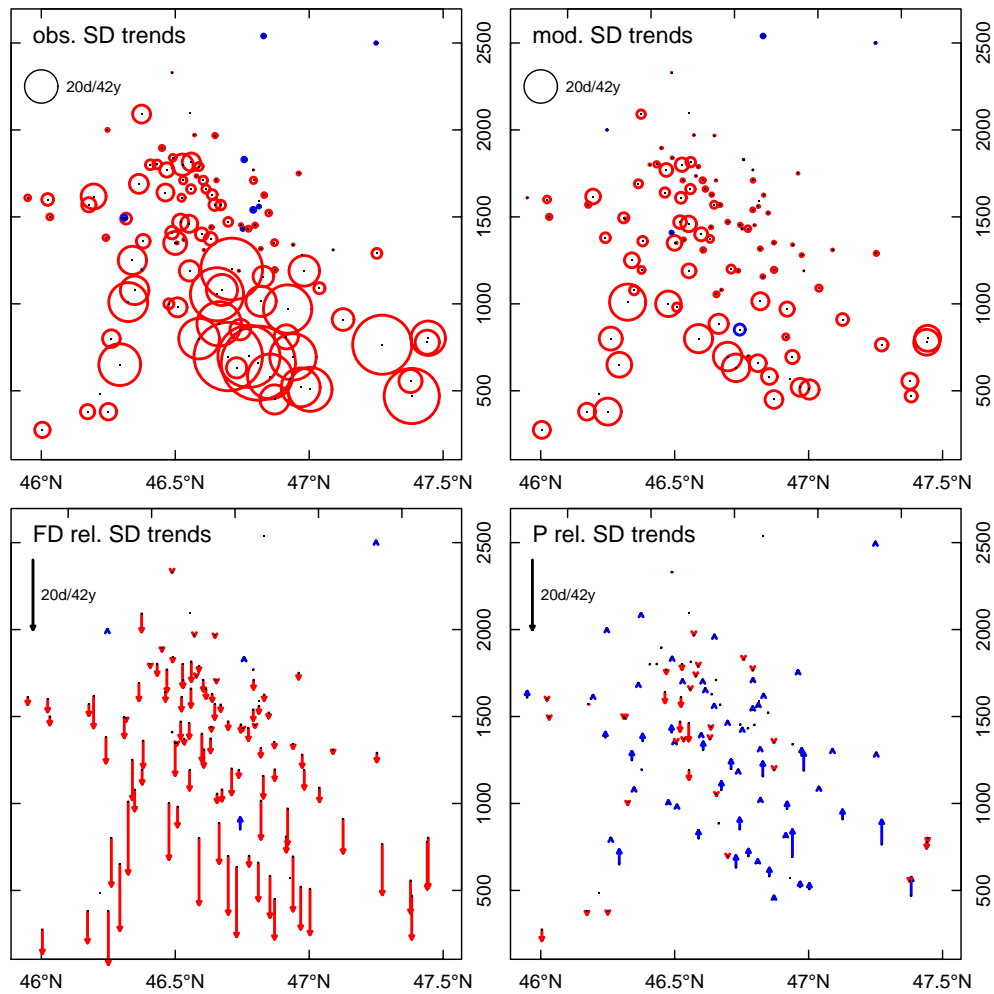
Figure 2.8: As Figure 2.7 but for the original temperature and precipitation model of Eq.2.1.
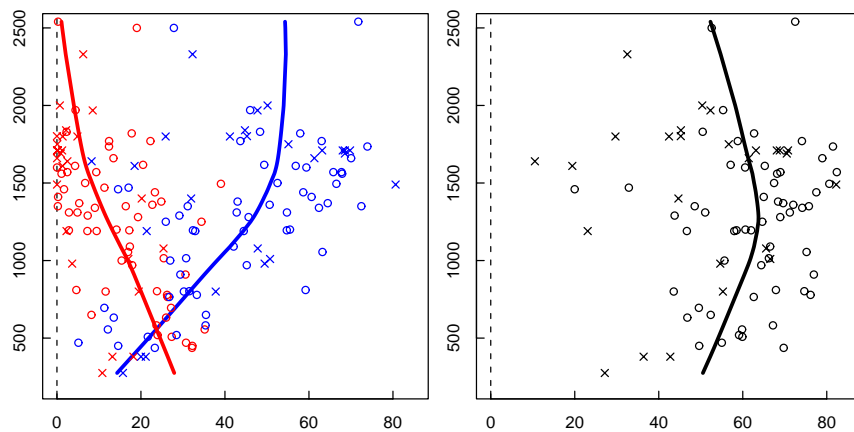
Figure 2.9: Height dependence (m asl) of new snow sum variability (%) explained by frost days alone (red), precipitation alone (blue) and together (black, right panel). Northern (southern) Swiss stations are shown as circles (crosses).

Chapter 3

Major patterns of Swiss Alpine snow pack variability: Links to local climate and large-scale flow

SIMON C. SCHERRER AND CHRISTOF APPENZELLER

Climate Services, Federal Office of Meteorology and Climatology (MeteoSwiss), Zürich, Switzerland

ABSTRACT

The impact of interannual climate variability on seasonal averaged Swiss Alpine snow cover is addressed. A principal component analysis is performed for the winters (DJF) 1958–1999. For the new snow and snow height series, three well separated leading patterns are found. The first (uniform) pattern explains ~50% of total variance and is spatially almost uniform over the entire Swiss area. The second (north-south) pattern explains ~15% of total variance and distinguishes between the northern and southern slope of the Alps. The height dependent third (low-high) pattern explains ~10% of total variance. For seasonal snow days the three patterns are similar, but the ranks of the north-south and low-high pattern are switched. Variability in the uniform new snow pattern is primarily related to positive seasonal precipitation anomalies. In contrast, variability in the uniform snow days is primarily related to negative mean temperature anomalies. For averaged snow height both temperature and precipitation are important. This change from precipitation dominance for new snow sums to temperature dominance for snow days is consistent with physical reasoning (i.e. control by snow accumulation only or accumulation and ablation). The surface pressure anomaly pattern linked to the uniform new snow pattern is centred over south-eastern Europe – resembling the classical Euro-Atlantic blocking pattern. For snow days the pressure anomaly pattern is shifted further south-eastward. The north-south snow pattern is mainly influenced by an East Atlantic like pattern, whereas only the temperature dependent low-high snow pattern is directly linked with the North Atlantic Oscillation.

3.1 Introduction

Alpine snow pack is an important economic factor for Switzerland. Revenues from winter tourism are highly correlated with snow abundance (Elsasser and Messerli, 2001). Snow pack also plays a major role in hydro-power electricity production and shaping mountain ecosystems (Beniston et al., 2003a; Gyalistras et al., 2005). Interannual and long-term changes in snow accumulation and ablation processes have a direct impact on the socio-economic system in the Alpine region (Abegg, 1996; Bürki, 2000).

In the Swiss Alps significantly negative trends have been observed in several snow pack variables in the late 1980s and 1990s (Laternser and Schneebeli, 2003). It has also been shown that these observed trends can be mainly attributed to a temperature increase and that the precipitation impact is small (Scherrer et al., 2004b). Similar results have been found for the mountain ranges in the north-western USA (Mote, 2003; Mote et al., 2005).

Local snow pack variability is determined to a large degree by local temperature and precipitation (Scherrer et al., 2004b; Mote et al., 2005). It is well known that there is an almost linear relation between melt and air temperature on glaciers and ice sheets (Ohmura et al., 1996; Hock, 2003). On the other hand are local climate variables determined to a substantial degree by large-scale flow. It predefines specific thermal and humidity characteristics of the air masses reaching the mountain range. In numerous studies the link between snow pack and circulation pattern variability has been confirmed. Some studies investigated snow on the continental to hemispheric scale (Gutzler and Rosen, 1992; Walland and Simmonds, 1997; Frei et al., 1999; Corti et al., 2000), others addressed links to regional issues (Dettinger and Cayan, 1995; Cayan, 1996; Hartley and Keables, 1998; Clark et al., 1999; Bednorz, 2002; McCabe and Dettinger, 2002; Morinaga et al., 2003).

In the Euro-Atlantic region the North Atlantic Oscillation (NAO) is the leading mode of large-scale circulation variability on seasonal to decadal time scales (Hurrell, 1995; Marshall et al., 2001; Wanner et al., 2001). The NAO was found to play a major role in determining snow pack in Poland (Bednorz, 2002) and Eastern Europe (Clark et al., 1999; Hori and Yasunari, 2003; Bednorz, 2004). For the Swiss Alps, Beniston (1997) found that high pressure episodes are linked with the NAO and accompanied by positive temperature anomalies and below average precipitation, both of which are unfavourable for Swiss Alpine snow accumulation. The role of the NAO as a possible explanation of the decadal trends was confirmed in a recent study (Scherrer et al., 2004b). However, on the northern slopes of the Swiss Alps seasonal to interannual variability is explained only to a very small extent directly by the NAO, while its influence on the southern slopes is stronger.

In this study, three different seasonal snow variables are used. Seasonally averaged snow heights (abbreviated as SH hereafter) and snow days (SD hereafter) are determined by all processes that accumulate and ablate snow. Seasonally averaged new snow sums (NSS hereafter) are primarily determined by the conditions during the relatively short periods in which the snow fall event takes place (accumulation only).

It is the aim of this work *(i)* to determine the major patterns of Swiss Alpine seasonal mean snow pack variability, *(ii)* to explore the local relation between seasonal mean temperature, precipitation and different variables of seasonal snow pack, and *(iii)* to investigate the influence of seasonal mean large-scale circulation patterns on the seasonal snow variability.

After the introduction of the data sets and methods (Section 3.2), the major patterns of snow variability and trends are determined and discussed (Section 3.3). In Section 3.4 the relation between seasonal temperature, precipitation and snow pack is worked out. A short analysis of the new snow sum – NAO index relation (Section 3.5.1) is followed by investigations to shed light on the relation between large-scale circulation and the local snow pack variability (Section 3.5.2). In Section 3.5.3 statistical models using large-scale circulation patterns as predictors are used to explain snow pack variance. Finally, the main findings are summarised and conclusions drawn in Section 3.6.

3.2   Data and methods

3.2.1   Data sets

Switzerland has a dense network of snow measurement stations run by the Federal Office of Meteorology and Climatology (MeteoSwiss) and the Swiss Federal Institute for Snow and Avalanche Research. Some few regular snow observations date back to 1864, but most of the digitised data is available after 1931. Total snow heights as well as new snow sums are measured once (or twice) a day at least during the period from October to May. In this study only stations in the Alps and its close foreland are used. The number of stations is far from being constant over time. Very few ($<$10) stations are available in digital form before the 1940s. Up to the late 1970s the number of stations increased up to 190 snow height stations and declined somewhat later on (Laternser, 2002). Only quality checked December-January-February data from stations with less than 20% missing values in the period 1958–1999 are used. These restrictions lead to a reduction to 89 new snow sums (squares in Figure 3.1) and 110 snow height stations (diamonds in Figure 3.1, left panel). Their altitudes range from 275 m to 2540 m asl with the highest station density between 1250 and 1750 m asl (cf. Figure 3.1, right panel). The spatial distribution shows a certain under-representation of very high stations and some clustering of stations along valleys and railway lines in the eastern parts of the domain.

A snow day data set is derived using the snow height measurements. Following Hantel et al. (2000) a day is qualified as a snow day if snow height is more than 5 cm. For high stations snow days saturate in DJF, i.e. all 90 of 90 potential days are snow days, cf. Figure 1 in Scherrer et al. (2004b). As in Scherrer et al. (2004b) only snow day stations which show a certain amount of interannual variability are used in this analysis (stations below 1300m asl). Since the higher stations are excluded (in contrast to the new snow sum and snow height analyses) results need to be handled with care.

Most of the snow measurement sites are "snow only" stations, i.e. there are no local temperature and precipitation measurements available at the station directly. To obtain seasonal mean temperature and precipitation estimates at the stations themselves, data from 67 (360) carefully homogenized monthly temperature (precipitation) measurements are used (Begert et al., 2005).

Following Scherrer et al. (2004b), the absolute values are linearly interpolated to the snow station coordinates and altitudes using the 5 (10) nearest surrounding temperature (precipitation) stations as predictors.
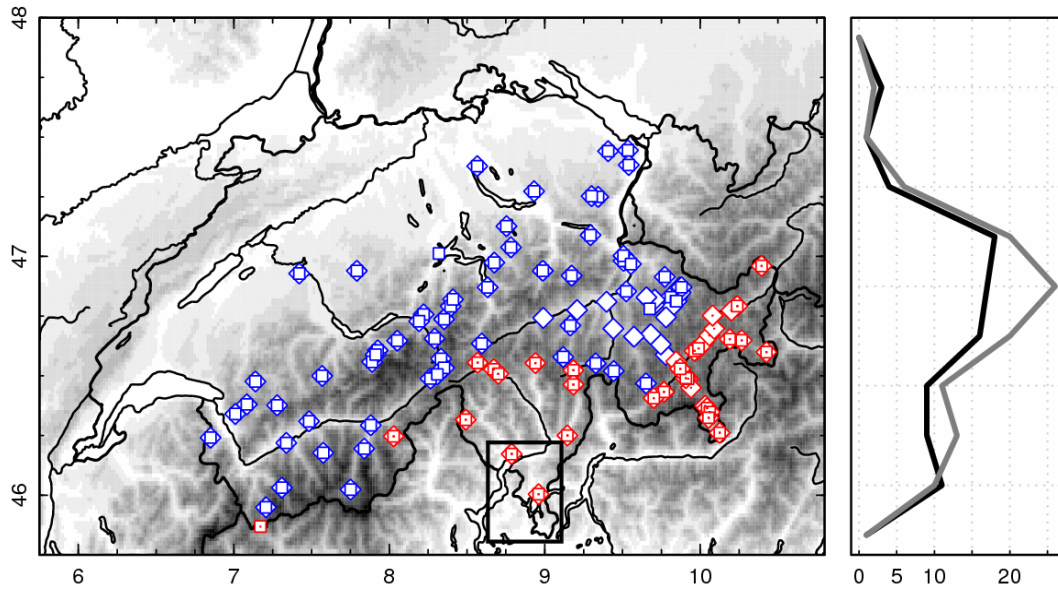
Figure 3.1: Left panel: Map of Switzerland showing the locations of the snow height (diamonds) and new snow measurement stations (squares) used in this study. Stations classified as northern (southern) Swiss are shown in blue (red with a point in the centre). The black rectangular box indicates the "Southern Ticino" region. Right panel: Altitudinal distribution of new snow (black) and snow height (grey) measurement stations. Shown are the number of stations in 250 m intervals centred around 500, 750, 1000, ..., 2500, 2750 m asl.

Sea level pressure data over the Euro-North Atlantic region (30°N–80°N and 80°W eastward to 60°E) is retrieved from the European Centre for Medium-Range Weather forecasts (ECMWF) reanalysis project ERA–40 data set (Uppala et al., 2006). The data are interpolated from an originally spherical harmonic T_L159 resolution onto a regular 1° latitude $\times$ 1° longitude grid. DJF mean values are computed using 6 hourly values at 00 h, 06 h, 12 h and 18 h UTC.

3.2.2 Statistical methodology

Standard unrotated Principle Component Analysis (PCA) (Preisendorfer, 1988; Widmann, 1996) is applied to determine the major patterns of seasonal mean snow variability. The resulting spatial loadings are called Empirical Orthogonal Functions (EOFs) hereafter. The time evolutions of these patterns, the temporal scores, are called principal components (PCs) below. One advantage of PCA compared to cluster analysis is its full objectivity. The results are completely independent (orthogonal) patterns of variance. At the same time the resulting patterns are not necessarily physical based. This makes a physical interpretation sometimes difficult or even impossible (e.g. Richman, 1986; Jolliffe, 1987; Cherry, 1997; Dommenget and Latif, 2002; Hannachi et al., 2006).

Before application of the PCA the snow series are standardized in order to circumvent the dominance of high stations caused by much larger absolute anomalies. No further power transformation is applied to the three monthly data since the resulting patterns are not very dependent on the power transformation applied. No weighting according to station density in space is made since tests showed that this had no substantial influence on the re-

sults. The fully objective method proposed by Beckers and Rixen (2003) is used to compute PCA with missing values. As a sign convention for interpretations, positive values of PCs are defined as positive contributions of snow for the northern slope of the Alps.

PCA of local temperature and precipitation is determined analogous to the snow data above. The same kind of PCA is conducted to determine the major patterns of large-scale circulation variability in the Euro-Atlantic sector. The large-scale sea level pressure fields are weighted by the cosine of latitude in order to give similar weights to all geographical regions accordingly.

North's rule of thumb (North et al., 1982) is applied to see whether an EOF is likely to be subject to large sampling fluctuations and to determine the maximum number of PCs that are well separated. Separation does not necessarily imply physical meaningfulness but gives an upper limit of the number of potentially meaningful patterns.

Standard Pearson correlation analysis is used to relate local variables such as snow, temperature and precipitation with Euro-Atlantic scale circulation fields (Wallace and Gutzler, 1981; Wilks, 1995). Correlation significance levels are determined using a Monte-Carlo approach of first order auto-regressive (AR1) processes to mimic the redness of the processes investigated. The significance level used in this study is 95% if not mentioned otherwise. Positive and negative (± 1 standard deviation) composite fields of sea level pressure are used to determine "absolute flow" fields and directions.

Alternatively, singular value decomposition (SVD) has also been used to explore the co-variability of snow and circulation fields (Bretherton et al., 1992; Widmann, 1996). The anomaly field results are very similar to the more simple point-wise correlation analysis (cf. Widmann, 2005). Therefore the SVD results are not shown in this paper.

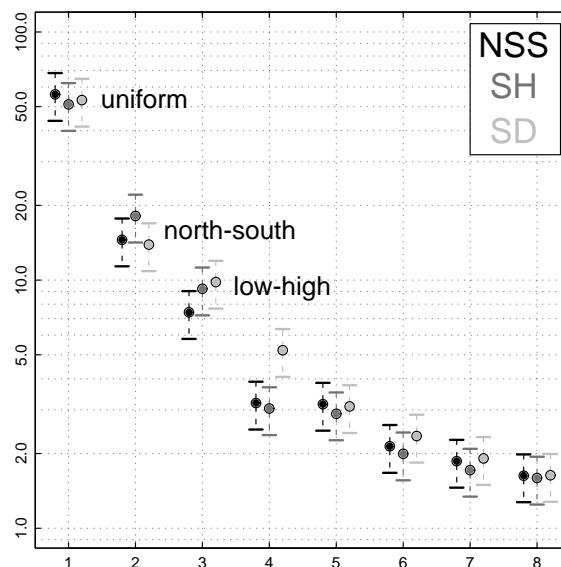*Figure 3.2*: Percentage of explained variance by the first 8 new snow sum (NSS), average snow height (SH) and snow day (SD) principal components. The season considered is DJF in the period from 1958 to 1999. The error bars give the range of uncertainty due to sampling fluctuations using North's rule of thumb. The leading three components are labelled. The vertical axis has a logarithmic scale.

Table 3.1: Summary table of the three leading principal components of Swiss Alpine snow pack. The columns show the names, variance explained for the three snow parameters (%) and the primary and secondary influence regions. A hash sign indicates that the pattern is not well separated according to North's rule of thumb. The "southern Ticino" region is defined in Figure 3.1.

pattern	new snow sum (NSS)	snow height (SH)	snow days (SD)	primary influence	secondary influence
uniform	56	51	53	everywhere except southern Ticino	-
north-south	14.5	18	10#	Southern Alpine slope	Northern Alpine slope
low-high	7.5	9	14#	low stations, esp. in the south	high stations
sum	78	78	77		

In Section 3.5, multiple linear models are used to investigate large-scale climate sea level pressure patterns explaining Swiss snow pack variance. To avoid overfitting a stepwise optimization procedure as in Junge and Stephenson (2003) is applied.

3.3 Major patterns of Swiss snow variability

3.3.1 Spatial patterns

The PCA of the new snow sum, average snow height, and snow day data yields three similar leading patterns of variability which explain roughly 50%, 15% and 10% of the total of the variance respectively (cf. Table 3.1 for details). The variance explained by the eight leading PCs is shown for all three snow variables in Figure 3.2 together with an estimation of the eigenvector error using North's rule of thumb of sampling errors (North et al., 1982). The three leading new snow sum and average snow height patterns are well separated and potential candidates for further interpretation. For snow days only the first pattern is well separated. The second and third pattern are switched and not well separated, indicating that results based on these patterns should be interpreted with care. The missing separation is likely related to the snow day saturation with height.

Since the spatial patterns of all three snow variables are very similar (the second and third pattern is switched for snow days), only the new snow sum results are discussed here in detail. The left panels of Figure 3.3 show the spatial patterns of the three leading new snow sum components expressed as correlation coefficient between station and principal component series. The leading pattern is almost uniform over the entire investigation area. The loadings are all of the same sign and the correlation with the corresponding station based snow series is statistically significant for all but the two low-altitude southern Alpine stations Locarno and Lugano.

The leading pattern indicates that the primary interannual mid-winter Swiss new snow variability can be expressed as either winters rich or poor in snow, almost independent of sub-regions. It is called *uniform* pattern hereafter. The second pattern clearly separates be-

tween the northern and southern slopes of the Alpine mountain divide with strong (significantly) negative loadings in the south and some significantly positive loadings in the north. When this pattern is dominant, sites on the southern slopes tend to have opposite anomalies than those on the northern slopes. It is called *north-south* pattern hereafter. The third pattern shows positive and often significant loadings in the low Alpine forelands (north and especially south of main ridge of the Alps) and small mostly insignificant negative loadings in the higher inner Alps. This pattern is called *low-high* pattern below. The primary and secondary regions of influence of the three leading patterns are summarized in Table 3.1.
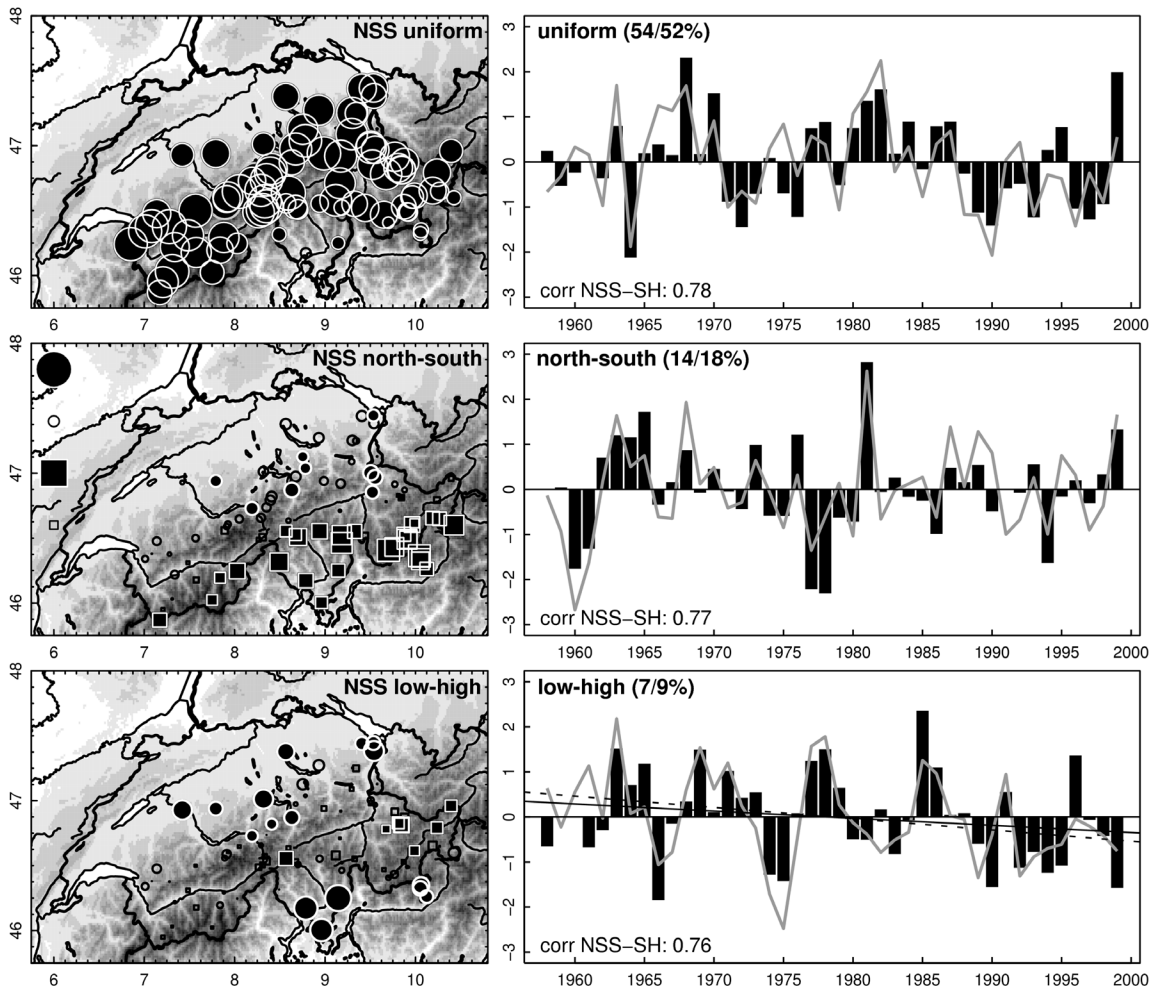
Figure 3.3: *Left panels:* Spatial patterns of the three leading components of DJF new snow sums (NSS). Positive correlations of station series with the principal component series are shown as circles, negative correlations as squares. Statistically significant correlation values (95% level) are filled and have a white border. The large (small) symbols in the left middle panel indicate correlations of 1 and 0.3. *Right panels:* Principal component time series of NSS and average snow heights (SH). The NSS series are shown as bar plot. The SH series are plotted as grey line. Percentage of explained variance as well as the correlation coefficient between NSS and SH series are given in the panels. For the low-high component, linear trend estimations are shown (NSS: solid line, SH: dashed line).

Note that caution is needed in the interpretation of the overall explained variance numbers. For specific stations or regions, the *north-south* pattern may explain much more variance than the overall averaged ~15% in the southern Swiss region. The same is true for the *low-high* pattern that dominates at low lying stations on both sides of the Alps. However, the leading *uniform* pattern is quite stable and also found for an analysis using only data from stations with altitudes below 800 m asl (not shown).

A comparison with a PCA of an independent precipitation data set reveals ample similarities (Widmann and Schär, 1997; Schmidli et al., 2002). The two leading precipitation patterns explain about the same amount of total variance. The *uniform* pattern shows more or less the same loadings all over the country. Similarly, the *north-south* pattern is also found for precipitation, and it represents the cross-alpine climate contrast well known in Switzerland (Begert et al., 2005). An exception is the *low-high* snow (i.e. solid precipitation) pattern. It has no direct counterpart in the precipitation PCs nor in precipitation clusters (Baeriswyl and Rebetez, 1997).

3.3.2 Temporal components

Overall 1958–1999 linear trends in the three leading new snow sum PCs are rather small (cf. Figure 3.3). The *low-high* components show the most prominent linear trend. For snow height the *low-high* component trend is significant on the 95% level (p-value = 0.04). The new snow sum *low-high* component trend p-value is 0.21. The *low-high* components show relatively large autocorrelation values, comparable with that of the NAO index. The other PCs considered have autocorrelation coefficients below 0.15. Although the lag-1 autocorrelation coefficient of the *uniform* PC is small, it is characterised by a rather pronounced decadal variability. A positive phase from the late 1970s to the mid 1980s is followed by a strong negative phase since the late 1980s (cf. Laternser and Schneebeli, 2003). The *north-south* component shows strong interannual and less decadal variability. The *low-high* component comes along with a fair amount of decadal variability (similar to the NAO). Correlations between corresponding PCs of new snow sums, snow heights and snow days are large (~0.77, see correlation numbers in panels of Figure 3.3) but there are several differences that are important for the interpretation of the different local influences as will be shown below.

3.3.3 Height dependence

The loadings of the *uniform* pattern can be separated into northern slope and southern slope stations, but there is no clear height dependence (Figure 3.4). For the *north-south* pattern the separation is more pronounced, but again the height dependence is small. A clear negative height dependence (r~-0.6) is found for the *low-high* pattern. This is true for both, northern as well as southern Swiss stations. The clear height dependence with a strong loading at lower altitudes together with the fact that no corresponding pattern is found in the precipitation data makes this pattern an attractive candidate to explore recent snow trends (see below).
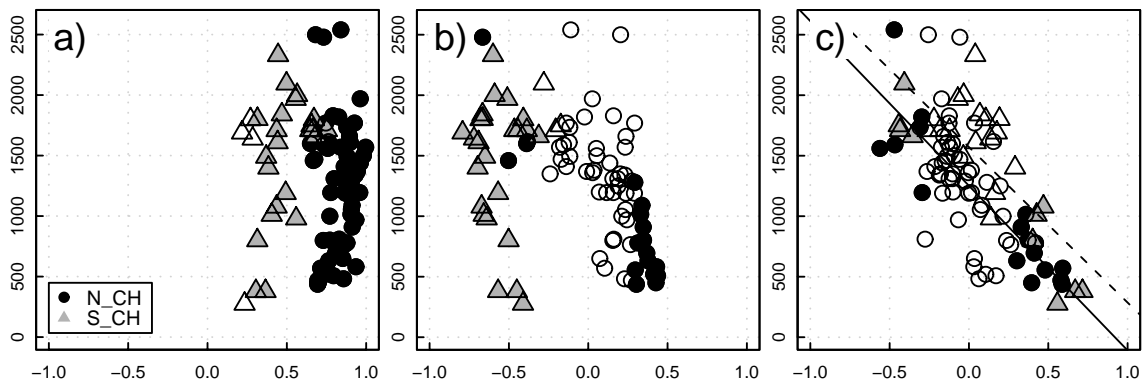
Figure 3.4: Correlation coefficients between all new snow sum station time series and the loadings of the principal components plotted vs. station altitude. Shown are the results for the three leading principal components. a) uniform pattern, b) north-south pattern, c) low-high pattern. Circles (triangles) denote northern (southern) Switzerland stations. Significant correlation coefficients (95% level) are filled, insignificant ones open.

3.4 Relation between temperature, precipitation and Swiss Alpine snow

It is well known that there exists an almost linear relation between melt and air temperature on glaciers and ice sheets (Ohmura et al., 1996; Wild et al., 2003). This relationship allows to construct simple, but for a large number of applications accurate enough temperature-index models to compute melt rates of snow and ice (Ohmura, 2001; Hock, 2003). Also seasonal snow pack variability in midlatitude mountain regions has been shown to be determined to a large degree by local temperature and precipitation variability (Mote, 2003; Scherrer et al., 2004b; Mote et al., 2005). However, details depend crucially on the different snow variables considered. New snow sums are primarily determined by the meteorological conditions during the relatively short periods in which the snow falls. Average snow heights and snow days are influenced by all processes that accumulate and ablate snow. In the following we explore how well the three snow variable's seasonal variability can be explained using only seasonal averages of local temperature and precipitation as predictor.

Table 3.2: Summary of the two leading patterns of seasonal Swiss Alpine temperature and precipitation principal components. The columns show the variance explained and the primary influence regions.

pattern	temperature	precipitation	primary influence
uniform	90	74	northern and central Alps
north-south	5	9	southern Alps
sum	95	83	

Table 3.3: Pearson correlation coefficients of the leading three DJF new snow sum (NSS), snow height (SH) and snow day (SD) components with the first two (uniform and north-south) principal components of temperature (temp) and precipitation (precip). Values greater than 0.5 are shown bold, values between 0.3 and 0.5 in italic. Sign convention: Positive snow, temperature and precipitation PC values mean positive correlation with northern Switzerland foreland stations.

correlation	uniform			north-south			low-high		
	NSS	SH	SD	NSS	SH	SD	NSS	SH	SD
uniform temp	*-0.43*	*-0.44*	**-0.64**	*-0.40*	*-0.33*	-0.16	**-0.59**	**-0.62**	**-0.55**
uniform precip	**0.76**	*0.46*	0.28	-0.17	0.12	0.09	*-0.40*	-0.10	-0.08
north-south temp	*-0.47*	*-0.31*	-0.25	*0.49*	*0.41*	*0.44*	0.01	-0.11	0.08
north-south precip	-0.10	-0.17	-0.17	**-0.80**	**-0.62**	**-0.70**	*0.33*	*0.38*	0.14

For further analysis, regional information about temperature and precipitation is quantified with the two leading temperature and precipitation principal components of the 67 (360) temperature (precipitation) series considered. For both temperature and precipitation, only the first two components proved to be well separated according to North's rule of thumb. Table 3.2 summarizes the results. The leading principal component of DJF temperature explains roughly 90% of the variance and is highly representative for most parts of Switzerland but with the primary influence on the northern slopes. It is called *uniform* temperature pattern subsequently. The second component shows a dipole structure with larger loadings on the southern slopes. It is therefore called *north-south* temperature pattern below. The leading precipitation component (~74% variance explained) is representative of most parts of Switzerland (*uniform* pattern), the second shows a dipole structure with high correlations especially at southern Swiss stations (*north-south* pattern).

Table 3.3 lists correlation coefficients of all snow variables' three leading components with the leading two temperature and precipitation PCs. The correlation coefficients with the *uniform* snow component depend strongly on the type of snow data. Positive *uniform* new snow sum anomalies are related to both positive *uniform* precipitation anomalies (linear correlation coefficient r = 0.76, Figure 3.5a) and negative *uniform* temperature anomalies (r = -0.43), but the relation to precipitation is dominating.

Different results are found for snow height and snow days that measure an integral over processes that accumulate and ablate snow. Positive *uniform* snow height anomalies correlate again with both negative *uniform* temperature (r = -0.44) and positive *uniform* precipitation (r = 0.46) anomalies. Both influences seem to be approximately equally important. The positive *uniform* snow day sum anomalies are primarily related to *uniform* temperature (r = -0.64, Figure 3.5b) and only weakly related to *uniform* precipitation (r = 0.28). In both quantities the *uniform* temperature influence is large. For snow days, the correlation with the *uniform* temperature pattern is clearly dominating over the one with the *uniform* precipitation pattern.

The *north-south* components show high negative correlations with the *north-south* precipitation PC (-0.62 and -0.80, cf. Figure 3.5c). In other words, interannual variability of the primary snow component at the southern Alpine slope is highly correlated with the

north-south pattern precipitation variability. The *low-high* snow component shows high negative correlations with the *uniform* temperature PC (Figure 3.5d) and (for new snow sums) is slightly negatively correlated with the *uniform* precipitation PC.

In several cases both temperature and precipitation components seem important to explain snow PCs. It is known that climatological temperature and precipitation values are often correlated with each other. This mutual correlation can cause misleading conclusions.
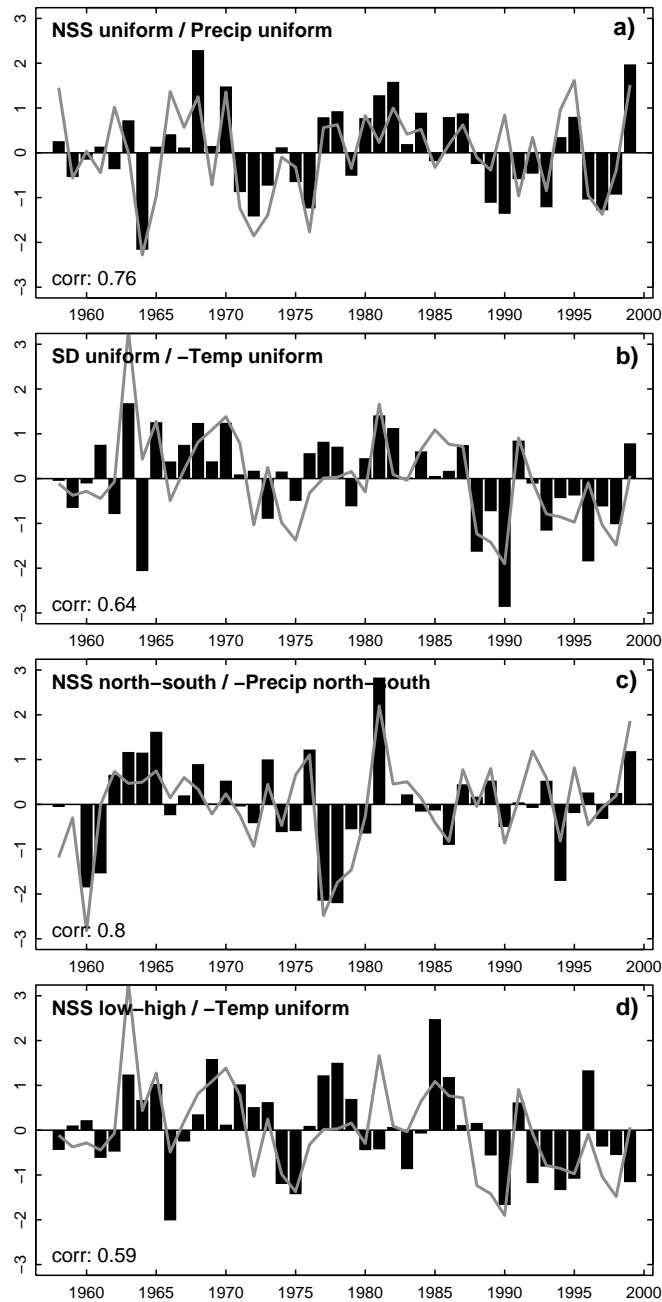

Figure 3.5: Time series of selected new snow sum (NSS) and snow day (SD) PCs (bars) and temperature and precipitation PCs (grey lines). See labels in panels for details. Correlation coefficients between the two series shown are printed in the lower left corner of the panels.
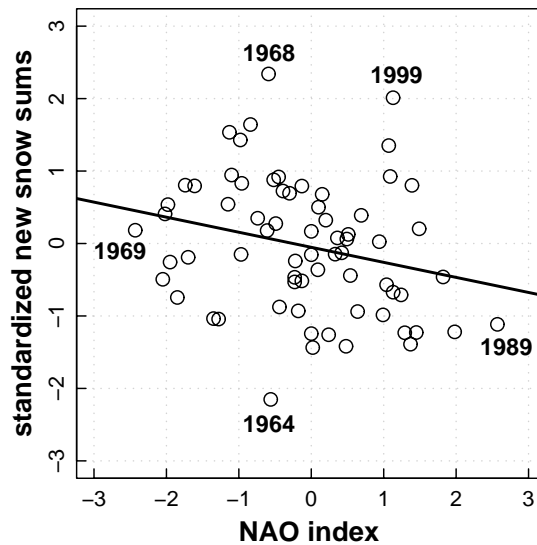
Figure 3.6: Scatterplot of DJF NAO index vs. DJF mean normalized new snow sums for the period 1931–1999. Shown are also a linear least square fit and the labels of five extreme new snow sum or NAO index years.

Following Junge and Stephenson (2003) a simple bivariate coupled model is used to discriminate the important direct effect from indirect effects mediated by mutual correlation between the explanatory variables. Results show that for all but one component the largest fraction of total correlation comes from direct correlation. The exception is the correlation of the new snow sum *north-south* component with the *north-south* temperature PC where the indirect part (0.37) is more than three times the direct part (0.12) of the correlation. This means that the second temperature PC is predominantly correlated with the *north-south* snow patterns via its mutual correlation with the *north-south* precipitation PC. More advanced techniques such as Granger causality could be used to gain more information about cause and effect (cf. Mosedale et al., 2005).

As demonstrated in this section variability in the leading local temperature and precipitation patterns have ample influence on the variability in leading snow patterns. At the same time local climate variables can be considerably affected by large-scale circulation, the topic of the next section.

3.5 Influence of the large-scale flow on local variability

3.5.1 Seasonal snowpack – NAO index relation

The NAO is the circulation pattern explaining most of winter upper-air variability in Europe (Wanner et al., 2001; Hurrell et al., 2003). The direct relation to Swiss climate variability is ambiguous and highly dependent on the variable considered (Schär et al., 1998; Appenzeller et al., 2000; Appenzeller et al., 2001; Massacand and Davies, 2001a; Schmidli et al., 2002). Figure 3.6 shows a scatterplot of DJF NAO indices versus normalized DJF Swiss new snow sums for the period 1931 to 1999. In accordance with earlier results which found a rather

pronounced effect of the NAO on Swiss snow pack (Beniston, 1997), the relation is negative (r~-0.30) and statistically significant on the 95% level (p-value = 0.04). In other words, positive (negative) NAO index values associated with strong (weak) westerlies over north-western Europe are linked with small (large) sums of Swiss Alpine new snow. However the relation is weak. Extreme new snow sum years are not extreme in seasonal NAO indices. The years 1968 and 1999, both extremely rich in new snow, and the year 1964 which was extremely poor in snow are accompanied by moderate NAO index values. Also the extreme NAO index years (positive: 1989, negative: 1969) are not extreme snow years.

Figure 3.7 shows 31-year running window correlations of the NAO index with the new snow sum PCs. The correlation with the *uniform* PC is negative (oscillating around the 95% significance level) and rather constant over the years. The correlation with the *north-south* PC is positive, shows a weak increase over the years from not statistically significant values at the beginning to slightly significant values at the end of the period considered. The *low-high* PC correlation is not statistically significant and almost zero at the beginning of the observation period, but starts decreasing in a rather monotonic manner in the late 1950s. The correlation becomes statistically significant in the mid 1960s and the maximum correlation is found at the end of the century with values of almost -0.8. The results are very similar using detrended data (thick lines in Figure 3.7) or original data (thin lines). This indicates that the high correlations are no artefact of possible linear trends in the series.

The above results show that interannual variability of the first two leading patterns is only moderately correlated with NAO variability. Only the *low-high* snow PC is highly correlated with interannual NAO variability since the 1960s.
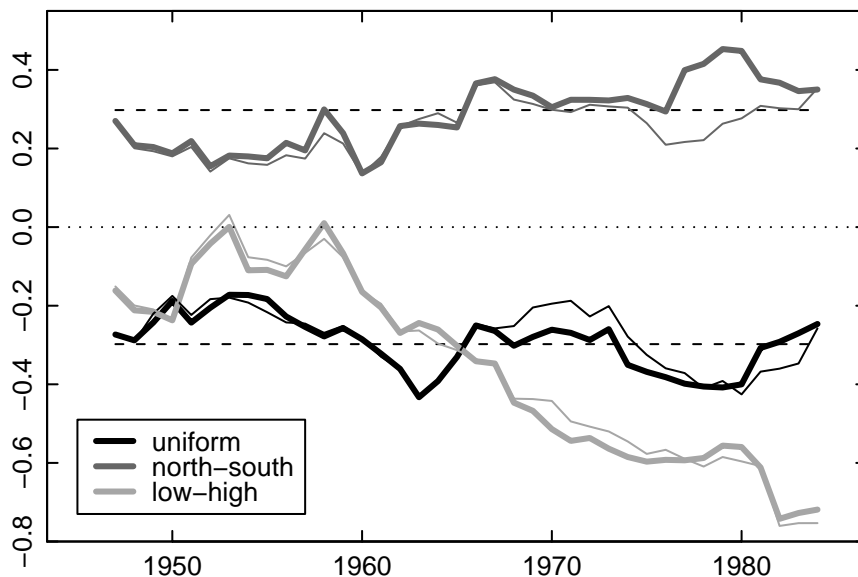
Figure 3.7: 31-year running window correlations between DJF NAO index and leading DJF Swiss new snow PCs for the period 1931–1999. Bold lines: linearly detrended 31-year windows, thin lines: original data. The uniform pattern series is shown in black; the north-south and low-high pattern series in dark grey and light grey respectively. The dashed lines represent the 95% significance levels. Note that the left panel ordinate is not centred on zero (dotted line) but runs from -0.8 to 0.5.

3.5.2   Relation between snow patterns and large-scale flow

Figure 3.8 shows grid point based correlation maps of the three leading DJF new snow sum PCs and the leading snow day PC with DJF sea level pressure variability. The *uniform* new snow sum PC (Figure 3.8a) is negatively correlated with sea level pressure over middle and south-eastern Europe (r_{min}~-0.65). Switzerland lies at the western boundary of the north-west south-eastward tilted monopole of enhanced correlation (r~-0.4). In the anomalous low (high) pressure case there is anomalous north-westerly (southerly) flow towards the Alps accompanied by large surpluses (deficiencies) of snow. The anomalous low pressure (i.e. positive new snow sum anomaly case) composite field reveals that the Alpine region is influenced by a strong westerly flow component (not shown). The associated circulation is stronger and the incident flow is from more northerly directions than the overall climatological flow which is west-south-west. Since a westerly component brings usually wetter conditions, it is consistent with the finding above that the uniform pattern is primarily determined by precipitation and only secondarily by temperature (cf. Table 3.3). The anomalous high pressure (i.e. negative new snow sum anomaly case) composite is characterised by high pressure directly over the Alpine region which is part of a ridge stretching from the Azores to Eastern Europe.

The correlation map for the *uniform* snow day PC (Figure 3.8b) also shows a correlation monopole over south-eastern Europe, but in contrast to the *uniform* new snow sum PC, the coefficients are somewhat lower (r_{min}~-0.55) and the expansion of high negative correlation to middle and north-western Europe is missing. The Alps now lie at the northern boundary of the region with significantly negative correlation (r~-0.3). The interpretation is therefore different. The low pressure anomaly over south-eastern Europe is linked with an additional easterly component towards the Alps. The anomalous low pressure (i.e. positive snow day anomaly case) composite shows that the westerlies are further in the north and that continental influences (cold air) are important in this phase. This is in agreement with Table 3.3, where the *uniform* snow day pattern is better correlated with temperature than with precipitation. The anomalous high pressure (i.e. negative snow day anomaly case) composite shows that the Alpine region is determined by high pressure similar to new snow sum case discussed above.

The correlation maps for the new snow sum and snow day *north-south* PC (Figures 3.8c and 3.8d) are characterised by a monopole of positive correlation (r_{max}~0.65 and 0.55) over the easternmost Atlantic and the British Islands, similar to the spatial pattern known as East Atlantic pattern in the literature (Barnston and Livezey, 1987; Pavan et al., 2000a). The positive phase with additional flow from northerly directions is linked with a weak surplus (strong deficiency) of new snow sums on the northern (southern) slopes of the Swiss Alps (cf. Figure 3.3). The composite field (not shown) shows a ridge of the Azores High reaching the Alps which is unfavourable for southern Alpine precipitation. The negative phase (additional south-westerly flow component) is characterised by new snow sum surpluses (deficiencies) on the southern (northern) slopes. The composite field shows south-westerly flow towards the southern Alpine slopes which is favourable for additional precipitation. These flow situations are in good agreement with the high correlation with local precipitation on the southern slopes found above (Table 3.3).

The new snow sum and snow day *low-high* PC correlation maps (Figures 3.8e and 3.8f) show a negative NAO like dipole pattern (cf. Figure 3.9a) with centres over the Norwegian Sea and north-western Africa.
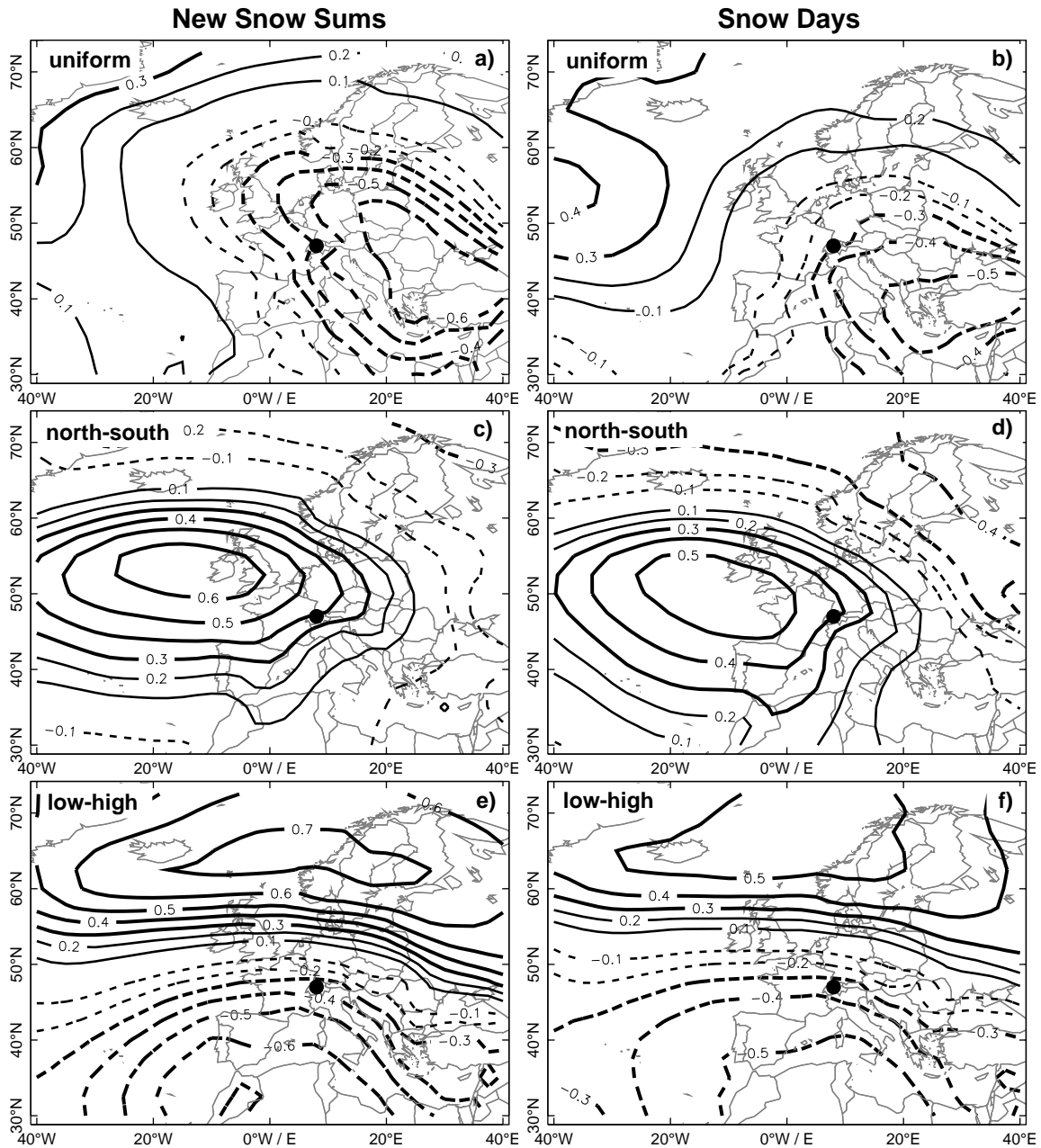

Figure 3.8: Correlation between DJF 1958–1999 sea level pressure and the uniform, north-south and low-high pattern of Swiss Alpine new snow sums (NSS: panels a, c, e) and snow days (SD: panel b, d, f). Contours for correlation values r ≥ |0.3| are shown in bold. Contour interval is 0.1. The zero contour is omitted. The black dot shows the approximate position of the Swiss Alpine region.

The additional westerly flow component in the years with negative (positive) pressure anomalies over northern (southern) Europe is linked with negative (positive) new snow sum anomalies at low (some high) lying stations north as well as south of the main ridge of the Alps. In the reversed case (reduced westerly flow) positive (negative) snow anomalies are found at low (some high) stations. The composite fields show that in the case with signs as in Figure 3.8e the Eurasian High is strong. The associated flat pressure distribution in central Europe and its flow from south-eastern Europe favours cold and dry conditions, in broad agreement with the correlation results in Table 3.3. In the opposite case there is a ridge spreading from south-western Europe to the Alps.

Analogous correlation maps are found for the second and third principal component pattern of snow height. Correlation maps based on geopotential height at the 500 hPa level show very similar results (not shown). The structures are smoother but the general interpretations remain the same and are not discussed further here.
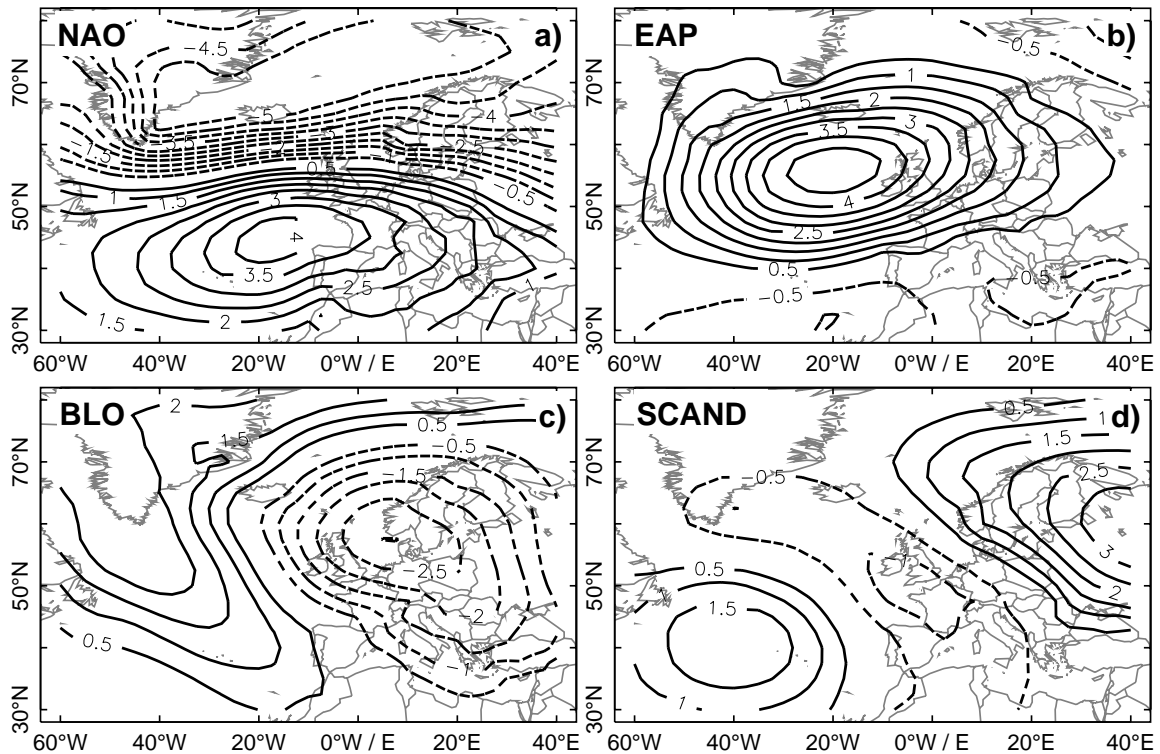
Figure 3.9: Spatial loadings of the four leading DJF sea level pressure principal components over the Euro-Atlantic region. a) North Atlantic oscillation (NAO), b) East Atlantic pattern (EAP), c) European blocking (BLO), d) Scandinavian pattern (SCAND). Shown are the sea level pressure anomalies in hPa associated with principal component amplitude of one standard deviation. Positive (negative) anomalies are given by solid (dashed) lines. Contour interval is 0.5 hPa.

3.5.3 Climatological sea level pressure pattern influences on Swiss Alpine snow pack

The linear correlation analysis is now extended using linear statistical model fits to determine the combination of large-scale sea level pressure patterns that have the largest impact on the Swiss Alpine snow pack components. A stepwise regression approach is used to avoid overfitting. For more methodological details the reader is referred to Junge and Stephenson (2003). Note that only PCA based sea level pressure patterns are used to fit Swiss Alpine snow pack components in this section.

Sea level pressure model predictors

The first 10 sea level pressure components explain about 98% of the DJF seasonal mean sea level pressure variance in the period 1958–1999. The four leading patterns (Figure 3.9) show ample similarities with circulation patterns in the literature (Barnston and Livezey, 1987; Pavan et al., 2000a; Scherrer et al., 2006b). The first PC (Figure 3.9a, NAO subsequently) turns out to be virtually identical with a station based NAO index as defined by Hurrell (1995). The spatial and temporal components of the second component (Figure 3.9b) are closest to the East Atlantic pattern (EAP hereafter). The third component (Figure 3.9c) is similar to the East Atlantic/Western Russia or Euro-Atlantic blocking pattern (BLO below). The fourth pattern (Figure 3.9d) is close to the Eurasian type-1 pattern also called Scandinavian pattern (SCAND below).

Statistical model fits

Figure 3.10 summarizes the results of the stepwise optimized linear model fits for the leading three new snow sum patterns together with some diagnostics. The models explain a large amount of the total principal component variance (*uniform* pattern: 67%, *north-south* pattern: 63%, *low-high* pattern: 73%, *uniform* snow days pattern: 59%). The fitted values vs. residual plots show that the difference between observations and modelled values are mostly within ±1 standardized anomalies and never greater than 1.5 or smaller than -2. The quantile-quantile plots show that the assumption of normally distributed residuals is very well satisfied for the new snow sum *low-high* pattern. There are some larger but still not dramatic deviations from the line with slope 1 for the *uniform* and *north-south* patterns. The model performance is worst for extreme years. In general, the diagnostic results confirm that the models do not violate the general assumptions of linear model theory.

   Table 3.4 lists the variance explained by individual sea level pressure components. BLO explains 44% of the *uniform* new snow sum variance. This result is not surprising when recalling the correlation map between the *uniform* new snow sum pattern and the sea level pressure field, which bears some similarity to the spatial pattern of BLO (cf. Figures 3.8a and 3.9c). A similar leading sea level pressure pattern has been identified for the first coupled pattern with European and Alpine precipitation (Widmann, 1996; Qian et al., 2000). With exception of PC5 (16%), all other components (including the NAO) play a minor role in explaining the *uniform* new snow sum pattern (e.g. EAP: 0%). The *north-south* pattern is mainly determined by EAP (34%), PC8 (12%) and to a rather small degree by the NAO (6%). Also in this case shows the correlation pattern large similarities with EAP (cf. Figures 3.8c and 3.9b). The *low-high* snow pattern is explained best by the NAO (31%) but also

EAP (24%) and SCAND (10%) explain larger amounts of the variance. This result is also plausible when comparing with the correlation pattern in Figure 3.8d.

Analogous models for snow height show that the same sea level pressure patterns are most important albeit with a smaller amount of total variance explained (not shown). As mentioned above, the leading snow day pattern seems to be more influenced by temperature than new snow sums. This is also mirrored in the sea level pressure model for the uniform snow day pattern. The BLO influence is still the most important (19% variance explained), but EAP (which explains 41% of the leading temperature component) is the second most important pattern explaining 14% of variance. There are several other components explaining between 4 and 8% of snow day *uniform* pattern variance.
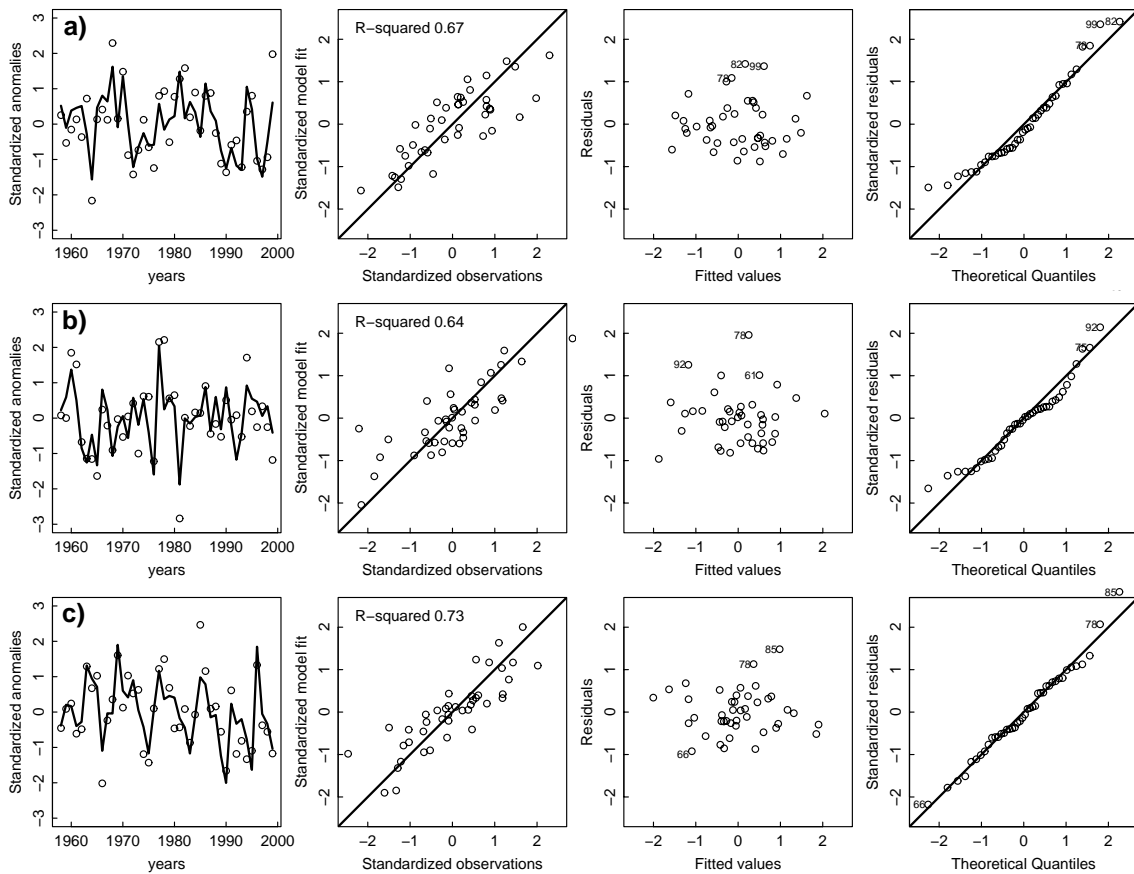
Figure 3.10: Model diagnostics for modelled standardized new snow sum principal components (PCs) using an optimal sea level pressure PC model. See text for details. a) uniform pattern, b) north-south pattern and c) low-high pattern. Sea level pressure PCs included in the models are shaded in Table 3.4. First column panels: Observed (points) and modelled values (line), second column panels: observed vs. modelled values, third column panels: fitted vs. residuals, fourth column panels: theoretical quantiles vs. standardized residuals.

Table 3.4: Variance explained (%) by sea level pressure (SLP) principal component (PC) models for the three leading new snow sum components and the leading (uniform) snow day (SD) component. PCs retained in the stepwise optimized model are greyed out. PCs explaining more than 30% of interannual variance are shown in bold. Total variance explained by the model is shown at the bottom. Numbers in parentheses are for the full model, regular numbers for the stepwise optimized model.

SLP PC	NSS			SD
	uniform	north-south	low-high	uniform
NAO	1.7	6.0	**30.6**	2.8
EAP	0.0	**34.3**	23.6	14.4
BLO	**43.5**	0.2	3.6	**18.8**
SCAND	0.3	4.5	10.1	4.0
5	16.3	0.2	0.4	7.9
6	5.5	0.2	0.0	4.3
7	0.0	0.5	1.6	0.0
8	1.3	11.7	3.4	6.2
9	0.0	4.9	0.0	1.2
10	0.5	2.1	0.0	0.5
total	67.0(69.1)	63.5(64.6)	72.9(73.3)	58.5(60.2)

3.6 Discussion and conclusions

In this study quality checked Swiss Alpine snow data are used to explore the major patterns of observed snow variability. The link between seasonal mean winter (DJF) snow variability and local temperature and precipitation variability as well as large-scale flow patterns is explored for new snow sums, average snow heights and snow days. For new snow sums and snow height three well separated patterns of variability are identified using principal component analysis. The first pattern explains more than 50% of total variance and the spatial pattern is almost *uniform* over the entire Swiss area. This indicates that interannual snow variability in Switzerland shows comparatively small geographical variations. The second pattern (explaining ~15% of total variance) shows a *north-south* dipole with positive (negative) loadings on the northern (southern) slopes of the Alps. The third (*low-high*) pattern (explaining ~8% of total variance) shows positive loadings at low altitude stations and negative loadings at high stations. It also has a weak decreasing trend. Such a pattern has not been found in winter precipitation data (Schmidli et al., 2002). It is well correlated with the NAO over recent decades (also detrended), has a similar high autocorrelation, is the only component that shows a linear trend in time, and is well correlated with the major pattern of temperature variability. For seasonal snow days, the three patterns are similar, but the rank of the *north-south* and the *low-high* pattern are switched and the second and third pattern are not well separated.

   Table 3.5 summarizes the main local and large-scale influences on the leading patterns of Swiss Alpine new snow sums, snow heights and snow days. Swiss Alpine temperature and precipitation are highly correlated with the snow pack patterns. However, the correlation depends on the snow variable considered. Although seasonal new snow sums are determined by conditions that are only characteristic for a small part of a season, they correlate better with local climate elements than snow height and snow days. Positive *uniform* new snow

sum anomalies are primarily related to positive seasonal precipitation anomalies. Positive *uniform* snow day sum anomalies on the other hand are primarily correlated with seasonal temperature and only weakly related to precipitation. This change from precipitation dominance for new snow sums to temperature dominance for snow days can be explained by the different character of the variables. Large *uniform* pattern new snow sum anomalies are only influenced by processes during snow accumulation (i.e. during snow fall events). Evidently these can be described well by seasonal *precipitation* sums. Large *uniform* pattern snow day anomalies are influenced by processes that control snow accumulation and ablation. It is well known that the melt process is almost linearly related to seasonal temperature (Ohmura, 2001; Hock, 2003). Here it was found that also the combined influence can be well described in a linear sense by seasonal *temperature*. The *north-south* snow pattern which explains most of snow variance in southern Switzerland correlates excellently with the *north-south* precipitation pattern. The *low-high* snow pattern correlates well with the *uniform* temperature pattern.

Table 3.5: Summary of the primary influences of local (temperature and precipitation) and large-scale (sea surface pressure) variability on the three leading patterns of Swiss Alpine new snow sums (NSS), snow height (SH) and snow days (SD). The numbers show the approximate mean fractions of total variance explained. Precip: precipitation, temp: temperature. BLO: Blocking pattern, EAP: Eastern Atlantic pattern, NAO: North Atlantic Oscillation.

snow pattern	local (temperature and precipitation)			large-scale (pressure patterns)
	NSS	SH	SD	NSS/SH/SD
uniform (~50%)	**precip**	**precip and temp**	**temp**	BLO
north-south (~15%)	precip	precip	precip	EAP
low-high (~9%)	temp	temp	temp	NAO

The influence of the large-scale flow is determined using descriptive techniques and statistical modelling. Results show that large-scale circulation pattern models can explain large amounts of local Swiss Alpine snow variance. The leading (*uniform*) snow patterns are primarily determined by a low (high) pressure anomaly pattern centred over the central and south-eastern Europe. It bears some resemblance to the third pattern of European sea level pressure variability (BLO) often referred to as Euro-Atlantic blocking (D'Andrea et al., 1998; Scherrer et al., 2006b). Similarities also exist with the midlatitude anomaly train pattern described in (Massacand and Davies, 2001a), the sea level patterns associated with the leading Swiss Alpine winter precipitation variability (Widmann, 1996), the leading European winter precipitation variability pattern (Qian et al., 2000), the second canonical pattern in extreme winter wet days (Haylock and Goodess, 2004) and the pattern connected to the second EOF of European and northern African winter precipitation (Rodriguez-Fonseca et al., 2006).

For snow days also the pattern explaining most of the leading temperature component, the East Atlantic pattern, explains a substantial amount of the *uniform* pattern variance. The second (*north-south*) snow pattern is mainly influenced by the East Atlantic anomaly

pattern. Only the third (*low-high*) snow pattern, which explains substantial amounts of interannual snow variance at low lying stations, is primarily linked with the interannual variability of the NAO and secondarily with the East Atlantic pattern.

Finally note the following points. First, our analysis is restricted to winter (DJF) condition and snow variability in autumn and spring remains to be explored. Second, our analysis is restricted to seasonally summed or averaged quantities. Sub-seasonal information, such as averaged climate conditions during snow fall events, has not been taken into account and remains to be explored. Third, in a first step only sea level pressure fields were used as large scale influence to explain local snow variance. Other influences like the large scale temperature fields as used e.g. in Widmann (1996) could possibly improve the model results. Finally, the different importance of precipitation and temperature for accumulation snow variables (new snow sums) and variables determined by accumulation and ablation (snow heights and snow days) could have implications for estimates of Swiss Alpine snow in global warming scenarios. Depending on the changes in precipitation and temperature it is conceivable that snow variables related to accumulation processes only (e.g. heavy snow events and avalanches) react differently than those related to the whole snow life cycle (e.g. snow days).

Chapter 4

Two dimensional indices of atmospheric blocking and their statistical relationship with winter climate patterns in the Euro-Atlantic region

Simon C. Scherrer[1], Mischa Croci-Maspoli[2], Cornelia Schwierz[2] and Christof Appenzeller[1]

[1] Climate Services, Federal Office of Meteorology and Climatology (MeteoSwiss), Zürich, Switzerland
[2] Institute for Atmospheric and Climate Science, ETH Zürich, Zürich, Switzerland

Abstract

The statistical relationship between the leading climate patterns of mid-tropospheric flow and atmospheric blocking over the Euro-Atlantic region during winter is investigated using three new two-dimensional blocking indicators. A focus is on the leading climate pattern of the 500 hPa geopotential variability, i.e. the North Atlantic Oscillation (NAO). The results indicate that the blocking-NAO relation is not restricted to the North Atlantic region where blocking and the NAO are known to be out of phase. All three indicators show that the positive NAO phase is characterised by an enhanced occurrence of blocking-type high-pressure systems over the European mainland. The sign change of the NAO–blocking relation from west to east is well detectable with the two-dimensional blocking indicators and found further south than at the traditionally studied blocking latitudes near 60°N. The analysis of blocking events by seasonal NAO indices leads to similar (albeit less significant) results as with a daily NAO index stratification. This indicates that the relation between the NAO and blocking is quite insensitive to the chosen time resolution.

The investigation is extended to the second to fourth pattern of mid-tropospheric flow variability using empirical orthogonal function (EOF) patterns. It reveals that one phase of each of the major Euro-Atlantic climate patterns is collocated with the region of maximum blocking frequency. The clearest separation between positive (negative) EOF phases and blocking (no-blocking) situations is found for EOF 2 and 3 and is associated with changes from zonal to ridge-like flow, similar to the so-called Northern European blocking signature. This is an indication that the purely statistically defined EOF patterns are related to the physical blocking phenomenon.

4.1 Introduction

From a climatological perspective, the North Atlantic Oscillation (NAO) is the statistical pattern explaining most of the European winter lower to mid-tropospheric flow variability on a wide range of time scales from months to decades (van Loon and Rogers, 1978; Barnston and Livezey, 1987; Hurrell, 1995; Appenzeller et al., 1998b; Stephenson et al., 2000; Marshall et al., 2001). From a synoptic perspective, persistent high-pressure systems are of prime interest for understanding European weather impacts on weekly time scales (Rex, 1950; Lejenäs and Økland, 1983; Tibaldi and Molteni, 1990; Tibaldi et al., 1994; Trigo et al., 2004). Several concepts about the dynamics of blocking exist, including blocking as a result of bifurcation of the zonal flow (Charney and Devore, 1979), modons (McWilliams, 1980; Verkley, 1990), planetary wave interaction (Hansen and Sutera, 1984; Lindzen, 1986; Lejenäs and Döös, 1987) possibly interacting with orographic forcing and nonlinear wave-mean flow interaction (Egger, 1978; Da Silva and Lindzen, 1993), multiple equilibria and resonance (Charney and Devore, 1979) or interaction between synoptic and planetary-scale processes (Lupo and Smith, 1995).

Similarly, different views exist concerning the nature of the NAO, especially about the dynamics behind its inherent time scales. Some argue that the NAO can be interpreted as a stochastic process with a relatively short time scale originating from synoptic-scale waves (Feldstein, 2000; Benedict et al., 2004). Other studies point to an influence of the Atlantic Ocean and hence much longer intrinsic time scales (Rodwell et al., 1999; Latif et al., 2000a; Czaja and Frankignoul, 2002; Sutton and Hodson, 2003). Considering the limited understanding of both, the time scale and dynamics of the processes, it is not astonishing that the relation between the NAO as a "climate mode" and the synoptic-scale blocking phenomenon is an issue not yet satisfactorily understood.

In several statistical analyses a significant anti-correlation between the NAO index and blocking events for the North-Atlantic region has been found (e.g. Pavan et al., 2000b; Stein, 2000; Shabbar et al., 2001). For Central Europe however, blocking-like persistent high-pressure systems do also exist and have an ample influence on local weather and even seasonal winter climate (Beniston et al., 1994). There are some indications that persistent high-pressure systems over central Europe are related to the positive NAO phase (Wanner et al., 2001).

Doblas-Reyes et al. (2002) classify blocking detection methods into objective and subjective procedures. Objective methods use statistical methods to classify the circulation patterns (e.g. Vautard, 1990). However, most common blocking indicators are subjective in the sense that they are based upon synoptic-scale experience and a set of calibration parameters. A majority of these subjective measures make use of the geopotential height field at 500 hPa (Z500). The methods can further be subdivided into indices that are based on meridional height gradients (e.g. Lejenäs and Økland, 1983; Tibaldi and Molteni, 1990; Corti et al., 1997; D'Andrea et al., 1998; Pavan and Doblas-Reyes, 2000) and those that detect geopotential height anomaly maxima (e.g. Dole and Gordon, 1983; Shukla and Mo, 1983; Liu, 1994; Sausen et al., 1995). The indicators of the first group essentially identify positive absolute geopotential elevations on an atmospheric level centred around a few chosen latitudes, e.g. 60°N. Pelly and Hoskins (2003) proposed an index where the latitude of detection varies zonally, in accordance with the changing latitude of the storm track. In the second group consideration of the anomaly field allows the definition of two-dimensional (2D) blocking index fields.

In this study we use a new 2D-extension of the TM90 blocking index and two recently introduced dynamical blocking indicators based upon vertically averaged potential vorticity (Schwierz et al., 2004). A robust statistical relationship between opposed NAO phases and atmospheric blocking is sought by quantifying and discussing the linkage of the two phenomena for the Euro-Atlantic region from a daily and seasonal perspective using the three 2D indicator fields. The season of interest is winter. In a second step the study is extended to the relation between higher-order Euro-Atlantic patterns of variability and blocking occurrence.

The structure of the paper is as follows: The data source, definition of blocking indices and statistical methodology are described in Section 4.2. The basic properties of the three different blocking indicators, their similarities and differences and also their relation to existing indices are discussed and their climatological blocking frequencies presented in Section 4.3. In Section 4.4 the statistical relation between the NAO and Euro-Atlantic blocking is addressed from a daily and seasonal perspective. The stratification of blocking in Central Western Europe with respect to the phase of the NAO is also investigated. The analysis is then extended to the next three higher-order climate patterns in Section 4.5. Finally some conclusions are drawn in Section 4.6.

4.2 Data and methodology

4.2.1 Data

The atmospheric data used in this study is based on the European Centre for Medium-Range Weather Forecasts (ECMWF) European reanalysis (ERA–40) dataset for 45 winter seasons, i.e. December-January-February (DJF), in the period from 1958 to 2002. The ERA–40 data set has a spectral resolution of T159 (~120 km) in the horizontal and 60 levels in the vertical (Uppala et al., 2006). The region considered is the North Atlantic and European area excluding the northern polar region [80°W–60°E, 30°N–80°N]. The height field at 500 hPa (Z500) is interpolated onto a 2.5° x 2.5° grid with a daily time resolution to construct the absolute geopotential blocking index. The same procedure is applied for the empirical orthogonal function (EOF) analysis of the geopotential field. The potential vorticity (PV) indices used in this study are based on the three-dimensional PV field, using Ertel's (1942) potential vorticity definition, with a 1° x 1° horizontal resolution and 60 vertical levels at six-hourly time steps.

4.2.2 Blocking indices

Three different atmospheric blocking indicators are considered and compared in this study. The first index is called absolute geopotential height (AGP) index hereinafter. It is an extension of the TM90 blocking index to a two dimensional map of blocking frequencies at every grid point. The following modifications are applied to the original index: The geopotential height gradients are computed not only for three central latitudes (ϕ_0=60°N+Δ, where Δ=-4°, 0° or 4° in TM90), but all grid latitudes between 35°N and 75°N (2.5 degree steps) are used as central latitude ϕ_0. Δ is fixed to one value only (0°). The difference between the central latitude ϕ_0 and the northern ϕ_N and southern latitudes ϕ_S for which the

linear gradient is computed is taken to be 15° each (instead of 20° in TM90). With this change of 5° it is possible to compute blocking frequencies up to 75°N. Sensitivity analyses show that the differences between indices based on $|\phi_0\text{-}\phi_{N/S}| = 15°$ or 20° are small in our context. The geopotential height gradient thresholds of 0 and -10 m per degree latitude remain unchanged to TM90 since the results are quite stable with respect to small changes in these thresholds (not shown). A 5-day persistence criterion is applied at every single grid point, i.e. a grid point is only considered blocked when the above gradient criterion is fulfilled for 5 or more consecutive days. There are no exceptions allowed to this rule as in some previous studies (D'Andrea et al., 1998; Doblas-Reyes et al., 2002). As a consequence blocking frequencies are lower since only blockings are captured that are stationary in space and uninterrupted in time. These characteristics typically correspond to a mature blocking state. The output is a daily binary 2D map of grid points with persistent quasi-stationary high pressure ("blocked") and other grid points which are classified as non-blocked.

Two dynamical blocking indicators based on vertically averaged potential vorticity between 500 and 150 hPa (VAPV) are used to capture the three-dimensional structure of the deep upper-tropospheric dynamical core of the blocking phenomenon. The definition of the PV indicators will briefly be discussed here. For more details the reader is referred to Schwierz et al. (2004). The first blocking indicator (APV) is based upon closed contours of the absolute VAPV field. Temporal and spatial quasi-stationarity is ensured respectively by application of a 5-days persistence criterion and a fractional area-overlap criterion at every time step, to allow for moderate movement of the blocking pattern. As with AGP, binary 2D APV blocking index maps are computed for every time step. It is important to note that APV blocking represents rare events that are persistent, large-scale and often characterised by – on an isentrope – sequestered upper-tropospheric air masses within the stratosphere. Likewise, persistent, closed contours of the VAPV-anomaly field relative to the corresponding daily climatological 30-day running mean value result in the binary 2D APV^* blocking index field.

Note that the blocked regions for the APV and APV^* indices are allowed to move as long as there is a large enough overlap between consecutive time steps, whereas stationarity in space is more rigorous for the AGP index where temporal persistence is required at every grid point. Additionally, the APV^* index is the only field which is based upon an anomaly field.

For all three indices, the blocking frequency is defined as the percentage of the number of blocked days at a given grid point compared to a total number of days considered. For the winter climatologies (Section 4.3.2) the total number of days is the number of days in the season, i.e.1% blocking frequency corresponds roughly to one blocked day per season. For the composite frequencies (Sections 4.4 and 4.5) the total number of days is the number of days in the corresponding tercile (e.g. days for which the daily NAO index is in the positive tercile).

4.2.3 Statistical methodology

To define climate pattern indices for the Euro-Atlantic region first a standard EOF analysis on the DJF Z500 seasonal anomaly is computed (Wilks, 1995). The anomalous Z500 fields are cosine-latitude weighted before application of the EOF analysis. No detrending and no standardisation are applied to the data before the EOF computation. Similar to Thompson

and Wallace (2000) daily (seasonal) indices of the leading climate patterns are determined by a regression of daily (seasonal) Z500 fields onto the first four EOFs of the seasonal mean Z500 fields. In analogy to the terminology of the US Climate Prediction Center (CPC) we call the daily and seasonal indices of the first pattern daily NAO index and seasonal NAO index in this paper. The EOF analysis was repeated with monthly instead of seasonal Z500 data. The first four patterns considered were very similar to the seasonal patterns and are therefore not studied further here.

The daily climate pattern indices created above are grouped into terciles (low, neutral, upper) to composite geographical maps of blocking frequencies for the opposed phases of the climate patterns. A grouping into three categories using the standard deviation σ ($\sigma < -1$, $-1 < \sigma < 1$, $\sigma > 1$) has also been tested but the results are very similar to the tercile categorisation and therefore not further discussed.

A Monte Carlo approach is used to determine whether the corresponding tercile blocking frequencies are significantly linked to the major EOF patterns. Our null hypothesis is that the binary blocking series and the principal component (PC) tercile time series are independent. To test this, 1000 surrogate PC tercile series are generated that mimic the original PC series. For simplicity a red noise (AR1) process is chosen to create these artificial "out of phase" series. Then the mean blocking frequency for each of the 1000 surrogate series is determined at every grid point, resulting in 1000 surrogate mean blocking frequencies. The grid points where the observed blocking frequencies are in the most extreme 1% (for the daily analysis) or 5% (for the seasonal analysis, and for APV) of the surrogate blocking frequency probability density function are identified as significantly linked. This procedure is applied for the upper and lower terciles of the NAO (i.e. the first EOF) in Section 4.4 for both, the daily and seasonal stratification, and for the tercile stratifications of EOF2–4 in Section 4.5. A comparison of the significant regions from the Monte Carlo method introduced above with the significant regions found by a simple binomial test which did crudely account for autocorrelation via a variance inflation factor (Wilks, 1995) shows good agreement.

4.3 Intercomparison of the blocking indices

4.3.1 Two case examples

A description of the behaviour and specific properties of the three blocking indices AGP, APV and APV^* will help to interpret the results of the climatological analysis below. To illustrate their basic characteristics, two selected blocking cases are discussed here. A Northern Atlantic blocking case snapshot is shown in Figure 4.1a (18 January 1963, 12UTC) where all three indicators coincide in location and scale and are co-located also with a pronounced Z500 cut-off high. The flow structure is typical of a mature block. The region of high pressure is straddled by lows to the south and to the east. This situation has developed from an Ω-configuration of which the western low and the high pressure have slightly rotated around each other to form the N-S vortex dipole visible in Figure 4.1. Figure 4.1b shows another case (12 December 1974, 12UTC) with an open, but persistent ridge structure. Although all indices detect blocking for this case, the identified regions show differences. The AGP index is able to catch the Z500 ridge well, but has a tendency to detect predominantly the centre of the blocked area and therefore underestimates the blocked region considerably – an effect of

the grid-point-based stationarity criterion. Note in passing, that AGP and APV also detect blocking over Russia at the eastern most part of the domain. Over the North Atlantic, the other absolute-field measure, APV, is co-located reasonably well with both the AGP field and the Z500 ridge, however detecting a larger area. The fact that the APV criterion shows a response for this blocking situation indicates the existence of a coherent, deep 3D upper-tropospheric PV signature associated with a cut-off-like elevation of the tropopause (not shown). Both the AGP and APV blocked regions are located further south towards the Azores-high than the APV^* blocked regions.

This shift is plausible since an index based on any full (absolute) field (here AGP and APV) differs fundamentally from using an anomaly measure (APV^*) which is likely to produce anomalies near regions of large gradients in the underlying climatological field (here VAPV). Consistently, the APV^* pattern is typically located further north-west than AGP/APV blockings in the North-Atlantic region. Similar results have been described for the SKS95 index, which is also based on an anomaly field and detects blocking maxima over the West Atlantic. The APV^* index highlights an area within the jet region (cf. Figure 4.1b), indicating the position of anomalously low upper-level PV (the PV gradient is reduced, i.e. the jet is weaker here than in the climatological mean). Using the invertibility principle (Ertel, 1942; Hoskins et al., 1985) this PV anomaly can be thought of as the dynamical core of the block and responsible for the associated anomalous anticyclonic circulation. Information on the origin and temporal evolution of the index regions can be gleaned from a succession of plots (not shown). They indicate that the APV^* measure is often activated already in the early stages of block development, in the westerly parts of the jet region, whereas blockings detected by APV and in particular AGP are likely to occur mainly during the mature stage of the block.

These case study examples illustrate the fact that results of automated blocking detection can differ with respect to the applied index definition and base field. However, the cases have also served to emphasize the indicators' consistency in determining blocked flow situations. For a more rigorous intercomparison, it is therefore useful to recognize their similarities and differences. Statistical relations that are found between a field under consideration and several independent blocking indicators can thus be interpreted as a robust result for the linkage.
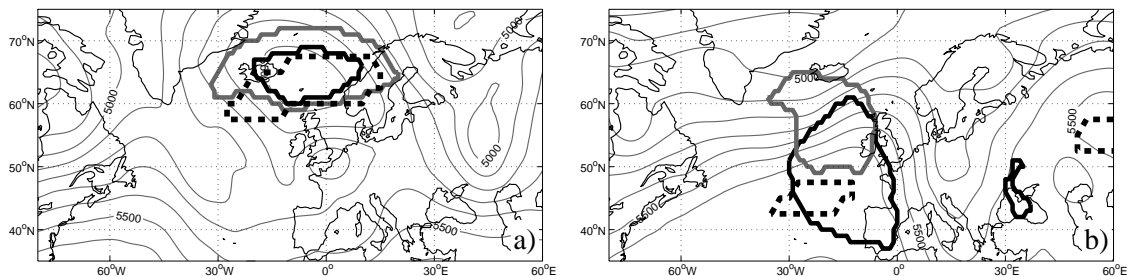

Figure 4.1: Geopotential height at 500hPa for a) January 18 1963, 12 UTC and b) December 12 1974, 12 UTC. Blocked regions are indicated for the AGP (dashed), APV* (grey) and APV index (black). Geopotential contour interval is 100 geopotential meters.
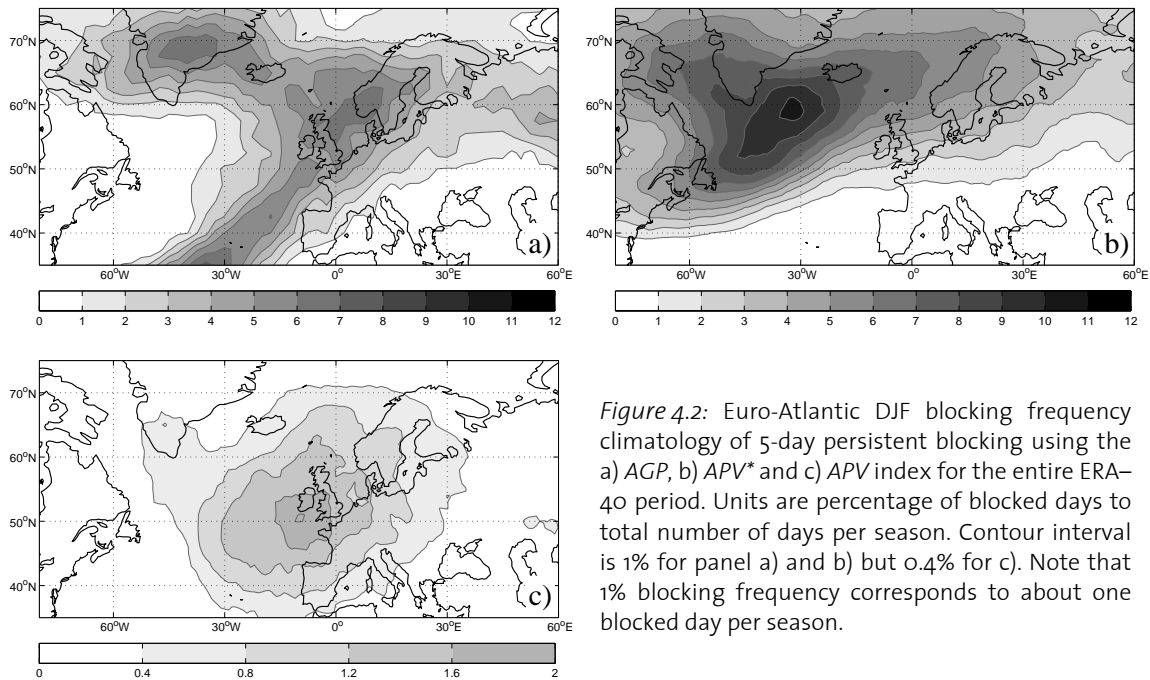
Figure 4.2: Euro-Atlantic DJF blocking frequency climatology of 5-day persistent blocking using the a) *AGP*, b) *APV** and c) *APV* index for the entire ERA–40 period. Units are percentage of blocked days to total number of days per season. Contour interval is 1% for panel a) and b) but 0.4% for c). Note that 1% blocking frequency corresponds to about one blocked day per season.

4.3.2 Euro-Atlantic winter blocking climatologies

The climatological winter blocking frequencies as detected by the three different indices are displayed in Figure 4.2. All three indices indicate the occurrence of blocking in the North Atlantic-European region during the cold season. The details of the geographical distribution depend to a large degree on the definition and selection criteria that pertain to each of the indices, as explained in Section 4.3.1.

Figure 4.2a shows a blocking frequency map based on the *AGP* index. It depicts two overlapping branches of amplified blocking frequency forming a "T-bone"-shape structure. One branch is stretching west to east from Davis Strait/Labrador Sea to Southern Scandinavia; the other extends south-west to north-east from the Azores to meet the first branch in Southern Scandinavia. Local maxima are found over Southern Greenland, over the North Sea and over the Azores, indicating three centres of enhanced blocking with highest frequencies of about 6%.

Figure 4.2b depicts the climatology for the *APV** anomaly-based blocking index with one broad maximum (frequency ~10%) centred near 30°W/60°N. Two short arms are stretching from the maximum in north-westerly (Davis Strait) and south-westerly (Newfoundland) direction and a longer extension is present in east-north-easterly direction towards Scandinavia. The overall shape is not unlike the "T-bone" found with the *AGP*, albeit with its leg somewhat shifted to the west.

The pattern of the (absolute) *APV* blocking frequency is, as the other absolute *AGP* pattern, located further east than the *APV** field (Figure 4.2c). Its almost circular structure exhibits highest frequencies southwest of the British Isles. A region of slightly increased frequency is directed from the centre towards Southern Greenland. Note that the maximum

frequencies amount to less than 2 blocked days per season compared to ~7 blocked days for AGP and ~10 blocked days for APV^*. The rareness of APV events has ramifications for the interpretation of the patterns and for the application of significance tests in Sections 4.4 and 4.5.

Concomitant inspection of Figures 4.2a, b and c again sheds light on the characteristics of the indices and are in line with our case study-based remarks in Section 4.3.1. *(i)* It is conceivable that the overall smaller blocking frequencies of AGP (compared to APV^*) are due to its grid-point-based spatial stationarity constraint that results also in smaller areas detected as blocked. *(ii)* The similar but in comparison to the AGP-field westward-shifted shape of the anomaly APV^* blocking index is related to the SW-NE oriented band of enhanced PV gradient (jet stream) in the climatological VAPV field. *(iii)* Another marked difference of the AGP index with respect to APV and APV^* is found near the Azores. The AGP index as an absolute measure detects phases of strong Azores highs that would not feature synoptically as a classic blocking phenomenon. Aspects *(ii)* and *(iii)* are possibly related since a strong Azores high detected by the AGP index is associated also with a northward shift of the band of large PV-gradient that can lead to an increase in APV^* blocks. A dynamical cause of such a shift by low-frequency (20 day period) westward travelling waves has been suggested by Doblas-Reyes et al. (2001) but will not be further investigated here.

Several similarities are found with blocking climatologies given in the literature. First we compare the 2D AGP distribution with Z500 composites resulting from the classical TM90 index. The AGP maximum at 60°N over the North Sea is close to the centre of the "blocking signature" (defined as the composite difference field of all blocked days to all non-blocked days) of TM90-classified Euro-Atlantic blockings and coincides with the frequency maximum at ~10°E (cf. Tibaldi et al., 1997; D'Andrea et al., 1998). However, the AGP blocking frequency values are much lower in comparison to TM90. The original TM90 index requires spatial persistence for one out of three base latitudes and no temporal persistence which results in maxima in blocking frequencies of ~20–30% for winter seasons (Tibaldi and Molteni, 1990; Corti et al., 1997). With an additional 5-day persistence criterion (e.g. Doblas-Reyes et al., 2002), the frequencies are lower by approximately a factor of two. The AGP frequencies are still somewhat smaller. This is a direct consequence of the strict spatio-temporal stationarity constraints for AGP introduced by the extension to 2D together with the strong persistence criterion which does not accept any interruptions of the 5-day interval.

Shabbar et al. (2001) find a similar maximum, but also one further west over Canada, which may correspond to the AGP maximum over Southern Greenland. Other studies based on Z500 find similar preferred blocking regions in the Northern Atlantic and Greenland (Liu, 1994; Lupo and Smith, 1995). The 1D-measure based on the absolute PV-θ field by Pelly and Hoskins (2003) shows a maximum between 10°W and 35°E, in agreement with AGP, but with much higher amplitudes of up to 30%. The location also compares quite well with that of APV at 60°N.

Anomaly-based 2D measures, such as those derived in Dole and Gordon (1983) and SKS95 reveal large similarities with the APV^* pattern. The SKS95 blocking frequency maximum is located between Greenland and Iceland with ~6–8% and thus slightly lower than the APV^* frequency. For APV^*, the occurrence of blocking is more seldom (~4–5%)

and the entire distribution is located much more northerly and westerly than in the AGP and APV index blocking regions. Similar differences between anomaly based indices and indices using absolute geopotential values is also found when comparing the SKS95 with the TM90 index (Doblas-Reyes et al., 2002). These climatological results show that there are many similarities between the three blocking indicators that also compare well with existing climatologies. Nevertheless there are some clear differences between the blocking climatologies by virtue of the index definitions, methodologies and base fields (cf. Section 4.3.1).

4.4 NAO-Blocking relation

A stratification of the blocking distribution for different NAO index phases sheds light on the relation between the NAO and blocking episodes. The NAO is defined as the first EOF of the anomalous Z500 field, as described above.
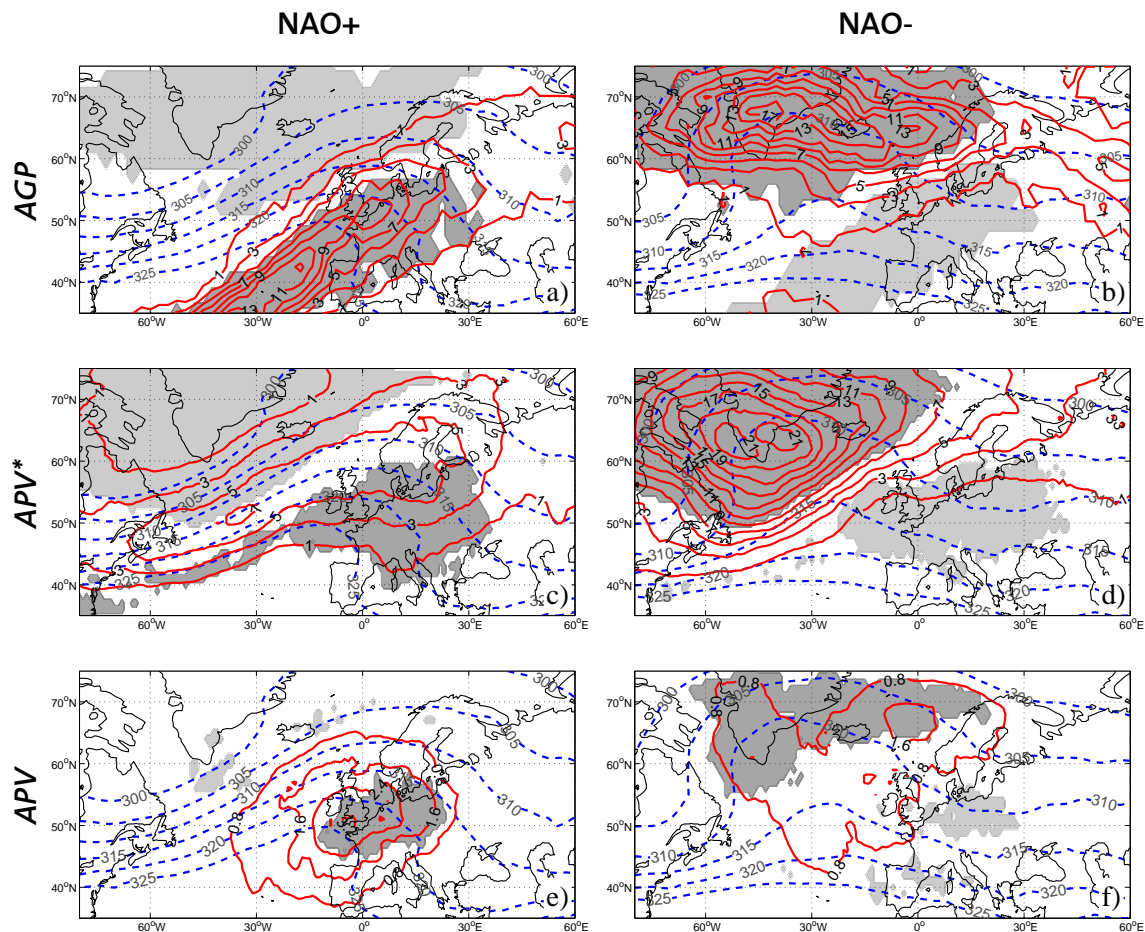
Figure 4.3: DJF blocking frequency composite maps for daily NAO+ (left panels) and NAO- (right panels) terciles (solid contours) for a, b) *AGP*, c, d) *APV** and e, f) *APV*. Blocking frequency contour interval is 2% for *AGP* and *APV** but 0.8% for *APV*. Regions of significantly higher (lower) blocking frequencies are shaded dark (light) grey. Significance level applied is 99%. Dashed contours indicate PV = 2 PV units on different isentropic surfaces from 300 to 325K in steps of 5K (1 PV unit = 10^{-6} m^{-2} s^{-1} K kg^{-1}).

4.4.1   Blocking relation to daily NAO index

General overview

In a first step the blocking climatologies are subdivided using daily NAO index (NAOI) values in the lowest (NAO-, i.e. NAOI < -0.37), medium (not shown) and highest (NAO+, i.e. NAOI > 0.51) tercile. The resulting NAO-blocking composite frequencies (red contours) with significance regions (grey shading) are depicted in Figure 4.3. Recall that blocking frequencies here means the percentage of blocked days when the index is in the corresponding tercile. In addition, the corresponding averaged structure of the dynamical tropopause is shown (blue contours). The tropopause potential temperature composites exhibit the archetypal upper-level flow structure for the respective NAO regime and its related jet position.

For both, blocking frequency and statistical significance, the daily NAO stratification of the AGP and APV^* blocking fields yield a clear distinction between the NAO phases (Figures 4.3a-d). The negative phase (NAO-) is characterised by a broad blocking frequency maximum over Southern Greenland and the western North Atlantic Ocean for both indices (maximum frequencies AGP ~17% and APV^* ~21%). These blocking areas are almost entirely significantly related to the NAO- phase and are co-located with the north-western part of the large-scale NW-SE oriented potential temperature ridge over the North-Atlantic. In the positive phase (NAO+) on the other hand, both indices detect blocking along a narrow SW-NE orientated band. For the AGP index this band lies within the weak potential temperature ridge and also extends into large parts of Western and Central Europe (~5–11% blocking frequency). For APV^*, the banded frequency pattern is positioned slightly more northerly, co-aligned with the strong potential temperature gradient and also extends further downstream of the upper-level jet (blocking frequency maximum ~7%). Interestingly, both NAO+ frequency patterns share a common significant blocking region in the NE-tilted ridge over Central and Western Europe. Note also that AGP and APV^* blocks both are absent over this area during the NAO- phase. Similarly, significantly reduced frequencies (< 1%) are found over the Northern and Western Atlantic region during the NAO+ phase.

Pronounced differences between the two indices are found over the Atlantic Ocean around the Azores and parts of the Iberian Peninsula, where, contrary to the AGP index, the climatological Azores high cases are not contributing to the anomaly-based APV^* blocking. Note also, that the large APV^* blocking frequencies along the jet axis over the Western Atlantic are not significantly related to a specific NAO phase.

The much lower APV-index blocking frequencies (maximum ~3%) are also separated rather well by the NAO phases (Figures 4.3e, f). The daily NAO+ composite shows a statistically significant increase of "cut-off" blockings over Western and Central Europe, at the right-exit of the jet stream, much like the AGP field. The NAO- composite is characterised by a significantly higher APV- blocking frequency over the Davis Strait, Southern Greenland and the Norwegian Sea in the northern part of the tropopause ridge. Although the frequencies and significant areas are much smaller for APV, they appear in similar regions as for the two other indices.

Latitudinal dependence of the NAO-blocking relationship

A more standard way to highlight the NAO-blocking relation for the European region is presented in Figure 4.4, which shows zonal sections across Figure 4.3 at a fixed latitude of 60°N (left panels) and further south at 50°N (right panels). In this way they can be directly compared to a similar analysis, using the TM90 blocking index presented by Pavan et al. (2000b) for monthly data, covering the 15 years of ERA–15.
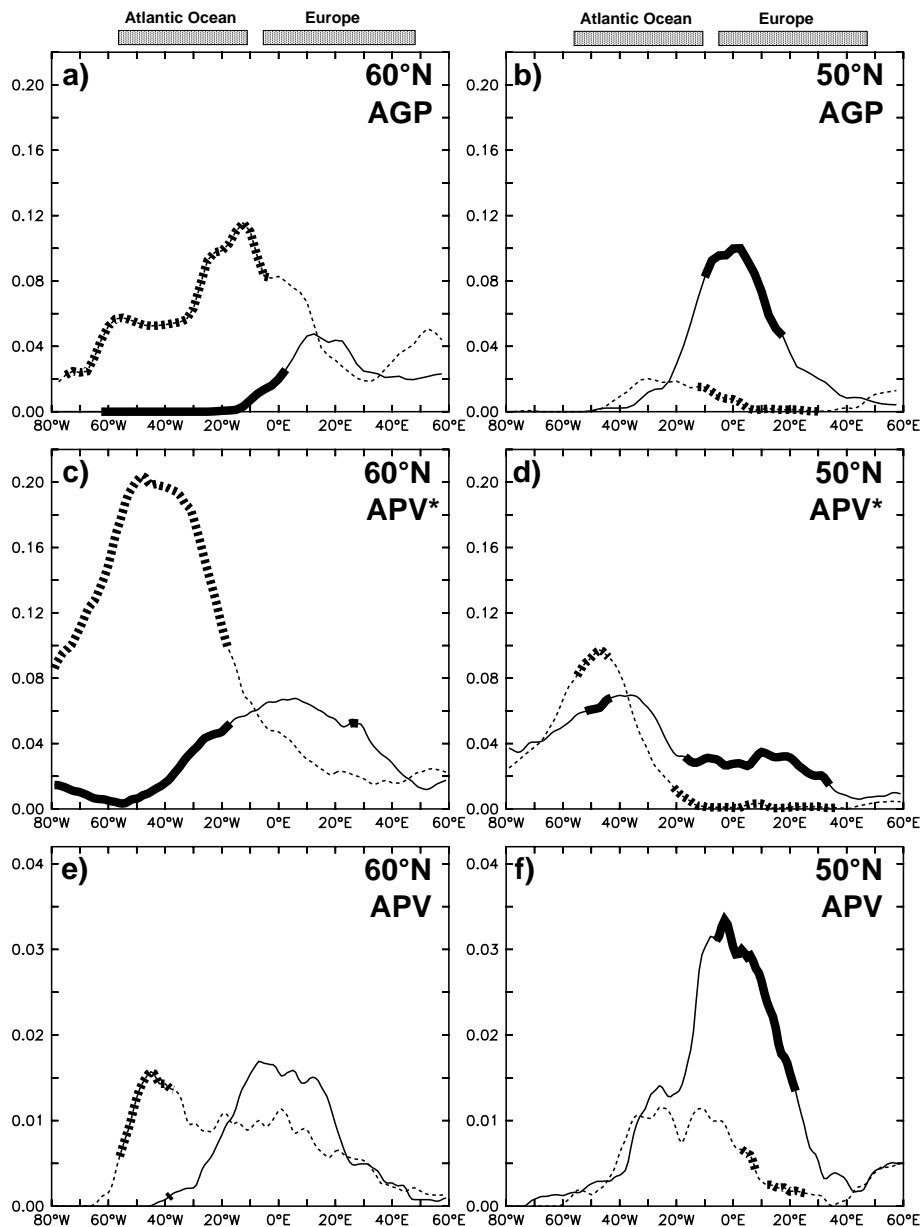
Figure 4.4: Blocking frequency sections at 60°N (left panels) and 50°N (right panels) for the NAO+ tercile (solid lines) and the NAO- tercile (dashed). Results are shown for *AGP* (a, b), *APV** (c, d) and for *APV* (e, f). Longitudes showing significantly increased or decreased blocking frequencies are indicated in bold. The frequencies shown are slightly boxcar smoothed (three point smoother). Note that the ordinate runs from 0 to 0.2 for *AGP* and *APV** but from 0 to 0.04 for *APV*.

At the classical latitude around 60°N all three indicators suggest, that the occurrence of blocking over the Atlantic Ocean and the negative NAO phase are correlated (Figures 4.4a, c, e), whereas the positive NAO phase coincides with a complete absence of blocking. Both results are significant for most of the longitudes covering the Atlantic Ocean, while over the European continent no significant differences are found. This is consistent with the results of Pavan et al. (2000b) (cf. their Figure 4.3a) and Shabbar et al. (2001). At the more southern latitude of 50°N no coherent statistically significant signal is found over the Atlantic Ocean. Instead, all three indicators now suggest a statistically significant relation over large parts of continental Europe, but with opposite sign compared to 60°N (Figures 4.4b, d, f).

The findings of this section show that the relation between blocking and the NAO strongly depends on both latitude and longitude. It is therefore important to consider the full spatial (and temporal) variability of these two phenomena to reveal further details of their interrelation.
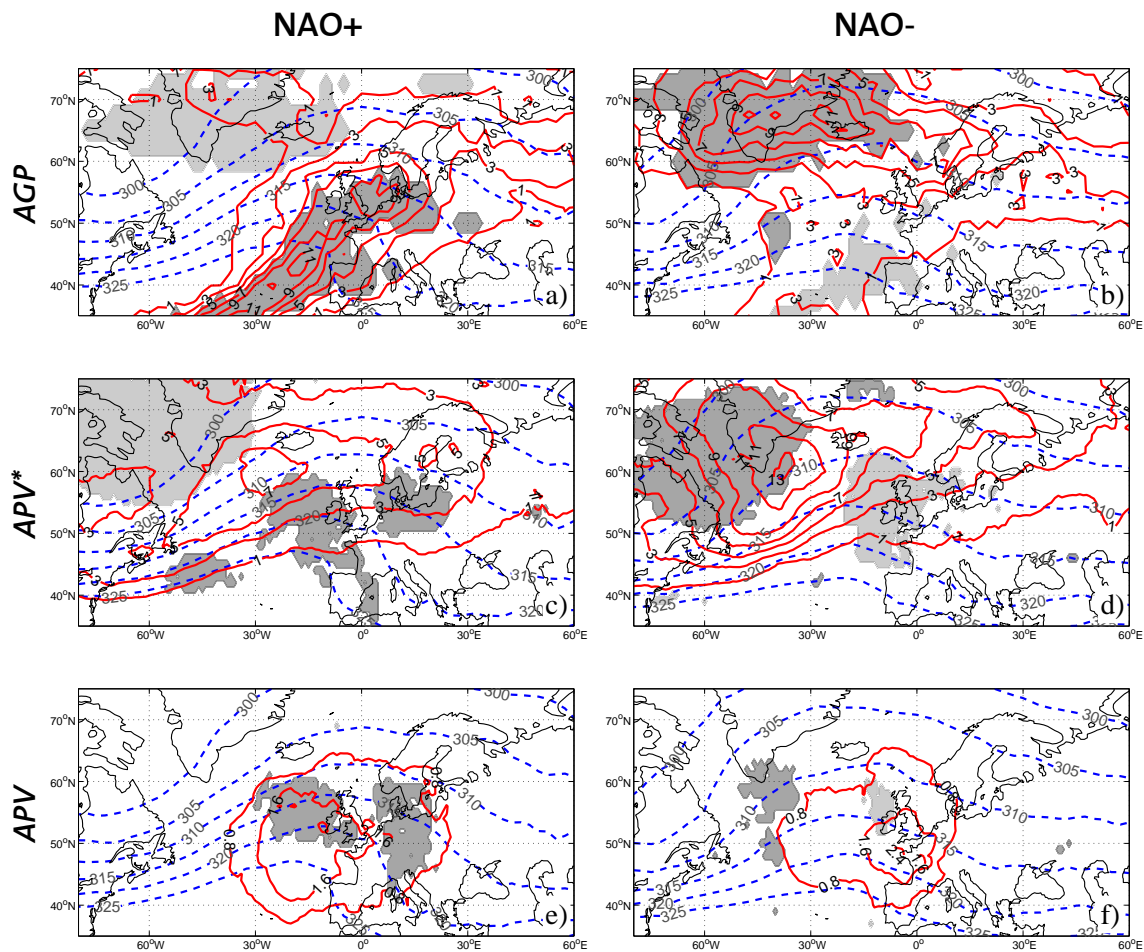

Figure 4.5: As Figure 4.3, but for terciles based on seasonal NAO values and a significance level of 95%.

4.4.2 Blocking relation to seasonal NAO index

The above stratification of blocking events is based on terciles of the daily NAO index. On this time scale, the regions of predominant blocking are well separated by the NAO index and the associated flow structure is in correspondence with weakened flow and ridge formation (cf. Figure 4.3). The question remains whether the NAO phase-separation of preferred blocking regions persists if the blocked days are grouped by seasonally averaged quantities instead of daily ones.

To tackle this question, the same composites as in Figure 4.3 are computed for the three blocking indices but using the winter (DJF) seasonal-mean NAO index. In general, similar patterns are found using a three-monthly instead of a daily NAO index stratification (Figure 4.5). The frequency distributions are not as distinct as with a daily separation, and in general the frequency maxima are now reduced. The regions that exhibit a significant correlation of blocking with the NAO phase are smaller but the general statements hold (especially for AGP and APV^*): During "NAO+ winters", significantly intensified blocking is found over Western Europe, whereas blocking is strongly reduced around Greenland and Iceland. During "NAO- winters" blocking episodes are more frequent over the western North Atlantic and the Davis Strait, but are reduced over Europe. The potential temperature structure of the dynamical tropopause and the co-location of blocking events identified with different indices are similar if somewhat less sharp than for a daily NAO stratification. However, all 2D blocking frequency maps show that there is a clear anti-correlation between NAO phases and blocking in the Atlantic region and a positive correlation of the NAO with blocking over Central and Western Europe. These results are an addition to earlier statements in the literature where only a clear anti-correlation between NAO phases and blocking in the Atlantic and Canadian region was reported (Pavan et al., 2000b; Stein, 2000; Shabbar et al., 2001).
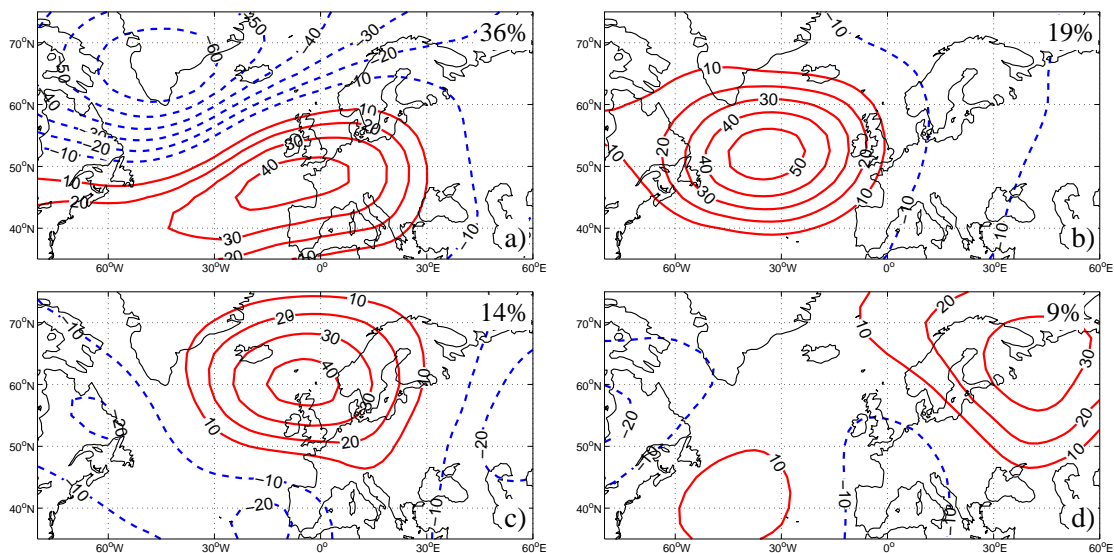
Figure 4.6: Spatial EOF1–4 patterns of DJF seasonal Z500 fields over the Euro-Atlantic region (panels a-d). Shown are the Z500 anomalies in geopotential meters associated with a principal component amplitude of one standard deviation. The variances explained by each of the 4 EOFs are shown in the upper right corner of the corresponding panel. Contour interval is 10m. Positive values are solid, negative values are dashed. The 0m-line is omitted.
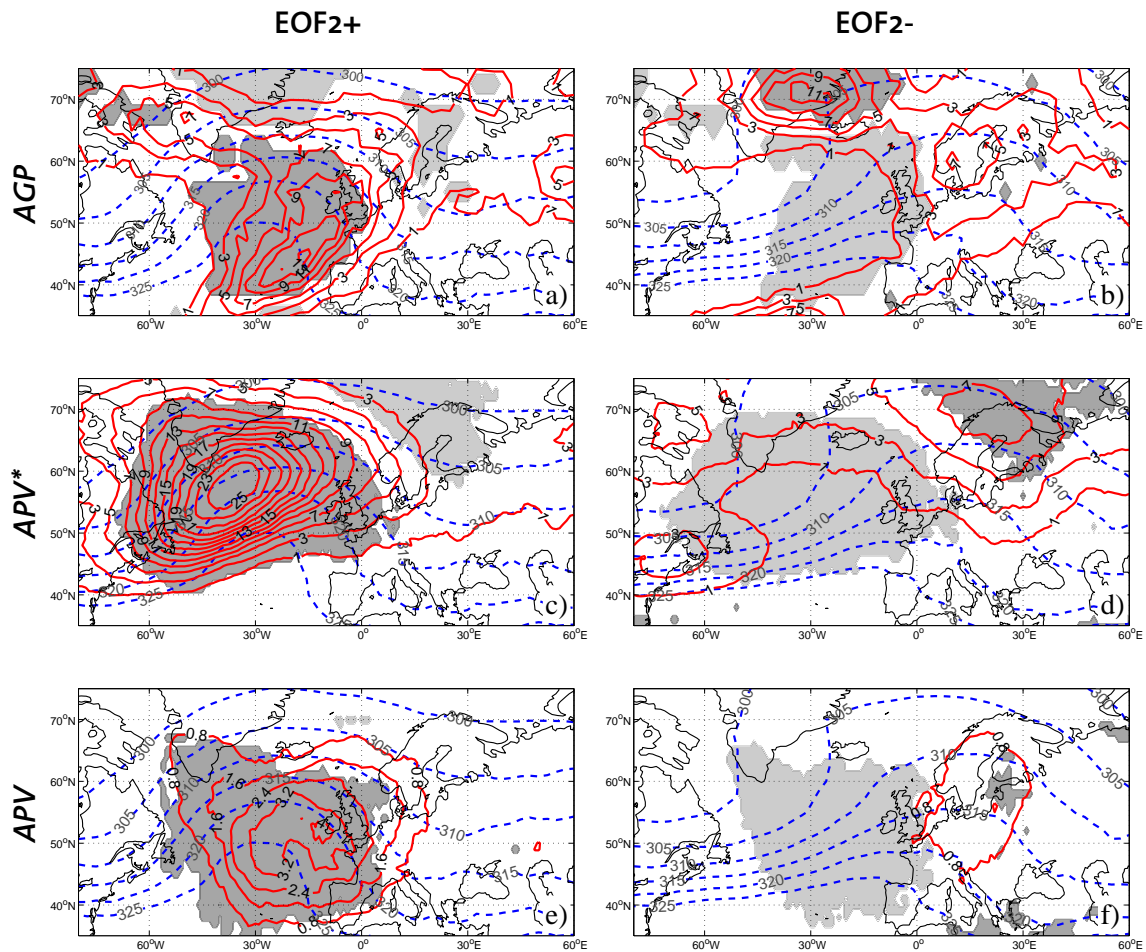
EOF2+   EOF2-

Figure 4.7: As Figure 4.3, but for daily EOF2+ (left panels) and EOF2- (right panels) terciles. Significance level applied is 99% for the *AGP* and *APV** and 95% for *APV*.

The above results imply that the NAO-blocking relation holds from daily to seasonal time resolution, but it is a purely statistical result and does not allow speculation about the question whether the NAO phase determines the blocking frequencies or vice versa. More process-based investigations would be needed to address this question in detail A first indication of a potential cause-and-effect relationship can be gleaned from Figure 8 of Schwierz et al. (2005), which suggests that long-lived Euro-Atlantic blocks precede the development of the large-scale flow into a NAO- phase.

4.5 Blocking relation to higher order climate patterns

The NAO (EOF1) explains roughly one third of the seasonal winter geopotential (Z500) variability. Another 42% of variability can be explained by the next three leading EOF modes. In this section the relation between these climate patterns and blocking is investigated on a daily basis as done for the NAO index in Section 4.4.1.

The spatial patterns of the first four EOF modes are given in Figure 4.6. They show large similarities with well-known teleconnection patterns (Barnston and Livezey, 1987; Pavan et al., 2000a). Correlation coefficients between the EOF principal component time series and the respective pattern time series of Barnston and Livezey (1987) are larger than 0.7. EOF2 explains 19% of monthly Z500 variability and is clearly related to the "East Atlantic" pattern, with a massive positive height anomaly over the central Atlantic. EOF3 (14%) shows some similarity with the "East Atlantic/Western Russia" pattern, with a positive anomaly over the British Isles and the North Sea and negative centres west of the Azores and over the Ural mountains. EOF3 also substantially resembles the midlatitude anomaly train (MAT) tropopause pattern defined in Massacand and Davies (2001a), which is reminiscent of the Z500 "blocking signature" as derived using the TM90 blocking index (Tibaldi et al., 1997; D'Andrea et al., 1998). The MAT pattern has been described to be the mode with the highest co-variability with January central European precipitation (Massacand and Davies, 2001b). EOF4 (9%) is closest to the "Eurasian type-1" pattern also called "Scandinavian" pattern, with a positive anomaly over Scandinavia and negative centres over South Western Europe, Eastern Canada and South Western Greenland (Barnston and Livezey, 1987; Rodgers, 1990).

Figures 4.7, 4.8 and 4.9 show the blocking frequency composite maps for all three blocking indicators stratified by days being in the lowest and highest tercile of the EOF2–4 principle component time series (analogous to Figure 4.3 for the NAO). The EOF2 monopole anomaly over the central North Atlantic (Figure 4.6b) is accompanied by an almost symmetric ridge located further to the south than for the NAO- phase (cf. Figures 4.3 and 4.7). The opposite phase is characterised by a rather zonal flow in the west Atlantic which weakens already well before it reaches the European continent. Figure 4.7 shows that the blocking frequency distribution in the EOF2+ phase exhibits enhanced blocking frequency (AGP ~12%, APV^* ~25%) essentially over most parts of the midlatitude Atlantic stretching northwestward up into Davis Strait. All three indicators detect no blocking over the Atlantic during the negative EOF2 index days. At the same time enhanced blocking frequency anomalies are found over Greenland (AGP) and Scandinavia/North-East Europe (APV^*/APV).

A highly consistent relation between the large-scale variability pattern and the blocking frequency indicators is found for EOF3 (Figure 4.8). In the positive phase, strongly increased blocking frequencies (AGP, APV^* ~17%) centred over the North Sea and the southern parts of the Norwegian Sea are observed, stretching from Finland in the east to Iceland and Greenland in the west, co-located with the centre of the spatial EOF3 pattern (cf. Figures 4.6 and 4.8). In the negative phase blocking is completely absent over this region for all indicators. A similar partitioning of presence or absence of blocking can be seen in the 1-dimensional figures of Pavan et al. (2000b), valid around 60°N. The structure of the tropopause is closely associated with the blocking signature. In the positive phase the potential temperature ridge reaching from the Azores to Northern Europe indicates considerable meridional flow. In contrast to the strong EOF3+ ridge, the negative EOF3 phase is marked by a clear zonal regime. This indicates that EOF3 is primarily a blocking pattern in the traditional sense (cf. Rex, 1950). Hardly any AGP blocking is found for the EOF3- composite over Europe with exception of a slight enhancement of blocking frequency over the Ural Mountains and the Iberian Peninsula. A similar but weak relation over the Iberian Peninsula is found for APV. These maxima are associated with the Z500 EOF3 minima straddling the positive pole (cf. Figure 4.6). We note in passing that the zonal EOF3 regime is exhibiting a

weaker jet flow than for instance during the zonal phases of the NAO+ or EOF2-, which is consistent with the significant increase of persistent negative PV anomalies near Newfoundland and the West Atlantic Ocean (Figures 4.8c, d; ~11% blocking frequency).

Although the EOF4 explains only 9% of the Z500 variability, the blocking frequencies associated with the EOF4+ and EOF4- terciles are quite high (up to 11 (15%) for *AGP* (*APV**), cf. Figure 4.9). However, the relation between blocking and the wave-type anomaly pattern EOF4 is more complex. The broad and intense maximum over Northern Scandinavia (~11% for *AGP*, *APV**) is statistically significant for all three indices and coincides with the primary maximum of the EOF4+ pattern (Figures 4.6 and 4.9). The negative phase (EOF4-) is anti-correlated with Scandinavian blocking but exhibits significantly increased blocking frequencies over southern Greenland and in the Davis Strait to its west. This west-east dipole is complemented by a weak, but significant third blocking maximum over Western Europe and the Iberian Peninsula (especially for *AGP* and *APV*). The associated flow pattern changes from a marked split flow with its weakest centre over Northern and North Eastern Europe as well as Russia in the EOF4+ phase to a rather zonal flow with a slight, backward tilted ridge over the East Atlantic in the EOF4- phase.
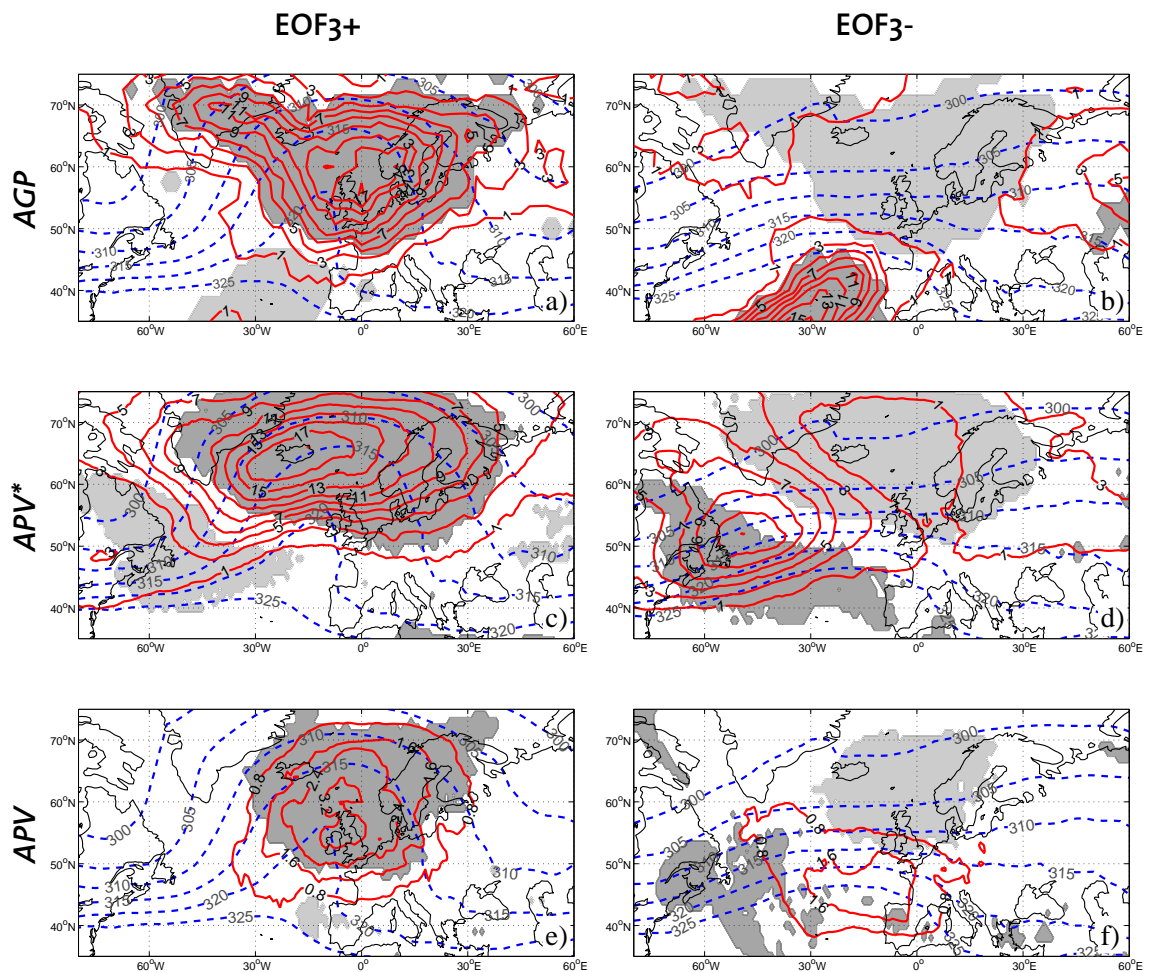

Figure 4.8: As Figure 4.7, but for EOF3.

As for the NAO, the APV^* frequency pattern within the jet region is not significantly different from the overall climatology. Pavan et al. (2000b) find also a distinct difference between the EOF4+ and EOF4- phases over Scandinavia but no clear differences at the more westerly longitudes in the Atlantic and Greenland.

In this section we have analysed the relation between blocking indicators and daily projections of purely statistical EOF climate patterns. Most of the EOF centres are linked with clearly enhanced blocking or complete absence of blocking. The different indicators agree considerably well with the regions where the blocking frequencies, are significantly different from climatology, (cf. the dark and light grey shade regions in Figures 4.7, 4.8 and 4.9). Near the EOF main centres all indicators show clearly increased or no blocking at all, depending on the EOF sign. In contrast to earlier studies, significant differences are sometimes found away from the main centre of activity (cf. EOF 4). As shown for the NAO, the climate pattern - blocking relations also hold for the seasonally defined EOFs, albeit at a considerably lower statistical significance (not shown).
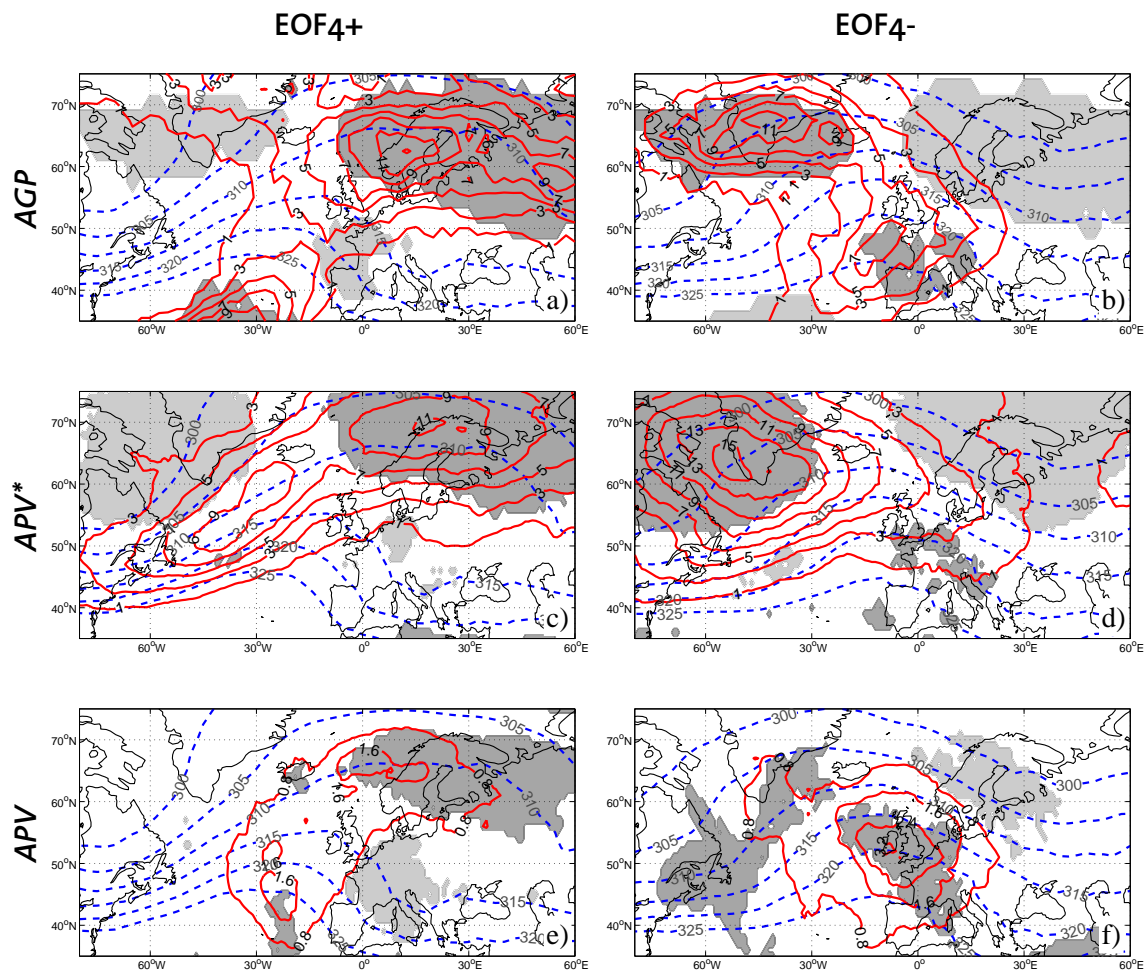

Figure 4.9: As Figure 4.7, but for EOF4.

4.6 Conclusions

In this study the statistical relation between climate patterns and three novel two-dimensional blocking indicators over the Euro-Atlantic region has been investigated. In addition to a two-dimensional extension of the TM90 index (using absolute geopotential heights for blocking detection) two dynamically based 3D-PV indices (one based on absolute, one on anomalous values) have been considered. A comparison of the three indices shows indicator-dependent differences in space, time and therefore also in climatological blocking frequencies. These dissimilarities can be made plausible by methodological and dynamical arguments. The performance of the indicators in capturing the block varies differently with the life cycle and structure of the phenomenon.

Despite these differences all indicators agree that both NAO phases (based on daily indices) are statistically related to distinct regions with increased/reduced blocking frequencies. Moreover they all highlight that there is not only a clear anti-correlation between NAO phases and blocking in the Atlantic region, as already described by several authors (Pavan et al., 2000b; Stein, 2000; Shabbar et al., 2001), but also a positive (if somewhat weaker) correlation of the NAO with blocking over Central and Western Europe. Although the NAO-blocking relation is weaker using a seasonal instead of daily NAO index stratification it remains statistically significant for the main centres. The results emphasise that the relation between blocking and the NAO strongly depend on both latitude and longitude. It is therefore important to consider the full spatial and temporal variability of these two phenomena to reveal further details of their interrelation.

An analysis of the relation between the daily projections of EOF2 to 4 and the blocking indicators shows that the EOF centres are linked with clearly enhanced or complete absence of blocking. For all EOF phases, the three indicators agree well on the regions identified as significantly different from overall climatological blocking frequency. Near the EOF centres all indicators show clearly increased or no blocking at all depending on the EOF sign. This is especially true for EOF2 and 3. The opposed phases of the patterns correspond to flow situations resembling the blocked-zonal flow equilibrium states that were proposed by Charney and Devore (1979) from idealised barotropic channel experiments. Significant blocking frequency differences are also detected away from the EOF main centre for certain climate patterns (e.g. EOF4). The climate pattern - blocking relations also hold (at a considerably lower statistical significance) for the seasonally defined index time series. The underlying dynamics and the associated consequences for regional impact studies merit further consideration.

Chapter 5

Recent temperature trends in Switzerland and Europe: Implications for climate normals

SIMON C. SCHERRER, CHRISTOF APPENZELLER AND MARK A. LINIGER

Climate Services, Federal Office of Meteorology and Climatology (MeteoSwiss), Zürich, Switzerland

ABSTRACT

This study discusses problems of the concept of normal period based anomalies arising from climate variability and ongoing climate change. The widely used WMO 1961–1990 (61–90) standard normal period is compared to other consecutive 30-year normal periods in detail. Focus is given to the temperature distribution in Switzerland and on the European continent. In these regions the temperature trend of the last decades led to an unusually high number of months with positive temperature anomalies relative to the WMO 61-90 standard normal period. Swiss anomalies based on the 61–90 normal are up to 1.25 K higher than those based on the Latest 30-years Running Normal (LRN). The probability to observe a positive temperature anomaly with respect to the 61–90 normal increased from 50% to near 80% for certain months of the year. Compared to the LRN, this change is statistically significant for 7 out of the 12 months on the 95% level. The strongest signal can be found for the summer months, whereas temperatures in fall do not show any trends. Similar results are found for more than 90% of the European continental area. For most regions 2–5 months are inconsistent with the 61–90 distribution. In southern France, parts of Spain and southern Scandinavia this number increases to 7–9 months.

5.1   Introduction

One of the operational tasks of every meteorological service is to provide climatological temperature and precipitation anomalies of the past months and seasons. The communication of this information constitutes an important analysis and decision basis for various applications such as planning, engineering works or managing energy consumption (Guttman, 1989). The official strategy of the World Meteorological Organisation (WMO) to determine climate

normals (and anomalies thereof) has been based on a *"uniform and relatively long period comprising at least three consecutive ten-year periods"* (WMO, 1959). The climatological standard normals were defined as *"averages of climatological data computed for consecutive periods of 30-years as follows: 1 January 1901 to 31 December 1930, 1 January 1931 to 31 December 1960 etc..."* (WMO, 1959). The choice for the 30-year averaging interval was a compromise. First the time series had to be long enough to average out short term fluctuations, second the length was limited by data availability and data inhomogeneity and third the framework had to be general enough to be easily implemented worldwide.

For precipitation, the applicability and usefulness of climate normals and anomalies thereof was discussed already in the 1930s (Gisborne, 1935; Mindling, 1940). With the introduction of 30-year means as normals in the USA, several studies focussed on so called "optimal normals", i.e. on the predictive skill of climate normals (Beaumont, 1957; Enger, 1959; Court, 1967-68). These and later studies showed that a base period of 30-years may not be an optimal choice, but there was no general agreement on what period length should be used. The suggestions varied from 5 up to 25 years (Lamb and Changnon, 1981; Dixon and Shulman, 1984; Kunkel and Court, 1990; Huang et al., 1996), which were also discussed at numerous WMO meetings. WMO Technical Note 84 states that it is essentially impossible to define a uniform time interval as a reference period for all climate elements that is independent of the region: *"a period which may be representative for one place may be totally unrepresentative at another (…)"*. A further criticism was on the influence of climatic fluctuations (decadal variability) on the reference period: *"owing to climatic fluctuations the statistics based on 30 or even 50 years may not be absolutely stable (…)"*.

Today, at the beginning of the 21st century temperatures are observed to increase in most parts of the world and Europe (Folland et al., 2001; Klein Tank et al., 2005). Climate temperature anomalies calculated on the current 1961–1990 standard normal period (61–90 normal hereafter) do not seem to be in line any more with their original meaning, namely the average is not zero over a longer time period. WMO recommended updating the 30-year normals at the completion of each decade (WMO, 1967). Hence the 1971–2000 period would be the actual reference period. In September 2004 still a majority of western meteorological services presented 61–90 normals and anomalies thereof on their websites (Table 5.1).

One of the aims of this paper is to explicitly quantify and discuss the effect of the recent temperature trends on the calculation of climate temperature anomalies, a quantity widely used for climate monitoring. It is clear that climate is much more than just mean temperature, and other climate elements could be considered. Similar changes in extreme values are of great importance for many applications (traffic, building codes, heating and cooling) and could also be analysed in a similar framework (cf. Sardeshmukh et al., 2000; Klein Tank and Können, 2003; Moberg and Jones, 2005).

After an introduction to the datasets and methodology used (Section 5.2), we will discuss the Swiss temperature distribution changes of the last 140 years (Section 5.3.1). Next, we focus on recent observations and quantify the effect of the observed temperature trends on the calculation of climate anomaly amplitudes (Section 5.3.2). The influence of the updating frequency of the normal periods on anomalies is also discussed (Section 5.3.3). In Section 5.3.4 the analysis is extended to a European scale. Finally the main results are summarised in Section 5.4.

Table 5.1: Temperature normal definitions used for public products on the internet on 24 September 2004. Considered were the weather service websites of all EUMETNET member countries (indicated by an asterisk) and some other western countries. For Luxembourg and Greece no information could be found online. In Austria, Australia and France both, the 1961–1990 and the 1971–2000 definition had been used.

Country	Institution	Normal definition on 24 September 2004	
		1961–1990	1971–2000
Australia	Bureau of Meteorology	X	X
Austria*	Zentralanstalt für Meteorologie und Geodynamik	X	X
Belgium*	The Royal Meteorological Institute of Belgium	X	
Canada	Environment Canada		X
Denmark*	The Danish Meteorological Institute	X	
Finland*	The Finnish National Weather Service		X
France*	Météo-France	X	X
Germany*	Deutscher Wetterdienst	X	
Greece*	Greek Meteorological Service	–	–
Hungary*	Hungarian Meteorological Service	X	
Iceland*	The Icelandic Meteorological Office	X	
Ireland*	The Irish Meteorological Service	X	
Italy*	Servizio Meteorologico dell' Aeronautica Militare Italiana	X	
Japan	Japan Meteorological Agency		X
Luxembourg*	Service Météorologique du Luxembourg	–	–
Netherlands*	Netherlands Royal Meteorological Institute		X
Norway*	Meteorologisk Institutt		X
Portugal*	Instituto de Meteorología	X	
Spain*	Instituto Nacional de Meteorologia		X
Sweden*	Swedish Meteorological and Hydrological Institute		X
Switzerland*	MeteoSwiss	X	
United Kingdom*	The Meteorological Office	X	
USA	National Weather Service		X

5.2 Data and methodology

5.2.1 Data sets and data quality

In this study two datasets of monthly mean temperature are used. The first set consists of carefully homogenized Swiss 2-m temperature series for the time period January 1864 to June 2004 (Begert et al., 2005). This dataset meets WMO recommendations on data quality for the proper determination of normal values (WMO, 1967). For northern Switzerland a composite time series of representative stations is formed and termed "northern Swiss series" hereafter. As in Schär et al. (2004) the equally weighted average is taken of the four stations Basle-Binningen, Berne-Liebefeld, Geneva and Zurich. The station of Lugano is used as the "southern Swiss series".

For the European scale analysis, 2-m temperature from the European Centre for Medium-Range Weather Forecasts (ECMWF) reanalysis (ERA–40) is employed (Uppala et al., 2006). The data used covers the period January 1960 to August 2002 and has been interpo-

lated onto a regular grid with a 1° x 1° resolution. Recent studies indicate that 2-m temperature in ERA–40 and direct observations such as CRUTEM2v (Jones and Moberg, 2003) are in good agreement in terms of short-term variability and trends (Simmons et al., 2004). This is true in particular over Western and Middle Europe (10°W–40°E, 36°N–65°N) the study area of this paper. A comparison of temperature data from the ERA–40 dataset (grid point: 47°N/7°E, period 1961 to 2002) with carefully homogenized Swiss observational data reveals a high overall consistency, both in correlation coefficient (r~0.98) and trend estimate (refer to Appendix for details). Trend values estimated with ERA–40 data slightly underestimate the observed changes in the mean for most months, especially in summer. The differences are not much larger than those from comparing homogenous data with inhomogeneous station data or CRUTEM2v 47.5°N/7.5°E grid point data, both of which also tend to underestimate changes in the mean.
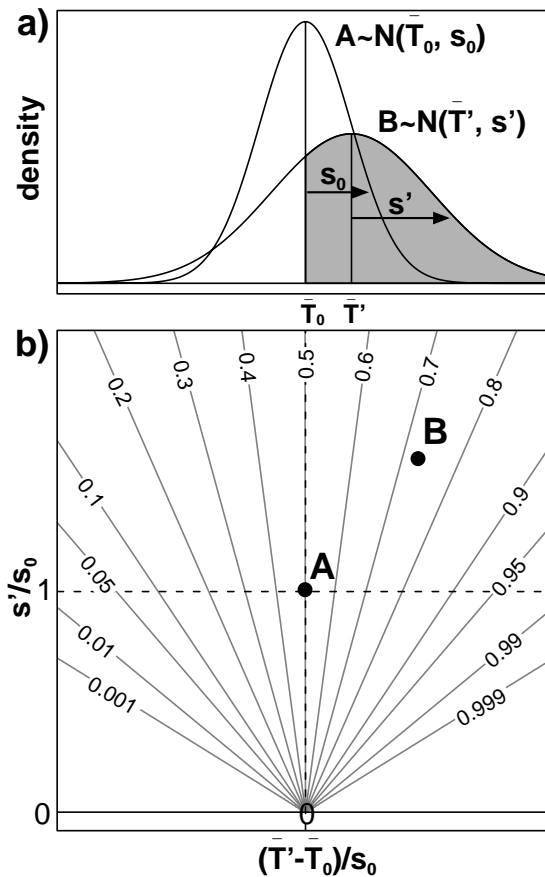
Figure 5.1: The impact of a simultaneous change in mean $(\overline{T}_o \rightarrow \overline{T}')$ and standard deviation $(s_o - s')$ on a climate distribution. Shown is a reference distribution A as well as a distribution B where mean and variability have increased. a) Probability density functions. The shaded area shows the Probability to observe a Positive Anomaly (PPA) with respect to the reference normal $\overline{T}_o$ for distribution B. b) Standardized mean change $(\overline{T}' - \overline{T}_o)/s_o$ vs. standard deviation change s'/s_o (MSC) plot with contours of equal PPA.

5.2.2 Methodology

A series of Shapiro-Wilk tests for normality (Shapiro and Wilk, 1965) applied to Swiss seasonal temperature data show that the monthly to seasonal 30-year samples of 2-m temperature observations are normally distributed (confidence level: 90%). Thus, it is justifiable to characterise the distribution solely by the mean (the normal value) $\overline{T_0}$ and standard deviation s_0. An example of a Gaussian probability density function (PDF) $A \sim N(\overline{T_0}, s_0)$ is shown in Figure 5.1a. For this reference PDF A, the Probability to observe a Positive temperature Anomaly (PPA) is 0.5 per definition. The 1961–1990 (61–90) period is used as the reference period hereafter (using the subscript zero). For a different period in time the PDF may have changed and the estimate for the mean and standard deviation is different from the reference PDF A (for example $\overline{T}' > \overline{T_0}$ and $s' > s_0$, as in PDF B of Figure 5.1a). The PPA with respect to the normal $\overline{T_0}$ of PDF A is:

$$PPA_{\overline{T_0}}\left(\overline{T}', s'\right) = \int_{\overline{T_0}}^{\infty} \frac{1}{\sqrt{2\pi}s'} \exp\left(-\frac{\left(T - \overline{T}'\right)^2}{2s'^2}\right) dT \qquad \text{(Eq.5.1)}$$

where T is the continuous value of the 2-m temperature. The PPA is shown as the grey filled area in Figure 5.1a. The PDFs are compared with each other in Mean change vs. Standard deviation Change (MSC) plots. The mean and standard deviation changes can be plotted as absolute ($\overline{T}' - T_0$ vs. $s' \rightarrow$ absolute MSC plot) or standardized ($[\overline{T}' - T_0]/s_0$ vs. $s'/s_0 \rightarrow$ standardized MSC plot) values. For most scientific questions the standardized form is preferred as illustrated in Figure 5.1b. In the standardized MSC plot, the example PDF A is located at (0,1) and PDF B in the upper right quadrant. Values of constant PPA are straight lines crossing (0,0). In the illustrative example of Figure 5.1b, the probability to observe a positive anomaly has increased from 0.5 for the original climate state (PDF A) to a value around 0.72 for the new climate state (PDF B).

Statistical significance and robust measures

Extreme climatic events like the cold winter 1962/63 or the hot summer 2003 have a considerable influence on the "stability" of statistics based on a 30-year period (WMO, 1967). Similarly the existence of long term trends (nonstationarities) affects the standard deviation (Scherrer et al., 2005). The confidence level of the results must therefore be assessed carefully. A bootstrapping approach using resampling with replacement (Efron and Tibshirani, 1993) is employed in order to determine whether the sample distributions PPA values differ significantly from the reference normal for which PPA is 0.5 by definition.

Figure 5.2a/b illustrates 1000 replications of the normal period mean change and standard deviation in a standardized MSC plot for the 61–90 seasonal DJF northern Swiss temperature series. The uncertainty of the parameter estimates for mean and standard deviation are in the order of 20 to 30% of s_0. A two dimensional kernel density estimator is used to highlight the "high-density centres". The primary density maximum is near (0,1). A secondary maximum is found near (0.1,0.82). This indicates that the 61–90 normal could underestimate the mean value and overestimate the variability due to the aforementioned

negative anomaly in winter 1962/1963. Panel b shows that the PPA is most probably around 0.5 but associated with a considerable uncertainty. A significant increase in the Swiss PPA is defined here as a value greater than the PPA 95th percentile, which is 0.64 for the 61–90 DJF temperature.

Due to the large sensitivity to extreme values one could argue to use more robust and resistant estimators of location and scale like the median and interquartile range (IQR) rather than mean and standard deviation (see e.g. Hoaglin et al., 1983; Ferro et al., 2005). Compared to mean and standard deviation, the median and IQR/1.349 estimates are much less coherent and the PPA PDF is far from being symmetric (Figures 5.2c/d). This shows that the median as well as the IQR are relatively inefficient, i.e. a large sample size is needed to determine a value with the same confidence compared to a more efficient measure. To estimate a standard deviation via IQR/1.349 and a sample size of 30 a Monte Carlo experiment suggests an efficiency of ∼0.40 with respect to the maximum likelihood estimator (relative efficiency). This value is close to the asymptotic relative efficiency of 0.37 (e.g. Staudte and Sheather, 1990). Thus, an IQR/1.349 based standard deviation estimate of a 30-year normal period is only as efficient as an estimate applying the standard deviation to a sample size of 0.4x30 = 12. Furthermore, depending on the method with which the IQR quartiles are determined, the IQR may have a negative bias for a small sample size (Hyndman and Fan, 1996). This analysis focuses on mean and standard deviation hereafter.
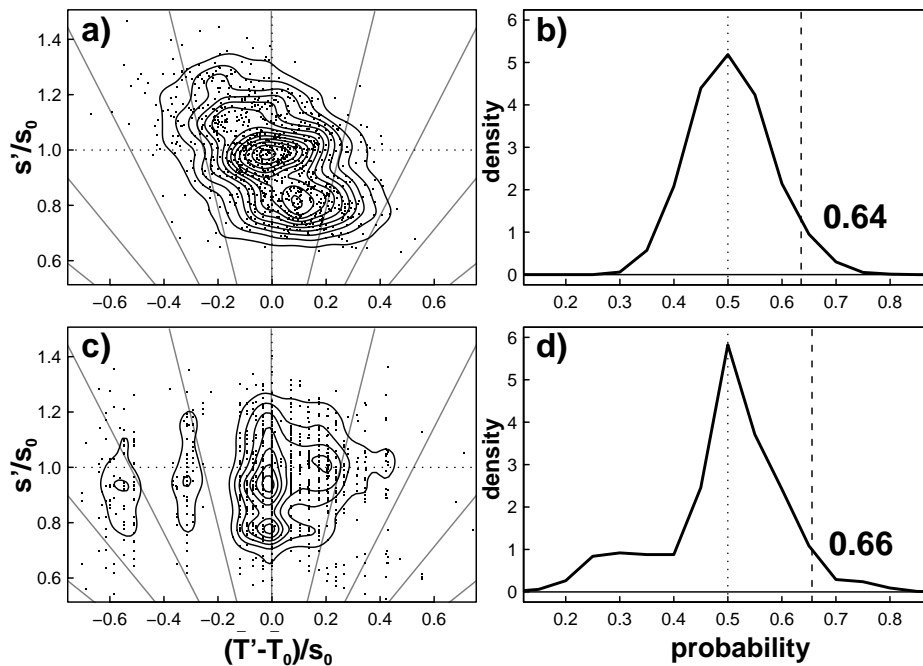
Figure 5.2: Bootstrapped uncertainty estimates for the DJF 61–90 northern Switzerland temperature normal definition. The MSC plots show estimates based on a) mean and standard deviation and c) median and IQR/1.349. For display purposes 1000 bootstrap samples are shown as dots. The density values are based on 5000 samples (contour lines, levels as in Figure 5.1). The corresponding PDFs of the PPA are shown in panel b) and d). The 95th percentile confidence limit for the mean-standard deviation (median-IQR/1.349) estimator is 0.64 (0.66).

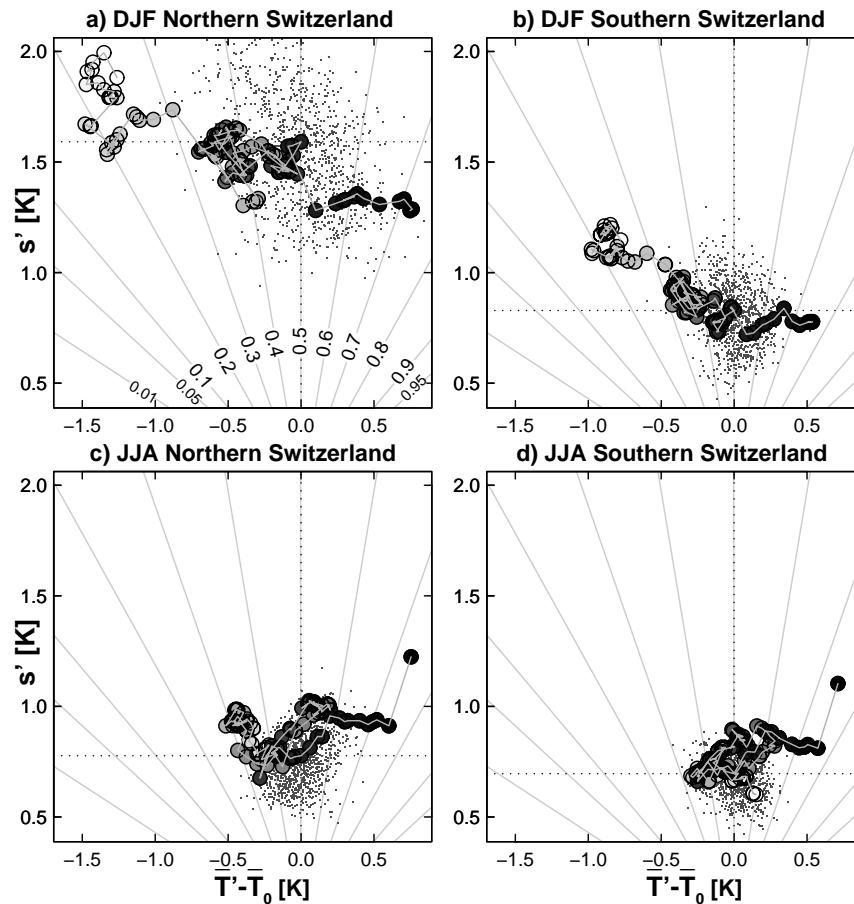*Figure 5.3*: Absolute MSC plots for Swiss 2-m temperatures. Shown are observations for northern (a, c) and southern Switzerland (b, d) for the DJF observational period 1865–2004 (a, b) and JJA 1864–2003 (c, d). The small dots show 1000 bootstrap realisations of the 61–90 period mean and standard deviation estimates. The PPA contour lines (grey solid) are based on the 61–90 normal period (position indicated by dotted lines). Units are in Kelvin.

5.3 Results

5.3.1 Swiss temperature distribution changes over the past 140 years

Figure 5.3 shows changes in the 2-m temperature distribution using an absolute MSC plot for northern and southern Switzerland. Here the 61–90 reference period is located at $(0, s_0)$. Climatological normal periods of all possible consecutive 30-year windows between 1864 and 2003 (for JJA) and between 1865 and 2004 (for DJF) are depicted. The lightest point indicates the first 30-year period (1864/5–1893/4), the darkest point the latest period available (1974/5–2003/4). The normal values have changed substantially in the past 140 years. In northern Switzerland the 140 year differences between the normal values are roughly 2 K (1 K) for the DJF (JJA) season. In southern Switzerland there is a smaller change of ~1.5 K in DJF and ~0.8 K in JJA. Thus, the increase in absolute numbers is much stronger in win-

ter than in summer seasons and in the north than in the south. This change is consistent with linear trend approaches considering the 1864–2003 period (Bader and Bantle, 2004; Begert et al., 2005).

In northern Switzerland DJF variability is almost twice that of JJA. This seasonal difference is much weaker for southern Switzerland which might be related to the more Mediterranean character of the climate or the proximity of the Lake of Lugano. For the winter season a negative trend in variability is found for both northern and southern Switzerland. With the exception of the extreme year 2003, such a clear trend is not found for the summer season. The decrease in winter temperature variability can be assigned to a few large discontinuities that are a consequence of a few extremely cold winters. The large discontinuities in both mean and standard deviations occur when an extreme value enters or leaves the running window. For example, the standard deviation drops from 1.6 K to below 1.3 K for switching from the 1963–1992 to the 1964–1993 DJF period which does not include the 1962/63 winter. It is thus not a continuous narrowing of the distributions that leads to the winter trend in variability but rather the result of the absence of extreme cold winters in recent decades. The bootstrapped estimates applied to the 61–90 normal (point clouds in Figure 5.3) show that the latest 30-year periods are located outside the 61–90 range of uncertainty for all seasons and regions. This is also the case for the winter periods at the end of the 19th century which will be discussed in more detail below.
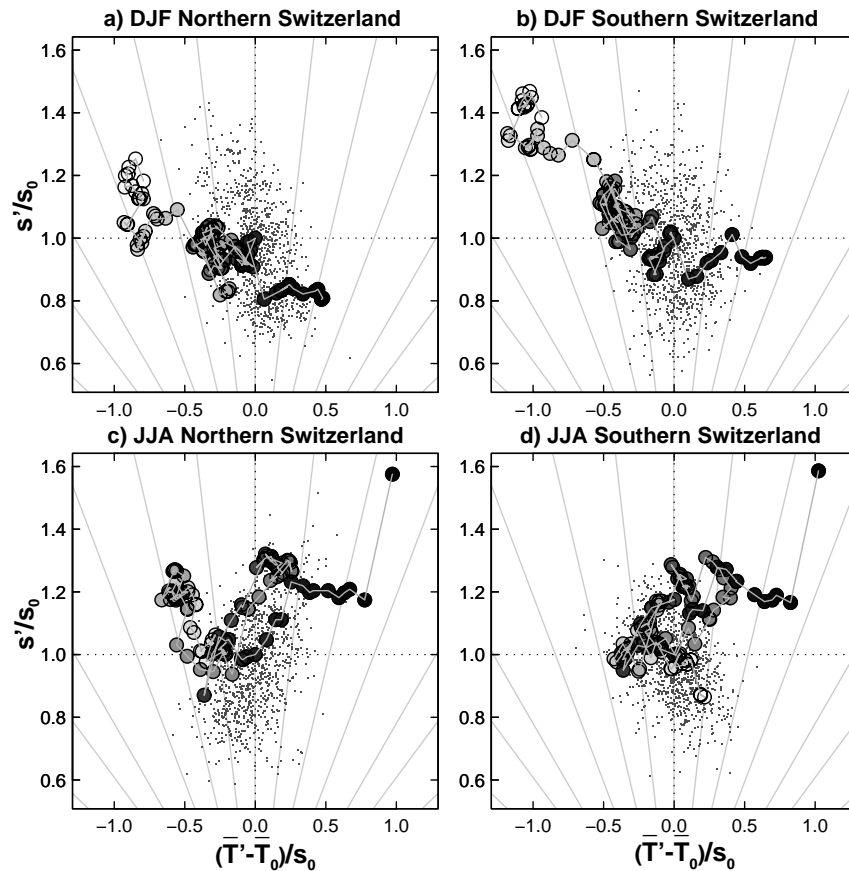

Figure 5.4: As Figure 5.3, but with standardized MSC plots. Axis units are dimensionless.
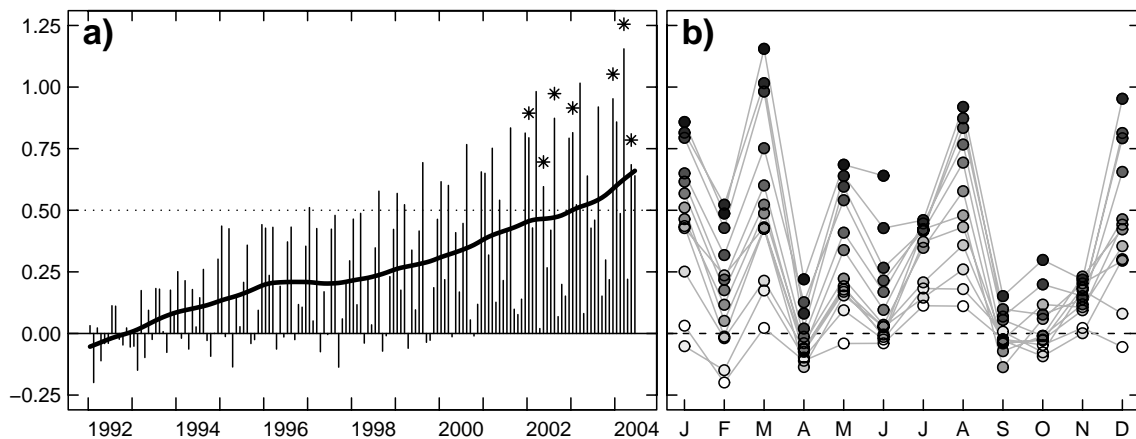
Figure 5.5: Northern Switzerland monthly differences between anomalies based on the 61–90 definition and the latest 30-year running period. a) Time series for the period January 1992 to June 2004. The thick solid line gives a spline smoothed estimate of the mean difference. Months with different signs in the two normal periods and an absolute difference larger than 0.5 K (dotted line) are indicated by asterisks. b) As a), but stratified for the months of the year. More recent observations are darker, i.e. 1992 anomaly differences are white, 2004 differences are black. Grey lines connect the months of the individual years. Units: Kelvin.

Figure 5.4 shows the data presented in Figure 5.3 using a standardized MSC plot. There are large similarities between the two figures. However, in contrast to the absolute plot the ranges of uncertainty in the standardized plot are now comparable for both, seasons and geographical regions. Moreover, the standardized decrease in winter variability is larger in southern than in northern Switzerland. As already indicated in Figure 5.3, the recent summer signals differ more clearly form the 61–90 values than the winter signals, even for the periods not including the extreme summer 2003 yet. This is a hint that statistical climate change detection over Switzerland might be easier in summer than in winter, see also (Scherrer et al., 2005). These findings agree with detection and attribution studies over Europe (e.g. Spagnoli et al., 2002; Klein Tank et al., 2005).

5.3.2   Recent monthly anomalies in Switzerland

From Figures 5.3 or 5.4 the PPA compared to the 61–90 normal can be determined. In northern (southern) Switzerland the values of the latest 30-year windows (1974/5–2003/4) are ~0.73 (0.74) for JJA and ~0.72 (0.76) for DJF respectively. Both are clearly above the desired value of 0.5. The implication of this finding is illustrated in Figure 5.5a. Shown are the differences between the monthly anomalies based on the 61–90 normal and the anomalies based on the corresponding Latest 30-year Running Normal (LRN) for all months from January 1992 to June 2004. The smoothed differences increase almost linearly from 0 K in 1992 to ~0.75 K in 2004. From 2001 onwards there was not a single month with a 61–90 anomaly smaller than the anomaly based on the LRN. For illustration the months where the difference between the 61–90 normal and the LRN is larger than 0.5 K and the sign of the resulting anomaly is additionally inversed are highlighted by an asterisk. All seven cases occur in the years 2002 to 2004 and the 61–90 anomalies are 0.6 to 1.2 K larger than the LRN anomaly. An illustrative example is March 2004 where the 61–90 anomaly suggests a marginally positive anomaly of about +0.1 K which would have been characterised as

"normal" or "average". In contrast the LRN anomaly suggests a negative anomaly of -1.0 K which would have been termed "below normal". Figure 5.5b depicts the anomaly differences stratified by months of the year. For most months the differences increase almost monotonically from one year to the next. For the months March, December, August and January the differences have reached values in the order of 1 K. In April and the autumn months September, October and November the differences between 61–90 and LRN based anomalies remain small, but are also positive. This lack of difference can be directly interpreted as lack of trend in these months.

The LRN PPA values with respect to the 61–90 normal can be used to quantify whether the LRN period normal is different from the 61–90 period normal. In Table 5.2 PPA values are given for each month separately. Significant differences in terms of PPA (95% level) are found for seven out of the twelve months, namely all summer months (June, July and August), two winter months (December and January), two spring months (March and May) but no autumn months.

Table 5.2: 1973–2002 northern Swiss monthly PPA values with respect to the 61–90 normal. Significant differences on the 95% level are shown in bold.

JAN	FEB	MAR	APR	MAY	JUN	JUL	AUG	SEP	OCT	NOV	DEC
0.65	0.59	**0.71**	0.53	**0.65**	**0.63**	**0.62**	**0.76**	0.52	0.55	0.54	**0.7**

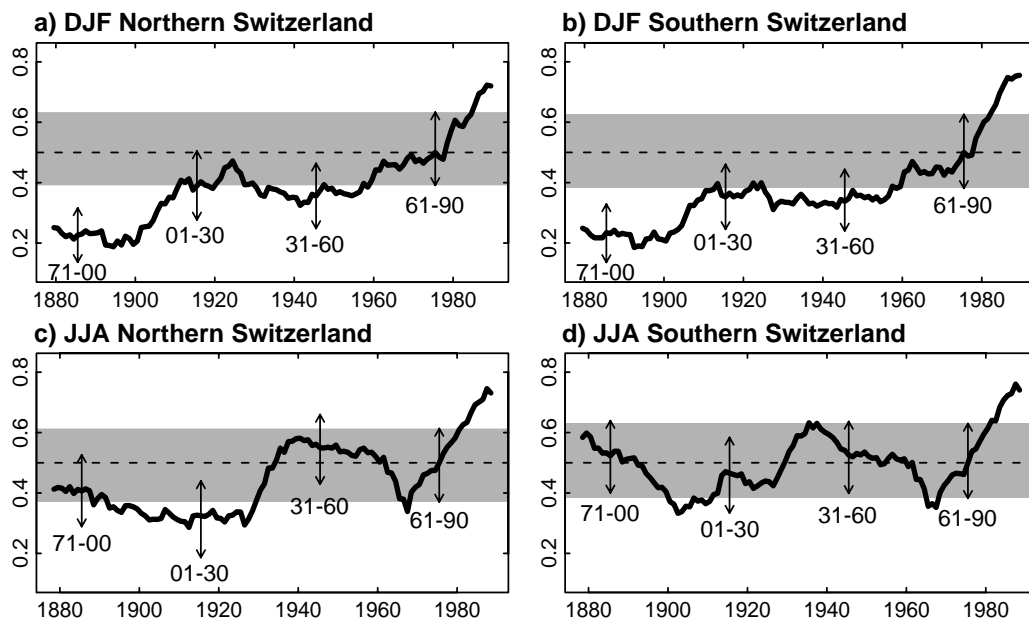*Figure 5.6*: PPA values from running 30-year periods for DJF (a, b) and JJA (c, d) northern (a, c) and southern Switzerland (b, d) 2-m temperature time series. The 61–90 value is 0.5 per definition. The bootstrapped 61–90 PPA 5–95% confidence range is shown as grey band. The PPA 5–95% confidence intervals of the 1871–1900 (71–00), 1901–1930 (01–30) and 1931–1960 (31–60) WMO standard normal periods are shown as double-headed arrows.

5.3.3 Updating normal periods

The results presented above prompt the question of adapting the normal period, such as an update to 1971–2000 or the introduction of a LRN concept in order to keep up with climate change. To investigate this issue it should be first assessed how representative the 61–90 normal period has been in the past. Such an analysis is also useful in the context of climate change detection (Hegerl et al., 2000; Stott et al., 2001).

In Figure 5.6 PPA values are shown as a function of time for all possible 30-year running windows with respect to the 61–90 normal ($PPA_{61-90} = 0.5$). Values for both DJF and JJA season are given and the associated 61–90 PPA 5–95% confidence range is shown. In analogy to the results from Figures 5.3 and 5.4 the latest 30-year values are clearly outside the 61–90 confidence range for both seasons and both Swiss regions. For the winter season, large parts of the time series are located outside the 61–90 confidence intervals. Similar strong deviations as in recent years occur in the winters of the late 19th and the beginning of the 20th century. The statistically significant deviations are in opposite direction (PPA $\ll$ 0.5; cf. also Figures 5.3 and 5.4 panels a/b). The DJF normal confidence ranges for the 1871–1900 and the 61–90 period are completely separated for both the northern and southern Swiss series (Figure 5.6a/b). For the summer season the 61–90 definition is more representative for the entire period than in winter, in particular the negative DJF deviation in the late 19th century is completely absent (Figure 5.6c/d). Interestingly, the 1931–1960 normal definition would have been more appropriate than the 61–90 normal period in describing the recent JJA periods. Table 5.2 shows that on a monthly basis all 12 months exhibit PPA values greater than 0.5 in recent years. This has never been observed in the past 140 years which makes the current situation unique in the record.
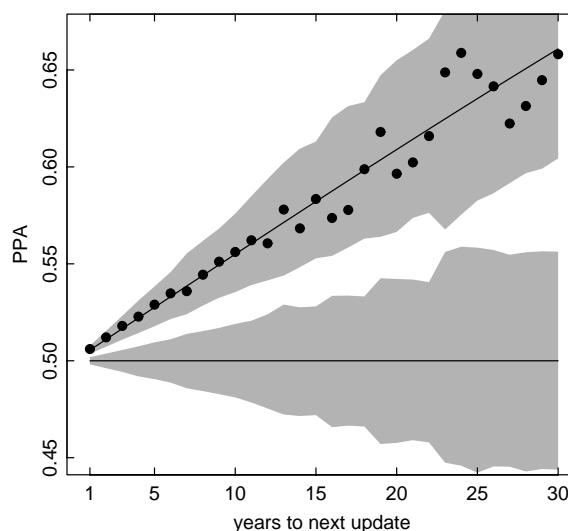
Figure 5.7: PPA values averaged over all 30-year update windows of a 120 year time series as a function of "number of years to next update of the normal period". The observed averages of the northern Swiss series from 1871–1990 are shown as black dots. Also given are the median (horizontal black line) and 5 to 95% confidence range of a white noise series (horizontally fanning grey band) as well as the result for a white noise series with the same trend as the observed series (inclined black line) plus its confidence range (inclined fanning grey band).

Figure 5.8: Isolines of PPA as a function of the "number of years to next update of the normal period" and relative trend (in standard deviations per 10 years). Line interval is 0.1. Dotted isolines indicate some half-intervals. The horizontal lines show the effect o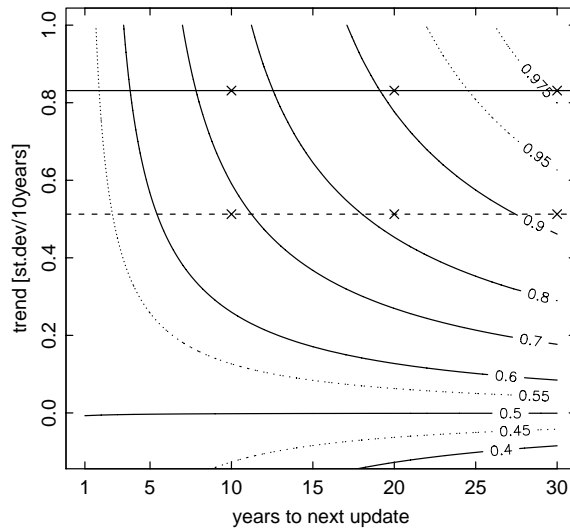n PPA for a trend equal the annual linear Swiss temperature trend of the 1974–2003 period (solid) and the 1961–1990 period (dashed).

From a scientific point of view it is obvious that more regular updates of the normal period would give more realistic PPA values, see also (WMO, 1967; Guttman, 1989). Whether such updates are feasible and make sense in a broader context is a different question.

The number of years until the next update of a 30-year normal period is discussed using Figures 5.7 and 5.8. Let t be the year in the record where an update takes place and x is the number of years until the next update of the normal period. Then $PPA_t(x)$ is the probability for the period (t-29,t) with respect to the normal of the 30-year interval (t-x-29,t-x). For a 120 year long white noise series $E(\overline{PPA}(x))$, the expected average over all years t is 0.5 for all update frequencies x = 1...30 years. The Monte-Carlo based 5 to 95% confidence range however increases linearly from almost zero for x = 1 year to roughly ±0.05 for x = 30-years (Figure 5.7). Thus, for a 120 year temperature record without autocorrelation and no intrinsic trend, PPA values between 0.45 and 0.55 can be expected when updating only every 30-years.

Also shown in Figure 5.7 is $\overline{PPA}(x)$ based on the northern Swiss annual temperature series for the time period covering four consecutive WMO standard normal periods from 1871 to 1990 (black dots). The values are clearly outside the white noise confidence range although the most pronounced trends observed in the record after 1990 are not included in the series used here. $\overline{PPA}(x)$ increases from values around 0.5 for updates every year to 0.66 for updates only every 30-years. The scatter increases with increasing x since the sample number of normal periods in the 120 year period decreases from 120 (for updates every year) to four (for updates every 30-years). The large difference between the white noise example and the observational time series is caused by the nonstationarity (i.e. the trend) in the data. This can be shown by repeating the white noise example with the added observed overall linear trend (i.e. ~0.9 K/100 years for the 1871–1990 period). The median agrees

very well with the results from the observations (compare the dots and inclined black line in Figure 5.7a). All averages from the observations lie within the 5–95% of the white noise with added trend series PPA values confidence range. The confidence ranges of the pure white noise and the white noise with added trend do not overlap. Hence, for large x, even a moderate trend (<1 K/100 years) can increase the PPA substantially. The trend over the whole observational record seems to be large enough to overcompensate the influence of decadal scale variability. Similar results were found for red noise processes mimicking decadal variability with and without additional trends (not shown).
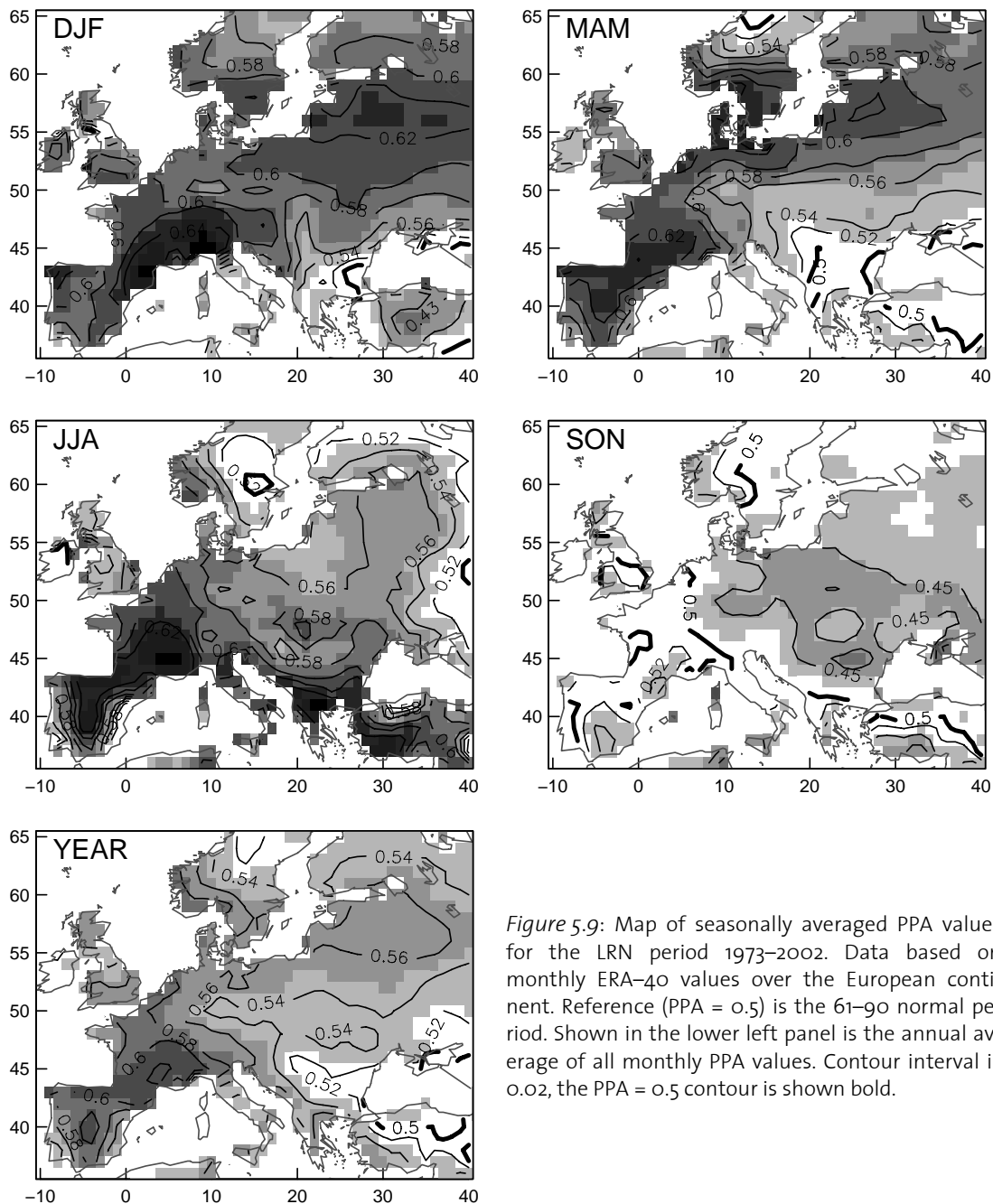

Figure 5.9: Map of seasonally averaged PPA values for the LRN period 1973–2002. Data based on monthly ERA–40 values over the European continent. Reference (PPA = 0.5) is the 61–90 normal period. Shown in the lower left panel is the annual average of all monthly PPA values. Contour interval is 0.02, the PPA = 0.5 contour is shown bold.

In Figure 5.8 the "error" in terms of PPA that is made without updating is shown as a function of the number of years to the next update of the normal period and the relative trend (standard deviations per 10 years) in the period. The horizontal lines indicate the observed annual trends in Switzerland for the 61–90 period and the "extreme trend" period 1975–2004. If the 61–90 (1975–2004) trend continues with the same magnitude and the normal is not updated, then the PPA reaches 0.68 (0.75) after 10 years, 0.82 (0.91) after 20 years and 0.92 (0.98) after 30-years. These numbers demonstrate that from a pure anomaly interpretation point of view it would be best to update normal periods "as often as possible" in a changing climate. Unfortunately even this may not be sufficient for extreme periods. For the northern Swiss temperature between January 1992 and June 2004 the number of months with positive anomaly is reduced from 78% (using the 61–90 normal) to 69% (using the LRN). Although this is a reduction of 9%, the running normal is still 19% above the desired value of 50%.

5.3.4 Recent probability for positive anomalies over Europe

In this section the PPA analysis is extended to a European domain. Monthly PPA values were averaged arithmetically to obtain seasonally averaged PPA maps for the LRN available in ERA–40 (1973–2002, Figure 5.9). For DJF the highest seasonally averaged PPA values are found over Eastern Spain, Southern France, the Alpine region and over western Russia. The few regions with values less than 0.5 are over parts of Bulgaria, Romania and the entire Turkey. For MAM the values are slightly less pronounced. Maxima are found over Spain, France as well as over the Netherlands, Northern Germany and Southern Scandinavia. The lowest values around 0.5 are found over South East Europe and Turkey again. For JJA all regions except some isolated grid points in Sweden and Southern Russia show PPA values greater than 0.5. Maxima (greater than 0.6) are found around the northern Mediterranean coast, in Spain, France and the western Alps. The SON season exhibits a completely different pattern than the three other seasons. PPA values are almost everywhere around 0.5 or somewhat lower (especially in Eastern Europe). This result is consistent with no or even negative temperature trends in fall during the 1976 to 1999 period as found by Klein Tank et al. (2005). Apart from SON, overall PPA values are greater than 0.5 for most of the European land area. The seasonal characteristics are consistent with the homogeneous Swiss series discussed above (cf. Figure 5.5b).

As for the Swiss temperatures (Table 5.2) the number of months inconsistent with the 61–90 normal period is calculated and plotted for every grid point (Figure 5.10). As confidence interval boundaries the 10 and 90 percentiles are used. This rather liberal interval was chosen since the two periods 61–90 and 1973–2002 overlap by 60%. Thus, the deviation from the 10 to 90% interval represents already substantial changes in the distribution. The general patterns are similar to the PPA maps in Figure 5.9. In particular, the SON season does not show many differences between the normal periods. For the other seasons, there are many grid points at which 1, 2 or even 3 months of a season are located outside the 61–90 confidence intervals. Note that the period used here does not include the extraordinary summer 2003.

Considering the sum of all 12 months of the year, 92% of all grid points show at least one month with values greater than the 90th percentile (61–90) confidence limit (Figure 5.10 lower-most panels). For most grid points, this holds true for two to five months. The most frequent value is five months (21% of the European land area).
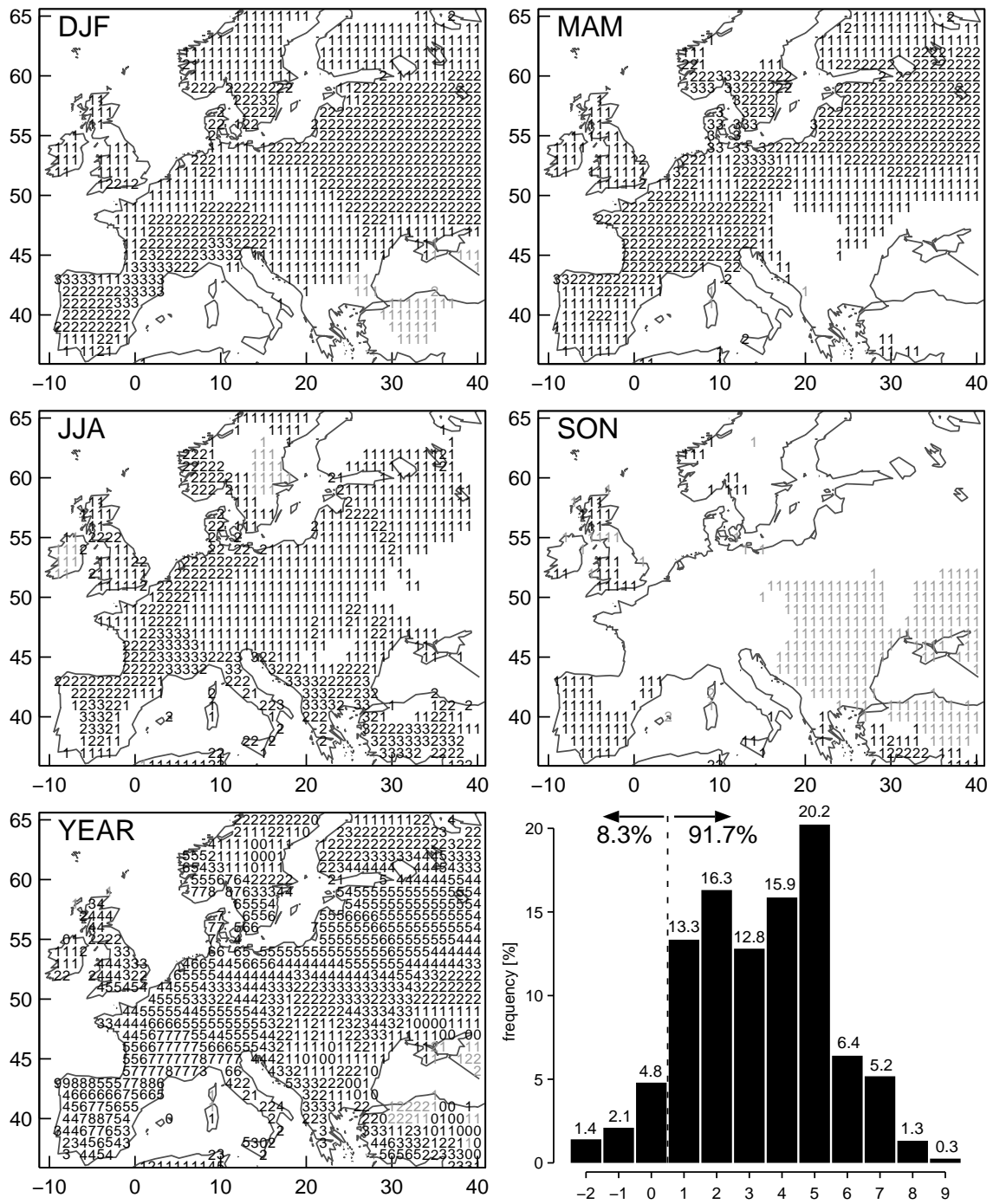
Figure 5.10: Number of months of the year in the LRN period 1973–2002 that are outside the 10–90 percentile confidence range given by the 61–90 period PPA. A value of 3 corresponds to a season with all months outside the confidence range. The number of months above (below) the confidence range is printed black (grey), zeros are omitted in the seasonal plots. The area-weighted frequency statistics for the whole year is shown as a histogram in the lower right panel.

In some regions of Spain, Southern France and Southern Scandinavia the PPA values of seven to nine months are not in line with the 61–90 normal. There are a few regions in South Eastern Europe and Turkey where most of the months are still consistent with the 61–90 normal. This agrees with findings of no clear trends in these regions (Kadioglu et al., 2001; Klein Tank et al., 2005).

5.4   Discussion and Conclusions

This study discusses problems of the concept of normal period based anomalies arising from climate variability and ongoing climate change. The widely used WMO 1961–1990 (61–90) standard normal period is compared to other consecutive 30–year normal periods in detail. The focus is on the temperature distribution in Switzerland and on the European continent. Other climate elements such as precipitation as well as problems arising when quantifying extremes are not considered. The differences between the normal periods can be expected to be even stronger at the tails of the distributions (Katz and Brown, 1992), but the changes of the mean values are communicated much more often and perceived as such more strongly by the public.

Results show that observed Swiss temperature in the last decade exhibit characteristics never found in the last 140 years. Absolute trends are greater in winter than in summer, but due to the smaller interannual variability the summer months exhibit higher statistical significance. The autumn months September, October and November show small trends and are still close to the 61–90 conditions. The recent strong temperature trends led to a high number of months with positive anomalies. For seven out of the twelve months, the last 30-years are statistically inconsistent with the 61–90 normal. Recent anomalies using the 61–90 normal as reference period are up to 1.25 K higher than those based on the last 30-years.

Similar results are found for the European continent. Most regions show two to five, southern France, parts of Spain and southern Scandinavia even seven to nine months statistically inconsistent with the 61–90 normal period. Again the autumn months are still close to the 61–90 conditions.

The significant changes may be only of minor relevance for studies where normals are used as a reference period to do direct comparisons, e.g. between data sets of different countries or in model intercomparisons. For applications where deviations from the normal are quantified without quoting the reference period the recent temperature trends make an interpretation difficult. The number of months with positive anomalies are very likely to increase strongly with the ongoing climate change (cf. Scherrer et al., 2005) and reinforce the problems described in this study.

Unfortunately there are no simple solutions to the problem presented. The traditional temperature normals are well established, easy to communicate, worldwide in use and provide a common basis for the determination of past climate variability. There is also no simple or obvious alternative to the current methodology. Running normals as investigated in this study are difficult to implement and mitigate the trend problem to a certain degree only as long as the trends are relatively small (smaller than those expected in the 21st century). A shortening of the period length to determine normals might not be a good idea either since a normal should be based on a relatively large sample in order filter out short term fluctuations. A potentially useful approach might be to supplement the normal values

with an additional trend information for the corresponding period. Official recommendations should be found in broader discussions on an international WMO level considering the influences on the largest possible number of applications and including other climate elements.

Appendix

A correct representation of trends in a time series is crucial for an adequate determination of the Probability to observe a Positive temperature Anomaly (PPA) values. In this section PPA values of four northern Switzerland temperature datasets are compared using monthly resolution for the period 1961 to 2002. Beside non-homogenized and homogenized station based series, ERA–40 47°N/7°E and CRUTEM2v 47.5°N/7.5°E grid point data are used. The differences are illustrated for the 1973–2002 period with respect to the 61–90 period, i.e. $PPA_{61-90} = 0.5$. Figure 5.11a shows that the standardized mean temperature changes are similar for the four datasets. The homogenous series shows the largest changes in mean for most months and differs strongest from the other three datasets, which show similar changes among each other. The differences are largest in May, June, September and October.
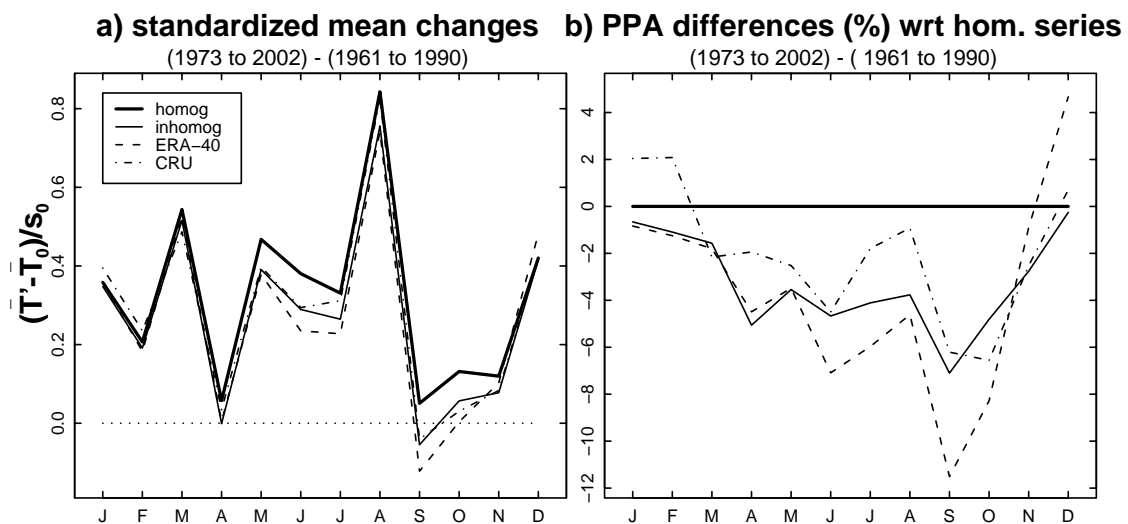
Figure 5.11: a) Standardized changes in 2-m mean temperature for the 1973–2002 period with respect to the 61–90 reference period for the homogenized station based series (bold solid), inhomogeneous station data (thin solid), ERA–40 (dashed) and CRUTEM2v (dash-dotted). The numbers are shown for all individual months of the year. b) PPA differences (in percent) of the inhomogeneous station data (thin solid), ERA–40 (dashed) and CRUTEM2v (dash-dotted) with respect to the PPA values using the homogenized station based series (zero line).

Figure 5.11b depicts the $PPA_{1973-2002}$ differences (in percent) with respect to the homogeneous numbers (values zero per definition, horizontal straight line). The results are similar to the standardized mean changes. ERA–40 and CRUTEM2v follow more closely the inhomogeneous than the homogeneous series. With the exception of December in ERA–40 and December/January/February in CRUTEM2v the PPA values are consistently smaller than the homogeneous ones. The underestimation is generally smaller than 5–6%. The largest underestimation (up to 11% for ERA–40) is found in summer and autumn. Overall the mean change and PPA difference reported are comparatively small and predominately negative.

Supplementary material

Efficiency and biases in simple estimations of standard deviation for small sample sizes

A good estimate of the variability of a time series is a crucial parameter for most studies in climate sciences. Several statistical properties are important to qualify a good estimator of variability. It should be unbiased, robust and resistant against outliers. Also well known for a long time in statistics is the desirable property called efficiency of an estimator. There are several problems with these desirable properties for small sample sizes ($N \ll 30$). Many estimators of variability are negatively biased, i.e. underestimate variability. These biases are in general only of importance for very small sample sizes (<10, cf. Figure 5.12). Small relative efficiency and biases in combination with relatively small sample sizes (e.g. 30, as used in climate normals) however can have a substantial influence on the estimations of moments. In those cases (and if outliers can be excluded) it can be advisable to use a less robust measure in favour of a more robust but less efficient one.

First we define relative efficiency, then compare simple estimates of standard deviation using small sample sizes and compare with debiased estimators.

Definition of relative efficiency

Textbooks of statistical inference define the statistical efficiency of an estimator as the ratio of the minimum possible variance to the variance of the estimator (e.g. Garthwaite et al., 2002). In our context we are interested in the relative efficiency of an estimator with respect to another estimator based on a different approach. If T_1 and T_2 are estimators for the parameter θ, then most people agree that T_1 is more efficient than T_2 if its mean squared error (MSE) is smaller for at least some value of θ and the MSE does not exceed that of T_2 for any value of θ. The relative efficiency RE is defined here as:

$$RE(T_1, T_2) = \frac{E\{(T_1 - \theta)^2\}}{E\{(T_2 - \theta)^2\}}, \qquad \text{(Eq.5.2)}$$

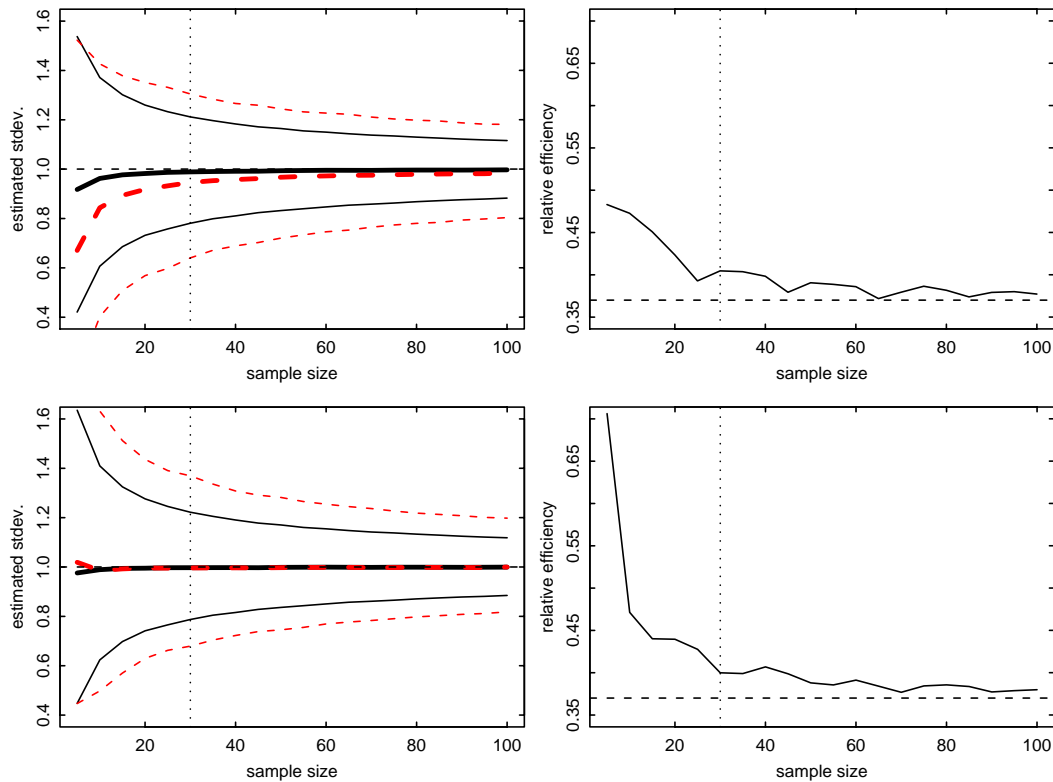where $E\{...\}$ stands for the expected value.

Figure 5.12: Left panels: Estimated standard deviation confidence intervals of 100'000 white noise samples with target standard deviation 1 as estimated by square roots of sample variance (solid) and IQR/1.349 (dashed) for different time series lengths. Shown are the median (bold), the 5th and 95th percentile of the estimated standard deviations. Right panels: relative efficiency of IQR estimation with respect to maximum likelihood standard deviation estimation. For both panels, a vertical dotted line indicates the classical 30-year normal. Top panels: Estimates using standard algorithms, bottom panels: Estimates using debiased measures (see text for details).

Estimating standard deviation using the maximum likelihood estimator and inter quartile range (IQR)

In this section a prescribed standard deviation of a normal distribution is estimated using two different estimators. The first is the square root of the sample variance and the second the estimation via IQR/1.349, where IQR $= q_{0.75} - q_{0.25}$ and q are the sample quantiles exceeding the proportion 0.25 and 0.75 of the data (see e.g. Wilks, 1995). Quantiles are determined using the default quantile algorithm in the free statistics software package R (R, 2005). 100'000 Monte Carlo samples of white noise time series with mean zero and standard deviation 1 and sample size 5 to 100 have been used. In the top left panel of Figure 5.12 the estimated standard deviation and the 5th to 95th percentile estimation range are shown for the square root of sample variance (solid) and the estimation using the more robust IQR/1.349 estimation (dashed). As well known in literature the square root of sample variance estimator is negatively biased. For sample sizes >10 the effect is negligible (Figure 5.12, upper left panel). The estimation range uncertainties decrease from >±50% (sample size 5) to ~±10% (sample size 100).

The estimations based on IQR/1.349 (dashed) show a substantially larger bias not only for very small sample sizes (<10) but also for sample sizes of 30 (bias >5%). The bias problem can be overcome quite easily as will be shown below. More fundamental is the fact that the 5th to 95th percentile estimation range is substantially wider than for the square root of sample variance estimate. Excluding very small sample sizes (<10), the effect is only weakly dependent of sample size. The top right panel of Figure 5.12 shows the relative efficiency of the IQR/1.349 estimator with respect to the square root of sample variance estimation. RE is larger for low sample sizes but approaches the asymptotic relative efficiency (ARE) of 0.37 (see e.g. Staudte and Sheather, 1990) relatively quickly. For a sample size of 30 a relative efficiency of ~0.40 is found. The straight forward interpretation is that an estimation of standard deviation of a normal period of 30-years by IQR/1.349 is only as efficient as estimation by standard deviation with sample size 0.4x30 = 12. Similarly, RE values for other robust estimators of e.g. measures of location can be found. For the median of a normal distribution with infinite sample size the ARE is 0.637 and RE is ~0.67 for sample size 30. There are more efficient robust alternatives discussed in statistical literature (see e.g. Pearson, 1920; David, 1998) but this is beyond the scope of this supplementary material.

Using debiased estimators

As demonstrated in Figure 5.12 biases can be substantial, especially when using blindly functions of statistical packages that need to estimate quantiles. There are many ways how sample quantiles can be determined, some are biased, others are not (Hyndman and Fan, 1996 and references therein). Here an unbiased estimate of quantiles (type = 8 in the R statistics package, version >2.0.0) is used. Also the square root of sample variance estimates can be biased corrected using a factor known as c_4 factor in statistical literature, hence

$$s_{unbiased} = \frac{s_{biased}}{c_4} \text{, where } c_4 = \left(\frac{2}{N-1}\right)^{\frac{1}{2}} \frac{\Gamma\left(\frac{N}{2}\right)}{\Gamma\left(\frac{N-1}{2}\right)} \qquad \text{(Eq.5.3)}$$

and Γ stands for the gamma function and N is the number of samples (cf. Wilks, 1995).

The bottom left panel of Figure 5.12 shows that the bias has indeed vanished for both estimates. There is no crucial impact on the relative efficiency (right panel).

Conclusion

Calculating "good" estimations of variability measures for small sample sizes (N ≤ 30) is difficult. Most standard methods to determine standard deviation are biased. More important however is the effect of inefficiency which can reduce the "effective sample size" N' considerably (e.g. N' = 12 for N = 30 and IQR/1.349 estimation). It is crucial to distinguish between the statistical properties of robustness (which means to be insensitive against outliers) and efficiency. A lot of well known robust measures are relatively inefficient and therefore (in case of no outliers) the less robust alternatives (e.g. the maximum likelihood estimate) may be preferred to determine normal-consistent estimates of standard deviation.

Chapter 6

European temperature distribution changes in observations and climate change scenarios

Simon C. Scherrer[1], Christof Appenzeller[1], Mark A. liniger[1] and Christoph Schär[2]

[1] Climate Services, Federal Office of Meteorology and Climatology (MeteoSwiss), Zürich, Switzerland
[2] Institute for Atmospheric and Climate Science, ETH Zürich, Zürich, Switzerland

Abstract

Changes in the distribution of seasonal surface temperature are investigated in central Europe using observations between 1961 and 2004 and a set of IPCC SRES A2 and B2 climate change simulations. A piecewise detrending methodology is used to distinguish between intrinsic and trend-induced variability changes. Mean and interannual variability changes are standardized with the intrinsic variability of the respective dataset. Within this framework, the strongest temperature changes in mean since 1990 are found for the summer season, both in observations and climate models. Estimates for variability changes show a weak increase (decrease) in summer (winter), but these changes are not statistically significant at the 90% level. For the 21st century all climate scenario runs suggest large relative increases in mean for all seasons with maximum amplitude in summer. Although changes in relative variability vary substantially between the models, there is a tendency for increasing (decreasing) variability in future summers (winters).

6.1 Introduction

In Central Europe eight of the ten warmest years in the 1851–2004 temperature record have been observed from 1989 to 2003, consistent with the increasing near surface temperatures on a global scale (Houghton et al., 2001; Jones and Moberg, 2003). Less clear is whether there are also changes in interannual variability (Houghton et al., 2001, p. 156), although the latter might be of importance in a socio-economic context (Kovats et al., 2004). Previous studies found indications for decreasing interannual variability in observational data

87

(Karl et al., 1995), whereas others report no changes or small increases (Parker et al., 1994; Räisänen, 2002). A recent climate modelling study found that European summer surface temperature variability might increase (by up to 100%) within the current century (Schär et al., 2004). Although there are substantial differences between models regarding the location and amplitude of this effect, these results have qualitatively been confirmed by several other models and studies (Meehl and Tebaldi, 2004; Brabson et al., 2005; Giorgi and Bi, 2005; Vidale et al., 2005).

In this paper, observed and modelled Central European land temperature distributions are investigated for each season separately. A temporal analysis of changes in mean and variance is conducted for recent observations and for scenarios of the 21st century. Relative changes in these quantities are compared between models and observations including the associated uncertainties.

6.2 Methodology

There are many different methodologies to quantify distribution changes, depending on both the parameter of interest and the space and time scales considered. For distributions described by large data samples, such as daily data, non-parametric quantile-based methods are more robust than parametric approaches (Ferro et al., 2005). For small data samples, such as seasonal mean temperature, moment-based methods are superior due to their higher statistical efficiency. For example, the estimation of the standard deviation from the interquartile range with a sample size 30 is only as efficient as its direct estimation with a sample size 12. Therefore we estimate mean ($\overline{T}$) and interannual standard deviation (s) of seasonal temperatures assuming a Gaussian behaviour. The moments are calculated for all possible contiguous (running window) 30-year periods available. The reference period is the World Meteorological Organization (WMO) 1961–1990 standard normal period if not indicated otherwise.

For Gaussian distributions, changes are described by a combination of a shift in mean (location) and/or a change in standard deviation (scale). Applying this simple conceptual model to real climate data can be difficult. For example high quality and homogeneous data are needed to avoid spurious shifts (see e.g. Begert et al., 2005). Another critical issue is the limited number of observations with which the climate space is sampled. This can result in considerable nonstationarities between 30-year windows (WMO, 1967; Scherrer et al., 2006a). These effects must be accounted for when making statements about changes in intrinsic variability as will be demonstrated below.

In order to properly compare observations against model results and the models among each other, standardized changes in mean $(\overline{T} - \overline{T}_0)/s_0$ and variability s/s_0 are used henceforth. Here the subscript 0 indicates the estimates based on the reference period. Plots with standardized Mean versus Standard deviation Change (referred to as MSC plots hereafter) are used to illustrate the changes in both parameters simultaneously (cf. Sardeshmukh et al., 2000; Scherrer et al., 2006a).

Time series with trends are not strictly Gaussian and the calculation of standard deviation measures using such data leads to a trend-induced inflation of variability as noted by Räisänen (2002) and Schär et al. (2004). The effect of a linear trend upon estimates of vari-

ability can be quantified by the ratio between the standard deviation s_t of the series with a superimposed linear trend of magnitude α per time step and the standard deviation s of the pure white noise series. The analytical derivation (see auxiliary material) shows that:

$$\frac{s_t}{s} = \left[1 + \gamma\left(\frac{\alpha}{s}\right)^2\right]^{1/2} \quad \text{with} \quad \gamma = \frac{N(N+1)}{12} \qquad \text{(Eq. 6.1)}$$

In this study the sample size $N = 30$ and therefore $\gamma = 77.5$. For Central European conditions, typical summer temperature trends are ~1–2 K for the last 30-years, and typical standard deviations are ~1 K. Thus, the inflation factors are in the order of 1.04–1.16. However, locally and for some specific periods the inflation can be much larger (cf. auxiliary material).

Figure 6.1 schematically illustrates the effect of variability inflation on time series, distributions and MSC plots. The period of interest is compared with the reference period, in general both having different trends. Figure 6.1a shows a case where the trend is constant over three consecutive 30-year periods. The distributions are broadened due to variability inflation. In the MSC plot no increase in variability can be detected since it measures changes with respect to the reference period. Figure 6.1b shows a case where the trends gradually increase from one 30-year period to the next. The distributions have different widths depending on their trends, which results in a variability change in the MSC plot. This effect needs to be corrected for when the focus is on changes in intrinsic variability. In this study piecewise detrending for both series (i.e. investigated 30-year period and reference period) is used to eliminate the influence of the trend on the variability estimates (cf. Figure 6.1c).
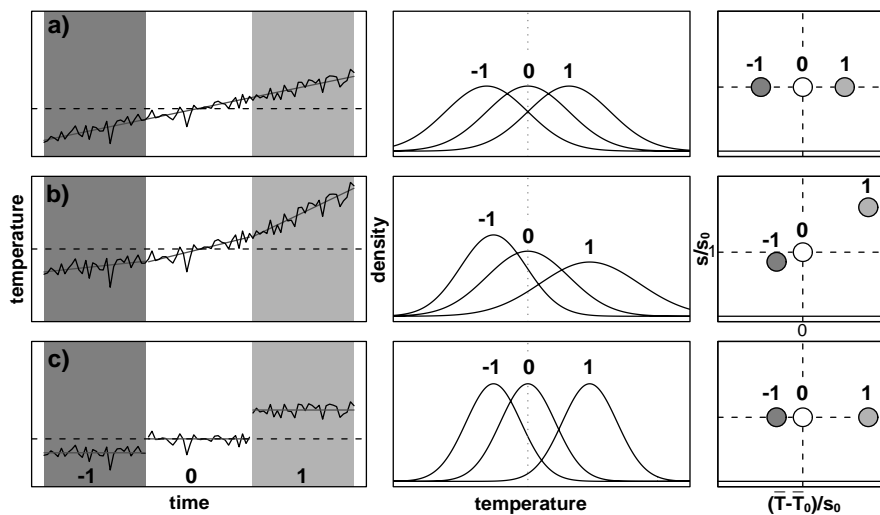
Figure 6.1: Schematic illustration of white noise climate realizations with constant intrinsic variability (reference interval 0). A constant (panel a) and an increasing trend (panel b) for the intervals I = -1, 0 and 1 is added. Shown are time series (left), interval dependent distribution functions (middle) and their representation in the MSC plot (right, see text for MSC definition). Panel c illustrates the piecewise detrending technique used in this study applied to the example in panel b.

Table 6.1: Models and scenarios used in this study. For details see Houghton et al. (2001).

model name	resolution	scenarios	availability	symbol
HADCM3	3.75×2.5deg	A2, B2	1950–2099	🔴
CSIRO-Mk2	R21	A2, B2	1961–2100	▼
GFDL-R30	R30	A2, B2	1961–2100	■
CCCma	T32	A2, B2	1900–2100	▲
CCSR/NIES	T21	A2, B2	1890–2100	◆
ECHAM4/OPYC3	T42	A2, B2	2000–2099	✖
NCAR PCM	T42	A2, B2	1980–2099	✖

6.3 Data and models

Two types of 2-m temperature datasets with seasonal resolution are considered. The first is the observed land-surface temperature dataset CRUTEM2v (Jones and Moberg, 2003). The second is a set of seven IPCC SRES A2 and seven B2 greenhouse gas scenario runs used in the third IPCC assessment report 2001 (available from `http://ipcc-ddc.cru.uea.ac.uk`). Ten of these scenarios cover the period 1961–2099, two are available for the 1980–2099 and two for the 2000–2099 period (Table 6.1). The region of interest is Central Europe, defined here as the model individual's land grid points in the area covering 3°W–27°E and 44°N– 55°N.

6.4 Observed changes since 1990

Figure 6.2 shows the standardized running 30-year estimates of mean and standard deviation for the observed Central European mean temperature from 1961–1990 onwards (i.e. the 30-year windows 1962–1991, 1963–1992, …, 1975–2004). Black (grey) lines show standard deviation estimates based upon raw (detrended) data. For DJF a more or less regular increase is found in the mean, corresponding to ~0.4 standard deviations of the 1961–1990 period (s_0 hereafter). A step-like decrease in variability of almost 20% occurs when the extraordinarily cold winter 1962/63 drops out of the running 30-year period (Scherrer et al., 2006a).

A bootstrap resampling technique is used to determine the 5–95% confidence range of the mean and standard deviation change (see shading). 5000 samples in combination with a kernel density estimator are used. The confidence range for the combined 30-year estimate is an ellipse-like area spanning ~±0.2–0.4 s_0 for both the mean and standard deviation. These values are used hereafter to determine the statistical significance of the results.

The 1975–2004 estimate for DJF just leaves the 1961–1990 confidence range. Larger positive mean changes are found for MAM (~0.5 s_0) and even larger ones for JJA (>0.75 s_0), indicating that the relative changes have been stronger in summer than in winter. Increasing variability is particularly found for the JJA season. An additional jump-like increase is observed if the extremely warm summer 2003 is included (last data point). The autumn season (SON) shows slightly negative changes in mean and no changes in variability (Klein Tank et al., 2005).
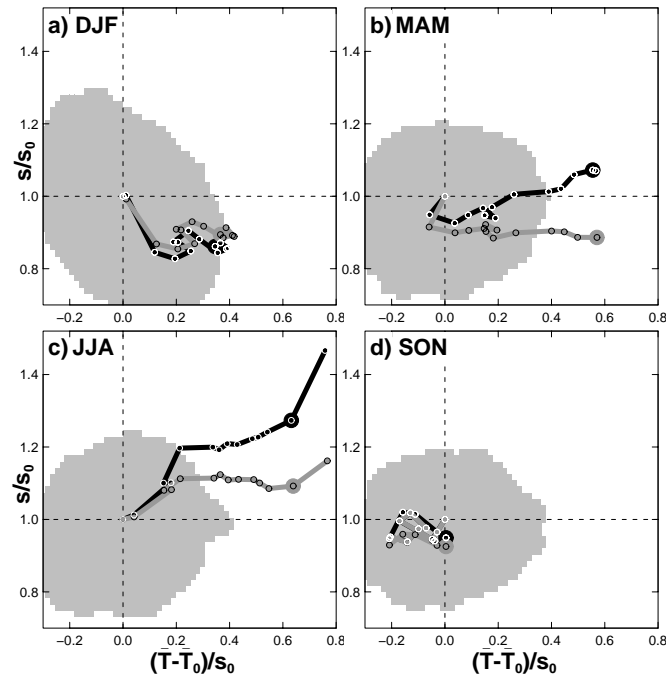
Figure 6.2: Seasonal MSC plots using running 30-year windows for Central European 2-m temperature after the 1961–1990 normal period. Data is shown till 2003 (2004 for DJF). The panels show raw (black line) and piecewise detrended data (grey line), the big black (grey) dots denote the estimates of the raw (detrended) 1974–2003 (1973–2002 for JJA) data. The approximate 1961–1990 5–95% confidence ranges of the raw data are shaded in grey.
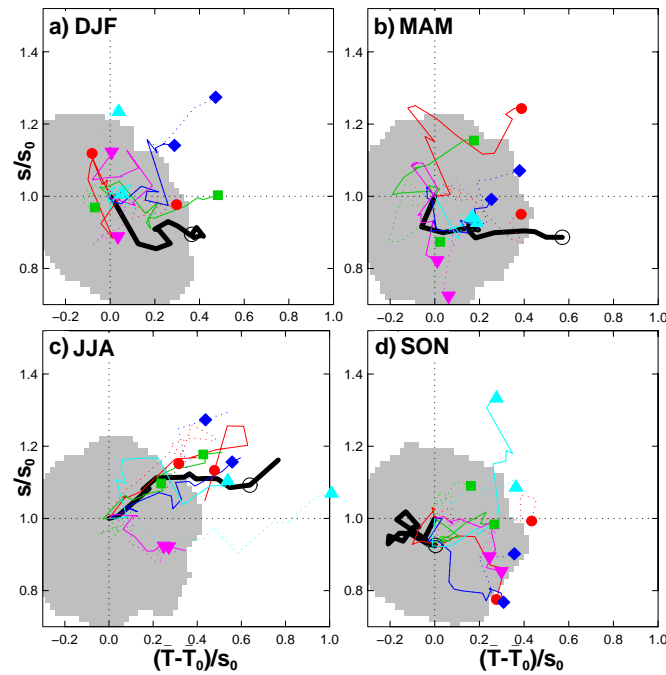
Figure 6.3: As Figure 6.2, but with five piecewise detrended IPCC SRES A2 (solid) and B2 (dotted) scenario runs for the same period. See Table 6.1 for symbol legend.

The differences between the analysis using raw or piecewise detrended data are small for DJF and SON (Figure 6.2, panels a/d). For MAM the moderate variability increase is reversed into a small decrease (Figure 6.2b). Most pronounced is the reduction of the variability increase for JJA from 20–50% to 10–15% (Figure 6.2c). This indicates that more than half of the observed variability increase is inflated due to the linear trend differences in the data.

6.5 Modelled changes from 1961 to 2003

The same analysis is now applied to climate simulations of the current climate using IPCC SRES scenario A2 and B2 runs for the years 1961–2003 (Table 6.1). In these runs the external forcing is prescribed in terms of time-dependent greenhouse gas and aerosol concentrations. This forcing is not identical to the observed 1961–2003 forcing, as for example discussed in Hansen and Sato (2001) and references therein. For both scenarios, the total radiative forcing from greenhouse gases plus direct and indirect aerosol effects with respect to the pre-industrial (1750) level amounts to 1.33 Wm^{-2} in the year 2000. By 2010, the A2 and B2 forcing amount to 1.74 and 1.83 Wm^{-2} respectively (Houghton et al., 2001, Table II.3.11, p. 823). The smaller A2 radiative forcing is due to a transiently higher aerosol load. In comparison, best estimates of the observed forcing in 2000 amount to ~1.8 Wm^{-2} (Houghton et al., 2001, p.393; Hansen et al., 2005).

Figure 6.4: As Figure 6.3 but for the future period 2005–2099. The black rectangle and the shading correspond to Figure. 6.3. The black (white) point denotes 1961–1990 (1975–2004) conditions, the coloured ones the last observational 30-year window estimates.

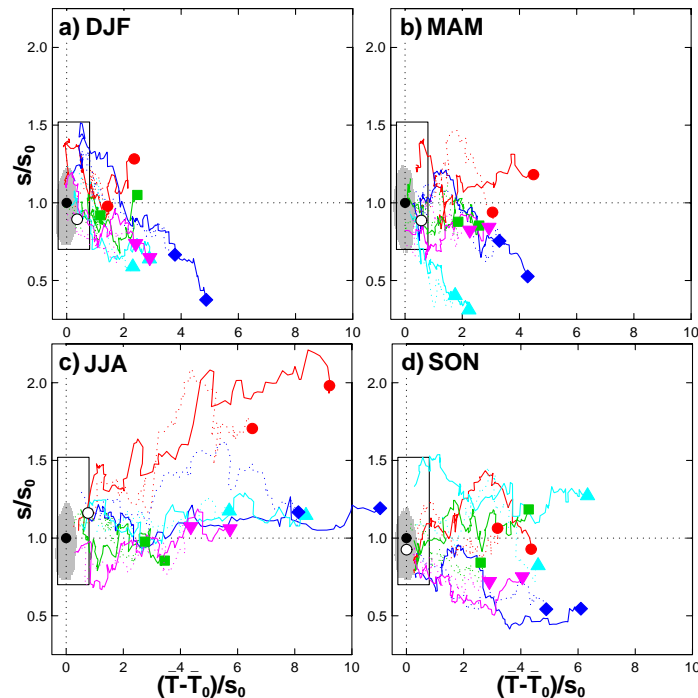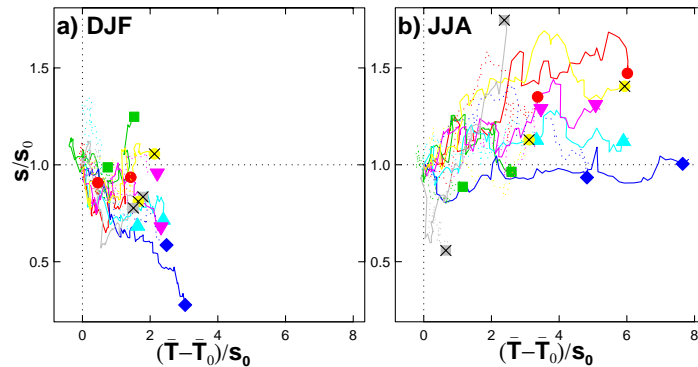*Figure 6.5*: As Figure 6.4 but for all models of Table 6.1 and the reference period 2000–2029.

Figure 6.3 shows the relative changes in mean and standard deviation for the periods 1961–1990 to 1975–2004 (DJF) and to 1974–2003 (MAM, JJA, SON) respectively. The analysis is performed using the piecewise detrending procedure. For JJA all models agree in showing a relatively large increase in mean which is somewhat smaller than observed. Four out of five model runs also indicate an increase in variability comparable to the observed one. For the other seasons there is less agreement among the models. The data are mostly within the large confidence ranges spanned by the observations. It is worth noting that several model runs show almost no changes in mean during the winter season (whereas the observations show a considerable trend), and all models suggest changes in mean during the autumn season (of the order 0.35 to 0.45 s_0), whereas no trend is found in the observations. The inter-model spread is larger than the spread between the two scenarios A2 and B2 of the same model. Changes in variability are less consistent and within the observed confidence ranges.

6.6 21st century scenario distribution changes

Piecewise detrended climate simulations are used to quantify the temporal evolution of the expected changes in mean and variability in a future climate. In Figure 6.4 results from five models are depicted for 2005–2099 relative to the 1961–1990 reference period. In Figure 6.5 results from all seven models are depicted for 2030–2099 relative to the 2000–2029 reference period. Overall the dominant changes are an increase in the mean values of the temperature distributions. By the end of the period (2070–2099), the largest relative changes in mean are found in summer (A2: 3.5–11 s_0, B2: 2.5–8 s_0) followed by autumn (A2: 4–6.5 s_0, B2: 2.5–5 s_0), spring (A2: 2–4.5 s_0, B2: 1.75–3.5 s_0) and winter (A2:~2–5 s_0, B2: 1–4 s_0). The inter-model spread in changes in mean is largest in summer.

Predicted changes in variability are less dominant and less consistent, both in terms of scenarios and models. Roughly three quarter of the values lie within the bootstrap range of the reference period uncertainties. In particular when considering all available model simulations (Figure 6.5), there is a tendency for increasing variability for both A2 and B2 runs in summer. This is consistent with recent studies using regional climate models (Giorgi et al., 2004; Schär et al., 2004; Vidale et al., 2005) and global climate models (Meehl and Te-

baldi, 2004; Brabson et al., 2005). For winter, decreasing variability is found for roughly two third of all A2 (B2) periods relative to 1961–1990. By the end of the period (2070–2099) changes are 0.35–1.3 (0.6–0.95) s_0 for A2 (B2). Predominantly decreasing variability is also found for spring season periods where $s_{2070-2099} = 0.3$–1.2 (0.4–0.95) s_0 for A2 (B2). The results for autumn are inconclusive although there is a tendency for decreasing variability with respect to the 2000–2029 period ($s_{2070-2099} = 0.5$–1.25 s_0). Again, the inter-model spread is larger than the spread between the A2 and B2 scenario results.

6.7 Concluding remarks

Temporal changes in Central European land temperature were examined in terms of relative changes in seasonal mean and interannual variability. Both observations and IPCC scenario runs have been scaled by their own intrinsic interannual variability to facilitate the comparison between the different datasets. Theoretical considerations show that the analysis of changes in variability requires a careful methodology, as temperature trends may imply an artificial inflation of variability. The effect is potentially large when distribution changes over a short time period are analyzed. We have corrected for this by piecewise detrending the time series.

Overall the analysis shows that the dominant changes in temperature distributions are an increase in the mean values in both observations and scenario runs, consistent with earlier studies (Houghton et al., 2001; Räisänen, 2002). In relative terms by far the largest change in mean is observed and predicted for summer. However, also the largest inter-model differences are occurring in the summer scenarios (by the end of the 21st century, the suggested warming varies between 3.5 and 11 s_0). These differences also imply different absolute temperature distributions.

With respect to changes in variability of observed seasonal mean temperature during the last decade, we estimate a decrease by ∼10% in winter, and an increase by ∼10 to 15% in summer. However, these changes are not statistically significant at the 90% level. For the 21st century, there is a large spread between the different climate change models analyzed. Overall, there is a tendency for increasing variability in summer and decreasing variability in winter and spring.

Finally note that this study uses a limited number of low-resolution global climate models to estimate future climate distributions on a continental scale. The estimates could be improved by using regional climate models or ensemble systems.

Auxiliary material

Derivation of the ratio between standard deviation of a white noise series with linear trend and standard deviation of the linearly detrended series

Let x be a discrete white noise time series of length N with mean zero and variance s_x^2. An additional linear trend αt (α is the trend per time step, t is time) is added to form an equation for a white noise series with "artificial" trend:

$$y_t = x_t + \alpha t, \text{ where } t = 1...N. \tag{Eq.6.2}$$

Note that the intercept has been set to zero since it drops out of the equations below. The mean $\overline{y}$ of the series y is

$$\frac{1}{N}\sum_{t=1}^{N} y_t = \frac{1}{N}\sum_{t=1}^{N}(x_t + \alpha t) = \frac{1}{N}\underbrace{\sum_{t=1}^{N} x_t}_{0} + \frac{\alpha}{N}\sum_{t=1}^{N} t = \frac{\alpha(N+1)}{2}. \tag{Eq.6.3}$$

The unbiased estimate of variance s_y^2 of the series y is defined as

$$\frac{1}{N-1}\sum_{t=1}^{N}\left(y_t - \overline{y}\right)^2. \tag{Eq.6.4}$$

Insertion of Eq.6.2 and Eq.6.3 into Eq.6.4 leads to

$$s_y^2 = \frac{1}{N-1}\sum_{t=1}^{N}\left(x_t + \underbrace{\alpha t}_{\text{trend}} - \underbrace{\frac{\alpha(N+1)}{2}}_{\text{mean}}\right)^2 = \frac{1}{N-1}\sum_{t=1}^{N}\left(x_t + \alpha t - \frac{\alpha N}{2} - \frac{\alpha}{2}\right)^2 =$$

$$\frac{1}{N-1}\left[\sum\frac{\alpha^2 N^2}{4} + \sum\alpha^2 t^2 - \sum\alpha^2 Nt + \sum x_t^2 - \sum\alpha^2 t + \sum\frac{\alpha^2}{4} + \sum\frac{\alpha^2 N}{2} + \sum\alpha N x_t + \sum 2t\alpha x_t - \sum\alpha x_t\right].$$

Using

$$\alpha N\sum_{t=1}^{N} x_t = 2\alpha\sum_{t=1}^{N} tx_t = \alpha\sum_{t=1}^{N} x_t = 0, \; s_x^2 = \frac{1}{N-1}\sum_{t=1}^{N} x_t^2$$

and further simplification leads to

$$s_y^2 = s_x^2 + \left(\frac{N(N+1)}{12}\alpha^2\right)$$

and therefore

$$\frac{s_y}{s_x} = \left[1 + \gamma \left(\frac{\alpha}{s_x}\right)^2\right]^{1/2} , \quad \text{where } \gamma = \frac{N(N+1)}{12} \qquad \text{(Eq.6.5)}$$

An example of the inflation factor using European land ERA–40 2-m temperature data is shown in Figure 6.6.
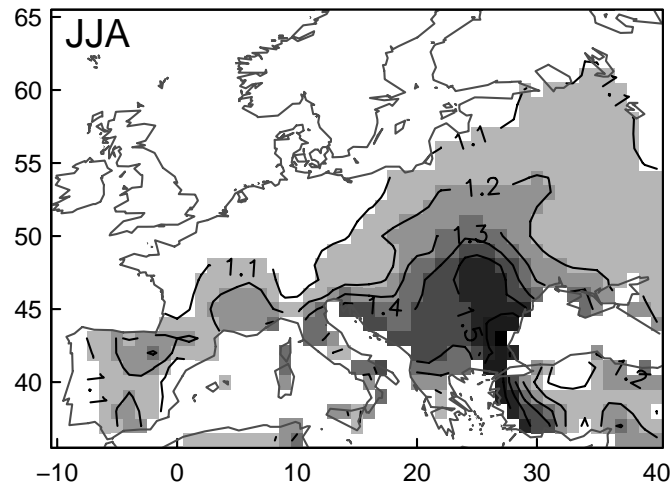

Figure 6.6: Map of inflation factor s_y/s_x as given in Eq.6.5 for ERA–40 JJA 2-m temperature data over Europe and the recent 30-year period 1973–2002.

Chapter 7

Conclusions and outlook

In this study the observed and projected interannual climate variability of the 20th and 21st century in the European and Alpine region has been explored. The relation between large-scale circulation variability and local climate variables has been investigated for different key parameters in a region with highly complex topography. Here, a brief summary of the main results and an outlook is presented.

7.1 Conclusions

The thesis focused on four distinct key issues related to interannual climate variability in the Alpine region. First, climate variability, trends and major patterns of Swiss Alpine snow pack have been analyzed and the relation with local climate elements and large-scale climate dynamics has been determined (Chapters 2 and 3). Second, the statistical relation between large-scale climate patterns and different indicators of atmospheric blocking in the Euro-Atlantic region has been worked out (Chapter 4). Third, the problems arising with the interpretation and perception of climate normals in a changing climate have been discussed from a user perspective (Chapter 5). Finally, near surface temperature changes in standardized mean and variability have been analyzed for central Europe using recent observational data and climate change scenario simulations (Chapter 6).

The key findings are as follows.

♦ Significant winter trends in Swiss Alpine snow pack are found for the end of the 20th century and stations below ~1300 m asl. It is shown that these trends can be mainly attributed to increases in local temperature. The local precipitation influence on trends is small. The North Atlantic Oscillation (NAO), as the major mode of large scale circulation variability over Europe, is found to be important in explaining the observed snow day trends, but not in explaining the large interannual snow day variability. The latter is primarily related to a flow anomaly pattern centred over southeastern Europe – resembling the classical Euro-Atlantic blocking pattern.
Swiss snow pack variability can be decomposed into three well separated patterns of variability. The leading pattern shows comparatively small geographical variations. It explains ~50% of total interannual variability. The second pattern distinguishes between the northern and southern slope of the Alps. It explains ~15% of total variability. The third pattern (explaining ~8% of total variability) shows large loadings in the lowlands and is height dependent. The relation to temperature and precipitation

depends on the specific snow parameter considered. Variability in seasonally averaged quantities that are determined by the conditions during the snow fall events is primarily related to local precipitation variability. Variability in parameters that are influenced by accumulation and ablation processes is related more to temperature or both temperature and precipitation variability.

♦ Three two dimensional atmospheric blocking indicators have been used to determine the relation between permanent high-pressure systems and the NAO. It is shown that the relation is not restricted to the North Atlantic region as previously reported. Over the European mainland, permanent high-pressure systems occur significantly more often during the positive NAO phase than in the negative phase. The sign change of the correlation between blocking and NAO from significantly negative values over the Atlantic Ocean to significantly positive values over Europe is well detectable with all three blocking indicators. An extension of the analysis to other major climate patterns shows that one phase of each of the Euro-Atlantic climate patterns is collocated with the region of maximum blocking frequency. The clearest separation between positive (negative) phases and blocking (no-blocking) situations is found for the second and third flow pattern.

♦ Ongoing climate change makes the interpretation and communication of climate temperature anomalies based on standard normal values (as defined by the World Meteorological Organization, WMO) increasingly difficult. The monthly anomalies based on the 1961–1990 normal are up to 1 K higher than those based on a running 30-year reference. For certain months of the year, the probability to observe a positive monthly anomaly increased from 50% for the 1961–1990 period to about 80% in the 1975–2004 period. In Switzerland, this change is statistically significant for seven of the twelve months of the year. The strongest changes of standardized temperature are found in the summer season. There are no changes in autumn. Very similar results are found throughout continental Europe where on average five months are outside the 1961–1990 10th to 90th percentile confidence limits. 92% of the area shows at least one month not consistent with the 1961–1990 normal.

♦ Changes in mean and variability of seasonally averaged quantities are key parameters in the current climate change debate. Both, observations of near surface temperature and present day IPCC climate change model output show the largest standardized changes in mean in the summer season. Estimates of the observed variability changes in recent observations show a weak increase (decrease) in summer (winter), which are not statistically significant at the 90% level. For the 21st century all model projections used in the third IPCC assessment report suggest large increases in standardized mean temperature in all four seasons. Largest changes in mean are found for the summer season. Although there are substantial inter-model differences in terms of changes in variability there is a tendency for increased variability in future summers and decreased variability in future winters.

7.2 Outlook

The results of this thesis contribute to a better understanding of some aspects of interannual climate variability in the Alpine region and its links with large-scale climate dynamics.

Further efforts are needed for an overall assessment of the links and relations between climate dynamics and local climate elements in a world with ongoing and accelerating climate change. In this section some aspects that merit further attention are presented.

Simple (mostly linear) methods have been used in this study to define the links between the phenomena and variables investigated. Other statistical methods such as generalized linear models, rotated PCA, cluster analysis or more advanced non-linear methods like neural networks could be used to define the links and to study the interrelations. Careful examination of alternative methods is important since non-linear extensions are not a priori superior to linear methods. An example in this context is non-linear principal component analysis (NLPCA) (see e.g. Monahan, 2000; Hsieh, 2001). In a recent study by Christiansen (2005), its usefulness has been questioned and it has been concluded that NLPCA is not recommended for detection of regime behaviour.
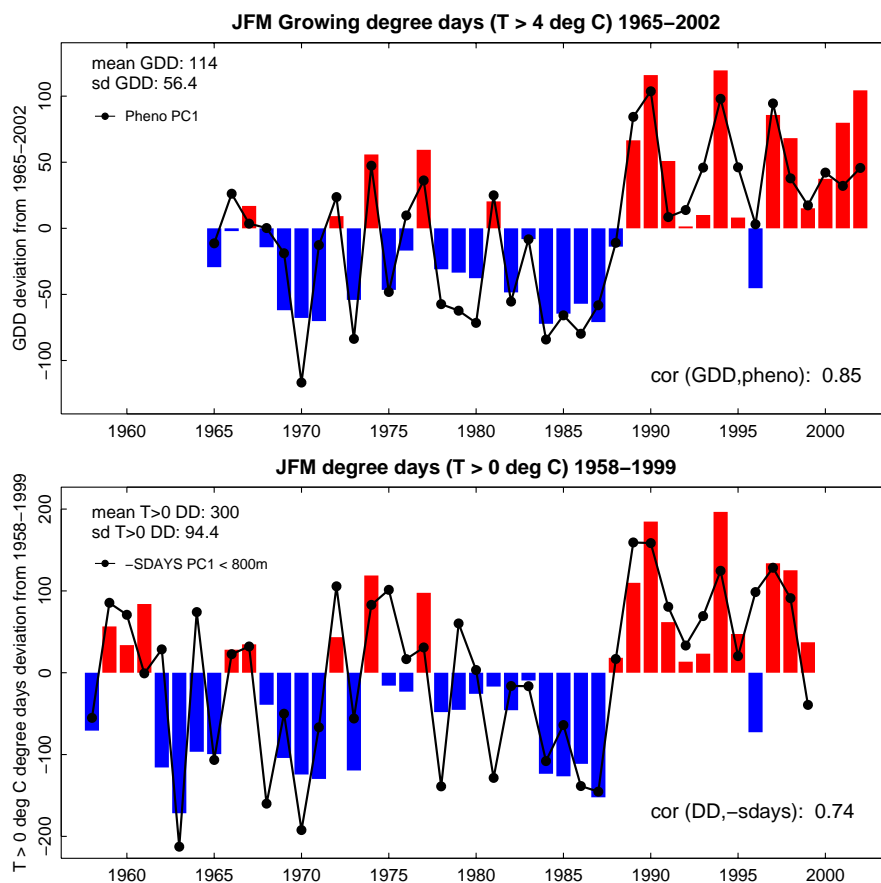
Figure 7.1: Interrelation between Swiss phenological phases and Swiss snow days with measures of degree days for the January, February and March period. Top panel: Growing degree days anomalies (histogram, summed temperatures for days where the daily mean exceeds 4 °C) and a multispecies index from ground observed phenological spring phases (line). For details see Studer et al. (2005). Bottom panel: Time series of degree days with a minimum temperature limit of 0 °C (histogram) and negative first principal component of snow days (line, for details see Chapter 3). Shown are deviations from long term means (see axis labels). Also shown are the correlation coefficient between the degree day measure and the first principal component time series of phenology and snow days. Further the mean and standard deviation of the corresponding degree day measure are indicated.
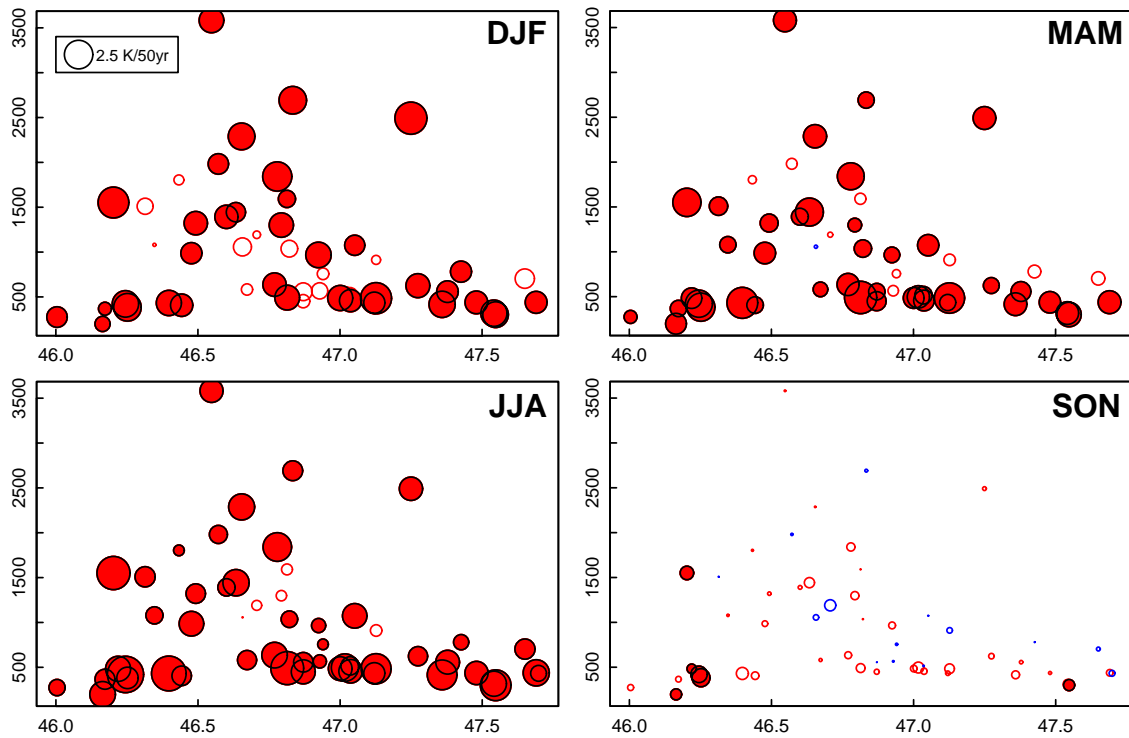
Figure 7.2: Linear trends in homogenized 2-m temperature measurements at 67 MeteoSwiss stations as a function of geographical latitude (°N, abscissa) and station altitude (m asl). The measurement period is 1958 to 2003. Shown are all four seasons: DJF (top left), MAM (top right), JJA (bottom left), SON (bottom right).

Climate in the Alpine region is definitely more than snow and temperature only. Many other climate elements or other derived variables used in applications (e.g. heating degree days) could be analysed in a similar manner. The links between local climate elements and other environmental variables can be of interest to a broad group of users (e.g. in the economic or agricultural sector). Swiss phenological phases as defined in Studer et al. (2005) are for example highly correlated with growing degree days (Figure 7.1). A similarly good relation is found for Swiss degree days with temperature limit 0 °C and the negative first Swiss snow day principal component analysed in detail in Chapter 3 of this thesis. The phenological series and the snow day series show large similarities. Note also the simultaneous jump-like increase for all variables (including the degree days) from 1987 to 1989. It seems plausible that the cumulated temperature measure determines the phenological phases and snow days to a substantial degree. For a more objective check of cause and effect Granger causality might be used (cf. Mosedale et al., 2005).

In Chapter 5 it was shown that temperature trends are different for different seasons, see also (Houghton et al., 2001; Klein Tank et al., 2005). Figure 7.2 shows 1958–2003 seasonal 2-m temperature trends for 67 homogenized temperature stations at different altitudes. In autumn no trends are found at most stations. The reason for this is not yet known. In agreement with findings in Pepin and Seidel (2005) no clear dependence of the trends with height is observed. A closer investigation of the relation between large-scale climate variability (e.g. in terms of blocking) and local temperature could be a promising approach to determine whether the missing autumn trends are due to compensating natural variability or not.

This study focuses on changes in the mean and variability. Climate change is definitely more than changes in mean. Changes in extremes are of interest for a large number of applications (cf. e.g. Zwiers and Kharin, 1998; Meehl et al., 2000; Frei and Schär, 2001; Benestad, 2003; Klein Tank, 2004; Schär et al., 2004; Ferro et al., 2005). A natural extension of this study is to analyse also changes in extremes. Figure 7.3 shows 1958–2004 monthly linear trends in every 5th percentile of the northern Switzerland daily mean temperature distribution following the method described in Robeson (2004). Note that an analysis using minimum and maximum temperatures might be more interesting but this would require carefully homogenized series not yet available. In some months the trends are different in various parts of the frequency distribution. In March the low values (5th to 30th percentiles) and the high values (70th to 95th percentiles) show large trends whereas the mean values do not change significantly. Trend estimates for September are positive for the low end of the distribution and negative for the high end. In May, August and December the trends are significant on the 95% level for the whole range of the distribution. A crucial question (not answered here) is whether the percentile trends are statistically significant different for certain percentile combinations. In other words, is e.g. the 50th percentile trend significantly different from the one on the 90th percentile.

Alpine tourism and hydropower industry are highly interested in expected changes of the Alpine snow pack in a changing climate. The regression coefficients of the statistical snow models applied in Chapter 2 could be used for estimations of climate change induced changes in snow pack (cf. Breiling and Charamza, 1999). These results should then be compared to the results using simple conceptual or physically based snow models.
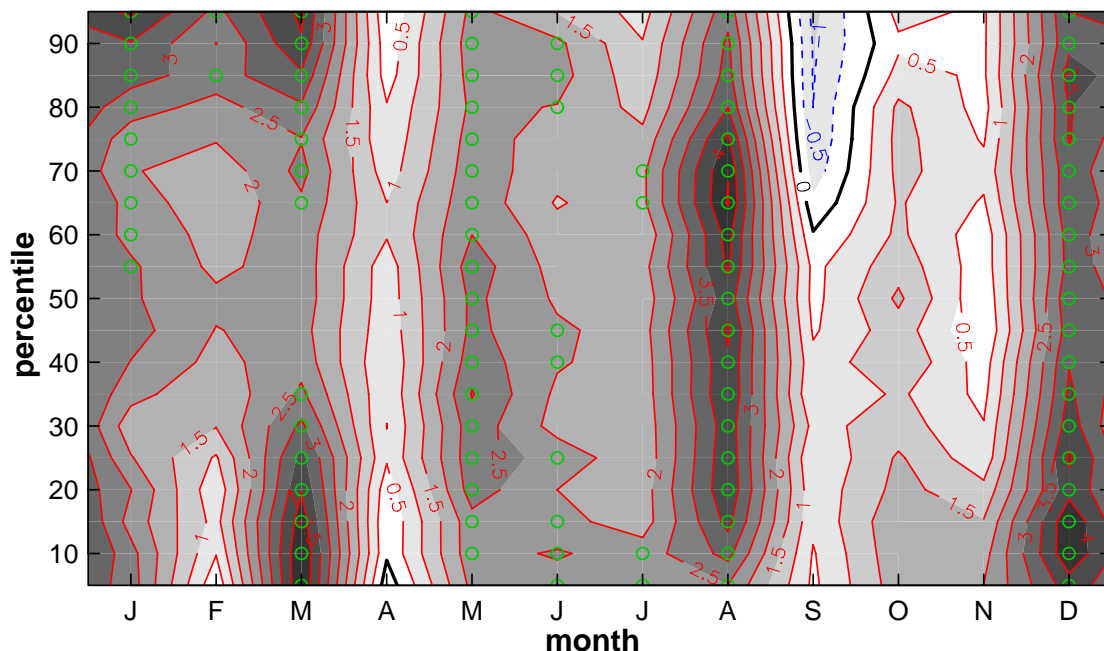
Figure 7.3: Linear trends in every 5th percentile (5th to 95th) of daily northern Switzerland 2-m temperature for every month of the year. Period used: 1958–2004. Units: K/50years. Contour interval is 0.5 K/50years, positive trend contours are solid and red, negative ones are dashed and blue. Trends with a p-value <0.05 are indicated with an open green circle. Percentiles have been determined using the approach in Robeson (2004).

The results presented in Chapter 6 showed that present day global models are able to reproduce recent trends relatively accurately. There are larger uncertainties in the representation of the modelled variability. A thorough understanding of interannual variability is a prerequisite to better predict the climate system both on seasonal and decadal time scales (Palmer, 1999; Palmer et al., 2004; Müller et al., 2005). Results of empirical statistical methods like those presented in this study could help to verify and calibrate physically based experiments using global or regional climate models.

Bibliography

Abegg, B., 1996: Klimaänderung und Tourismus: Klimafolgenforschung am Beispiel des Wintertourismus in den Schweizer Alpen (Climate change and tourism: climate impact research exemplified by winter tourism in the Swiss Alps). vdf Hochschulverlag AG an der ETH Zürich, Zürich, 222 pp.

Appenzeller, C., J. Schwander, S. Sommer, and T. F. Stocker, 1998a: The North Atlantic Oscillation and its imprint on precipitation and ice accumulation in Greenland. *Geophys. Res. Lett.*, **25,** 1939-1942.

Appenzeller, C., T. F. Stocker, and M. Anklin, 1998b: North Atlantic oscillation dynamics recorded in Greenland ice cores. *Science*, **282,** 446-449.

Appenzeller, C., A. K. Weiss, and J. Staehelin, 2000: North Atlantic oscillation modulates total ozone winter trends. *Geophys. Res. Lett.*, **27,** 1131-1134.

Appenzeller, C., T. F. Stocker, and A. Schmittner, 2001: Natural climate variability and climate change in the North-Atlantic European sector; chance for surprise? *Integrated Assessment*, **1,** 301-306.

Auer, I. and R. Böhm, 1994: Combined Temperature-Precipitation Variations in Austria During the Instrumental Period. *Theor. Appl. Climatol.*, **49,** 161-174.

Auer, I., R. Böhm, M. Brunetti, M. Maugeri, T. Nanni, and W. Schöner, 2001: Austrian long-term climate 1767-2000. Multiple instrumental climate time series from Central Europe (ALOCLIM), 147 pp.

Auer, I., R. Böhm, A. Jurkovic, A. Orlik, R. Potzmann, W. Schöner, M. Ungersbock, M. Brunetti, T. Nanni, M. Maugeri, K. Briffa, P. Jones, D. Efthymiadis, O. Mestre, J. M. Moisselin, M. Begert, R. Brazdil, O. Bochnicek, T. Cegnar, M. Gajic-Capkaj, K. Zaninovic, Z. Majstorovic, S. Szalai, T. Szentimrey, and L. Mercalli, 2005: A new instrumental precipitation dataset for the greater alpine region for the period 1800-2002. *Int. J. Climatol.*, **25,** 139-166.

Bader, S. and H. Bantle, 2004: Das Schweizer Klima im Trend: Temperatur- und Niederschlagsentwicklung 1864-2001 (in german). *Veröffentlichungen der MeteoSchweiz*, **No. 68,** 48 pp, available online (`http://www.meteoschweiz.ch`).

Baeriswyl, P. A. and M. Rebetez, 1997: Regionalization of precipitation in Switzerland by means of principal component analysis. *Theor. Appl. Climatol.*, **58,** 31-41.

Barnston, A. G. and R. E. Livezey, 1987: Classification, Seasonality and Persistence of Low-Frequency Atmospheric Circulation Patterns. *Mon. Wea. Rev.*, **115,** 1083-1126.

Beaumont, R. T., 1957: A criterion for selection of length of record for a moving arithmetic mean for hydrological data. *Trans. Amer. Geophys. Union*, **38,** 198-200.

Beckers, J. M. and M. Rixen, 2003: EOF calculations and data filling from incomplete oceanographic datasets. *J. Atmos. Ocean. Tech.*, **20,** 1839-1856.

Bednorz, E., 2002: Snow cover in western Poland and macro-scale circulation conditions. *Int. J. Climatol.*, **22,** 533-541.

Bednorz, E., 2004: Snow cover in eastern Europe in relation to temperature, precipitation and circulation. *Int. J. Climatol.*, **24,** 591-601.

Begert, M., G. Seiz, T. Schlegel, M. Musa, G. Baudraz, and M. Moesch, 2003: Homogenisierung von Klimamessreihen der Schweiz und Bestimmung der Normwerte 1961-1990 (in german). *Veröffentlichungen der MeteoSchweiz*, **No. 67,** 170 pp., available online (`http://www.meteoschweiz.ch`).

Begert, M., T. Schlegel, and W. Kirchhofer, 2005: Homogeneous temperature and precipitation series of Switzerland from 1864 to 2000. *Int. J. Climatol.*, **25,** 65-80.

Benedict, J. J., S. Lee, and S. B. Feldstein, 2004: Synoptic view of the North Atlantic Oscillation. *J. Atmos. Sci.*, **61,** 121-144.

Benestad, R. E., 2003: How often can we expect a record event? *Clim. Res.*, **25,** 3-13.

Beniston, M., M. Rebetez, F. Giorgi, and M. R. Marinucci, 1994: An Analysis of Regional Climate-Change in Switzerland. *Theor. Appl. Climatol.*, **49,** 135-159.

Beniston, M., 1997: Variations of snow depth and duration in the Swiss Alps over the last 50 years: Links to changes in large-scale climatic forcings. *Climatic Change*, **36,** 281-300.

Beniston, M. and P. Jungo, 2002: Shifts in the distributions of pressure, temperature and moisture and changes in the typical weather patterns in the Alpine region in response to the behavior of the North Atlantic Oscillation. *Theor. Appl. Climatol.*, **71,** 29-42.

Beniston, M., F. Keller, and S. Goyette, 2003a: Snow pack in the Swiss Alps under changing climatic conditions: an empirical approach for climate impacts studies. *Theor. Appl. Climatol.*, **74,** 19-31.

Beniston, M., F. Keller, B. Koffi, and S. Goyette, 2003b: Estimates of snow accumulation and volume in the Swiss Alps under changing climatic conditions. *Theor. Appl. Climatol.*, **76,** 125-140.

Böhm, R., I. Auer, M. Brunetti, M. Maugeri, T. Nanni, and W. Schöner, 2001: Regional temperature variability in the European Alps: 1760-1998 from homogenized instrumental time series. *Int. J. Climatol.*, **21,** 1779-1801.

Bostrom, A., M. G. Morgan, B. Fischhoff, and R. D, 1994: What do people know about climate change? 1. Mental models. *Risk Analysis*, **16,** 959-970.

Brabson, B. B., D. H. Lister, P. D. Jones, and J. P. Palutikof, 2005: Soil moisture and predicted spells of extreme temperatures in Britain. *J. Geophys. Res. Atmos*, **110,** D05104.

Breiling, M. and P. Charamza, 1999: The impact of global warming on winter tourism and skiing: a regionalised model for Austrian snow conditions. *Regional Environmental Change*, **1,** 4-14.

Bretherton, C. S., C. Smith, and J. M. Wallace, 1992: An intercomparison of methods for finding coupled patterns in climate data. *J. Clim.*, **5,** 541-560.

Broecker, W. S., 1997: Thermohaline circulation, the Achilles heel of our climate system: Will man-made CO2 upset the current balance? *Science*, **278,** 1582-1588.

Brown, B. G. and R. W. Katz, 1991: Use of statistical methods in the search for teleconnections: past, present, future. Teleconnections Linking Worldwide Climate Anomalies: Scientific Basis and Societal Impacts, M. H. Glantz, R. W. Katz, and N. Nicholls, Eds., Cambridge University Press, Cambridge, 535 pp.

Brown, R. D., 2000: Northern Hemispheric Snow Cover Variability and Change 1915-97. *J. Clim.*, **13,** 2339-2355.

Bürki, R., 2000: Klimaänderung und Anpassungsprozesse im Wintertourismus (Climate change and adaptation processes in winter tourism). Ostschweizerische Geographische Gesellschaft, St. Gallen, 206 pp.

Cayan, D. R., 1996: Interannual climate variability and snowpack in the western United States. *J. Clim.*, **9,** 928-948.

Charney, J. G. and J. G. Devore, 1979: Multiple Flow Equilibria in the Atmosphere and Blocking. *J. Atmos. Sci.*, **36,** 1205-1216.

Cherry, S., 1997: Some comments on singular value decomposition analysis. *J. Clim.*, **10,** 1759-1761.

Christiansen, B., 2005: The Shortcomings of Nonlinear Principal Component Analysis in Identifying Circulation Regimes. *J. Clim.*, **18,** 4814-4823.

Clark, M. P., M. C. Serreze, and D. A. Robinson, 1999: Atmospheric controls on Eurasian snow extent. *Int. J. Climatol.*, **19,** 27-40.

Corti, S., A. Giannini, S. Tibaldi, and F. Molteni, 1997: Patterns of low-frequency variability in a three-level quasi-geostrophic model. *Clim. Dyn.*, **13,** 883-904.

Corti, S., F. Molteni, and C. Brankovic, 2000: Predictability of snow-depth anomalies over Eurasia and associated circulation patterns. *Quart. J. Roy. Meteor. Soc.*, **126,** 241-262.

Court, A., 1967-68: Climatic normals as predictors: Part I-V. *Sci. Rep.*, Air Force Cambridge Res. Lab, Bedford, MA, Contract AF19(628)-5176.

Czaja, A. and C. Frankignoul, 2002: Observed impact of Atlantic SST anomalies on the North Atlantic oscillation. *J. Clim.*, **15,** 606-623.

Da Silva, A. M. and R. S. Lindzen, 1993: On the Establishment of Stationary Waves in the Northern-Hemisphere Winter. *J. Atmos. Sci.*, **50,** 43-61.

D'Andrea, F., S. Tibaldi, M. Blackburn, G. Boer, M. Deque, M. R. Dix, B. Dugas, L. Ferranti, T. Iwasaki, A. Kitoh, U. Pope, D. Randall, E. Roeckner, D. Strauss, W. Stern, H. van den Dool, and D. Williamson, 1998: Northern Hemisphere atmospheric blocking as simulated by 15 atmospheric general circulation models in the period 1979-1988. *Clim. Dyn.*, **14,** 385-407.

David, H. A., 1998: Early sample measures of variability. *Statistical Science*, **13,** 368-377.

Dettinger, M. D. and D. R. Cayan, 1995: Large-Scale Atmospheric Forcing of Recent Trends toward Early Snowmelt Runoff in California. *J. Clim.*, **8,** 606-623.

Dixon, K. W. and M. D. Shulman, 1984: A Statistical Evaluation of the Predictive Abilities of Climatic Averages. *J. Climate Appl. Meteor.*, **23,** 1542-1552.

Doblas-Reyes, F. J., M. A. Pastor, M. J. Casado, and M. Deque, 2001: Wintertime westward-traveling planetary-scale perturbations over the Euro-Atlantic region. *Clim. Dyn.*, **17,** 811-824.

Doblas-Reyes, F. J., M. J. Casado, and M. A. Pastor, 2002: Sensitivity of the Northern Hemisphere blocking frequency to the detection index. *J. Geophys. Res.*, **107,** doi:10.1029/2000JD000290.

Dole, R. M. and N. D. Gordon, 1983: Persistent Anomalies of the Extratropical Northern Hemisphere Wintertime Circulation - Geographical-Distribution and Regional Persistence Characteristics. *Mon. Wea. Rev.*, **111,** 1567-1586.

Dommenget, D. and M. Latif, 2002: A cautionary note on the interpretation of EOFs. *J. Clim.*, **15,** 216-225.

Efron, B. and R. Tibshirani, 1993: An introduction to the bootstrap. Vol. 57, Monographs on statistics and applied probability, Chapman & Hall, New York, 436 pp.

Egger, J., 1978: Dynamics of Blocking Highs. *J. Atmos. Sci.*, **35,** 1788-1801.

Egger, J. and K. P. Hoinka, 1992: Fronts and Orography. *Meteorol. Atmos. Phys.*, **48,** 3-36.

Ehrler, C., 1998: Klimaänderung und alpine Schneedecke - Auswirkungen auf das Abflussregime am Beispiel des Einzugsgebiets Rhein-Felsberg (Climate change and the alpine snow cover - Consequences for the runoff regime using the Rhein-Felsberg catchment as an example). vdf Hochschulverlag an der ETH Zürich, Zürich, 134 pp.

Elsasser, H. and P. Messerli, 2001: The vulnerability of the snow industry in the Swiss Alps. *Mt. Res. Dev.*, **21,** 335-339.

Enger, I., 1959: Optimum Length of Record for Climatological Estimates of Temperature. *J. Geophys. Res.*, **64,** 779-787.

Ertel, H., 1942: Ein neuer hydrodynamischer Wirbelsatz. *Meteorol. Z.*, **59,** 277-281.

Exner, F. M., 1913: Übermonatliche Witterungsanomalien auf der nördlichen Erdhälfte im Winter. *Sitzungsberichte der Kaiserlichen Akademie der Wissenschaften*, **122,** 1165-1241.

Feldstein, S. B., 2000: Teleconnections and ENSO: The timescale, power spectra, and climate noise properties. *J. Clim.*, **13,** 4430-4440.

Ferro, C. A. T., A. Hannachi, and D. B. Stephenson, 2005: Simple non-parametric techniques for exploring changing probability distributions of weather. *J. Clim.*, **18,** 4344-4354.

Fliri, F., 1974: Niederschlag und Lufttemperatur im Alpenraum. *Wissenschaftl. Alpenvereinshefte*, **24,** Innsbruck.

Fliri, F., 1984: Synoptische Klimatographie der Alpen zwischen Mont Blanc und Hohen Tauern (Schweiz, Tirol, Oberitalien). *Wissenschaftl. Alpenvereinshefte*, **29,** 686 pp.

Föhn, P., 1990: Schnee und Lawinen (in: Schnee, Eis und Wasser in einer wärmeren Atmosphäre). *Mitteilungen VAW-ETH Zürich*, **108,** 33-48.

Folland, C. K., T. R. Karl, J. R. Christy, R. A. Clarke, G. V. Gruza, J. Jouzel, M. E. Mann, J. Oerlemans, M. J. Salinger, and S.-W. Wang, 2001: Observed climate variability and change. Climate Change 2001: The Scientific Basis, J. T. Houghton, Y. Ding, D. J. Griggs, M. Noguer, P. J. van der Linden, X. Dai, K. Maskell, and C. A. Johnson, Eds., Cambridge University Press, Cambridge, UK, 99-182.

Frei, A., D. A. Robinson, and M. G. Hughes, 1999: North American snow extent: 1900-1994. *Int. J. Climatol.*, **19,** 1517-1534.

Frei, C. and C. Schär, 1998: A precipitation climatology of the Alps from high-resolution rain-gauge observations. *Int. J. Climatol.*, **18,** 873-900.

Frei, C. and C. Schär, 2001: Detection probability of trends in rare events: Theory and application to heavy precipitation in the Alpine region. *J. Clim.*, **14,** 1568-1584.

Fukuoka, A., 1951: A study of 10-day forecast (A synthetic report). *The Geophysical Magazine, Tokio*, **22,** 177-218.

Garthwaite, P., I. T. Jolliffe, and B. Jones, 2002: Statistical Inference. Oxford University Press, Oxford, GB, 328 pp.

Giorgi, F., X. Q. Bi, and J. S. Pal, 2004: Mean, interannual variability and trends in a regional climate change experiment over Europe. II: climate change scenarios (2071-2100). *Clim. Dyn.*, **23,** 839-858.

Giorgi, F. and X. Q. Bi, 2005: Regional changes in surface climate interannual variability for the 21st century from ensembles of global model simulations. *Geophys. Res. Lett.*, **32,** L13701, doi:10.1029/2005GL023002.

Gisborne, H. T., 1935: When a "normal" is not normal. *Bull. Amer. Meteor. Soc.*, **16,** 171-173.

Glantz, M. H., R. W. Katz, and N. Nicholls, 1991: Teleconnections Linking Worldwide Climate Anomalies: Scientific Basis and Societal Impacts. Cambridge University Press, Cambridge, 535 pp.

Grebner, D., 1978: Zur Berechnung der Höhenlage des Übergangs vom festen in flüssigen Niederschlag. *14. Tagg. Alp. Meteor. Rauris*, Heft, 31, 22/1-6, Zentralanstalt für Meteorologie und Geodynamik, Wien.

Guttman, N. B., 1989: Statistical Descriptors of Climate. *Bull. Amer. Meteor. Soc.*, **70,** 602-607.

Gutzler, D. F. and R. D. Rosen, 1992: Interannual Variability of Wintertime Snow Cover across the Northern Hemisphere. *J. Clim.*, **5,** 1441-1447.

Gyalistras, D., M. B. Rohrer, C. Wahrenberger, D. Lorenzi, and M. Schwarb, 2005: Assessing the sensitivity of local snow cover to global climate change: A general method and its application to five Swiss locations. *Clim. Dyn.*, submitted.

Hannachi, A., I. T. Jolliffe, D. B. Stephenson, and N. Trendafilov, 2006: In search of simple structures in climate: Simplifying EOFs. *Int. J. Climatol.*, **26,** 7-28, doi:10.1002/joc.1243.

Hansen, A. R. and A. Sutera, 1984: A Comparison of the Spectral Energy and Enstrophy Budgets of Blocking Versus Nonblocking Periods. *Tellus*, **36A,** 52-63.

Hansen, J., M. Sato, R. Ruedy, L. Nazarenko, A. Lacis, G. A. Schmidt, G. Russell, I. Aleinov, M. Bauer, S. Bauer, and N. Bell, 2005: Efficacy of Climate Forcings. *J. Geophys. Res.*, **110,** D18104, doi:10.1029/2005JD005776.

Hansen, J. E. and M. Sato, 2001: Trends of measured climate forcing agents. *P. Natl. Acad. Sci. USA*, **98,** 14778-14783.

Hantel, M., M. Ehrendorfer, and A. Haslinger, 2000: Climate sensitivity of snow cover duration in Austria. *Int. J. Climatol.*, **20,** 615-640.

Hartley, S. and M. J. Keables, 1998: Synoptic associations of winter climate and snowfall variability in New England, USA, 1950-1992. *Int. J. Climatol.*, **18,** 281-298.

Hartmann, D. L., 1994: Global Physical Climatology. International Geophysics Series, vol. 56., Academic Press, 411 pp.

Haylock, M. R. and C. M. Goodess, 2004: Interannual variability of European extreme winter rainfall and links with mean large-scale circulation. *Int. J. Climatol.*, **24,** 759-776.

Hegerl, G. C., P. A. Stott, M. R. Allen, J. F. B. Mitchell, S. F. B. Tett, and U. Cubasch, 2000: Optimal detection and attribution of climate change: sensitivity of results to climate model differences. *Clim. Dyn.*, **16,** 737-754.

Hirstein, A., 2005: Die Selbstzensur der Forscher wird die Welt nicht retten. *NZZ am Sonntag, 20.2.2005.*

Hoaglin, D., F. Mosteller, and J. Tukey, Eds., 1983: Understanding robust and exploratory data analysis. Applied probability and statistics, John Wiley & Sons, Inc., New York, 447 pp.

Hock, R., 2003: Temperature index melt modelling in mountain areas. *J. Hydrol.*, **282,** 104-115.

Horel, J. D., 1981: A rotated principal component analysis of the interannual variability of the Northern Hemisphere 500 hPa height field. *Mon. Wea. Rev.*, **109,** 2080-2092.

Hori, M. E. and T. Yasunari, 2003: NAO impact towards the springtime snow disappearance in the western Eurasian continent. *Geophys. Res. Lett.*, **30,** art. No.-1977.

Hoskins, B. J., M. E. Mcintyre, and A. W. Robertson, 1985: On the Use and Significance of Isentropic Potential Vorticity Maps. *Quart. J. Roy. Meteor. Soc.*, **111,** 877-946.

Houghton, J. T., Y. Ding, D. J. Griggs, M. Noguer, P. J. van der Linden, X. Dai, K. Maskell, and C. A. Johnson, Eds., 2001: Climate Change 2001: The Scientific Basis, IPCC Third Assessment Report. Cambridge University Press, Cambridge, UK, 944 pp.

Hsieh, W. W., 2001: Nonlinear principal component analysis by neural networks. *Tellus*, **53A,** 599-615.

Huang, J., H. M. VandenDool, and A. G. Barnston, 1996: Long-lead seasonal temperature prediction using optimal climate normals. *J. Clim.*, **9,** 809-817.

Hurrell, J. W., 1995: Decadal Trends in the North Atlantic Oscillation Regional Temperatures and Precipitation. *Science*, **269,** 676-679.

Hurrell, J. W., Y. Kushnir, G. Ottersen, and M. Visbeck, 2003: The North Atlantic Oscillation - Climatic Significance and Environmental Impact. Geophysical Monograph 134, AGU, Washington DC, 279 pp.

Hyndman, R. J. and Y. Fan, 1996: Sample Quantiles in Statistical Packages. *The American Statistician*, **50,** 361-365.

Jasper, K., P. Calanca, D. Gyalistras, and J. Fuhrer, 2004: Differential impacts of climate change on the hydrology of two alpine river basins. *Clim. Res.*, **26,** 113-129.

Jolliffe, I. T., 1987: Rotation of Principal Components - Some Comments. *J. Climatol.*, **7,** 507-510.

Jolliffe, I. T., 2002: Principal Component Analysis. 2nd ed. Springer, 502 pp.

Jolliffe, I. T., 2003: A cautionary note on artificial examples of EOFs. *J. Clim.*, **16,** 1084-1086.

Jones, P. D. and A. Moberg, 2003: Hemispheric and large-scale surface air temperature variations: An extensive revision and an update to 2001. *J. Clim.*, **16,** 206-223.

Jones, P. D., T. J. Osborn, and K. Briffa, 2003: Pressure-based measures of the North Atlantic oscillation (NAO): A comparison and an assessment of changes in the strength of the NAO and its influence on surface climate parameters. In : The North Atlantic Oscillation - Climatic significance and environmental impact, J. W. Hurrell, Y. Kushnir, G. Ottersen, and M. Visbeck, Eds., Geophysical Monograph 134, American Geophysical Union, Washington DC, 51-62.

Junge, M. M. and D. B. Stephenson, 2003: Mediated and direct effects of the North Atlantic Ocean on winter temperatures in northwest Europe. *Int. J. Climatol.*, **23,** 245-261.

Kadioglu, M., Z. Sen, and L. Gültekin, 2001: Variations and trends in Turkish seasonal heating and cooling degree-days. *Climatic Change*, **49,** 209-223.

Kaplan, A., Y. Kushnir, M. A. Cane, and M. B. Blumenthal, 1997: Reduced space optimal analysis for historical data sets: 136 years of Atlantic sea surface temperatures. *J. Geophys. Res. Oceans*, **102,** 27835-27860.

Karl, T. R., R. W. Knight, and N. Plummer, 1995: Trends in High-Frequency Climate Variability in the 20th-Century. *Nature*, **377,** 217-220.

Katz, R. W., 1988: Use of Cross Correlations in the Search for Teleconnections. *J Climatol*, **8,** 241-253.

Katz, R. W. and B. G. Brown, 1992: Extreme Events in a Changing Climate - Variability Is More Important Than Averages. *Climatic Change*, **21,** 289-302.

Kirchhofer, W., 2001: Klimaatlas der Schweiz. Bundesamt für Landestopographie, Wabern.

Klein Tank, A. M. G. and G. P. Können, 2003: Trends in indices of daily temperature and precipitation extremes in Europe, 1946-99. *J. Clim.*, **16,** 3665-3680.

Klein Tank, A. M. G., 2004: Changing temperature and precipitation extremes in Europe's Climate of the 20th century, PhD Thesis, Koninklijk Nederlands Meteorologisch Instituut (KNMI), De Bilt, De Bilt, 124 pp.

Klein Tank, A. M. G., G. P. Können, and F. M. Selten, 2005: Signals of anthropogenic influence on European warming as seen in the trend patterns of daily temperature variance. *Int. J. Climatol.*, **25,** 1-16.

Kovats, S., T. Wolf, and B. Menne, 2004: Heat waves of August 2003 in Europe: Provisional estimates of the impact on mortality. *Eurosurveillance Weekly*, **8(11)**, available online (`http://www.eurosurveillance.org/ew/2004/040311.asp`).

Kunkel, K. E. and A. Court, 1990: Climatic Means and Normals - a Statement of the American-Association-of-State-Climatologists (Aasc). *Bull. Amer. Meteor. Soc.*, **71,** 201-204.

Kutzbach, J. E., 1967: Empirical eigenvectors of sea-level pressure, surface temperature and precipitation complexes over North America. *J. Appl. Meteor.*, **6,** 791-802.

Lamb, P. J. and S. A. Changnon, 1981: On the Best Temperature and Precipitation Normals - the Illinois Situation. *J Appl Meteorol*, **20,** 1383-1390.

Lang, H. and M. B. Rohrer, 1987: Temporal and spatial variations of the snow cover in the Swiss Alps. Large-scale effects of Seasonal Snow Cover, B. E. Goodison, R. G. Bary, and J. Dozier, Eds., IAHS Press, IAHS Publication No. 166, Oxfordshire, UK.

Laternser, M. and M. Schneebeli, 2002: Temporal trend and spatial distribution of avalanche activity during the last 50 years in Switzerland. *Nat. Hazards*, **27,** 201-230.

Laternser, M. and M. Schneebeli, 2003: Long-term snow climate trends of the Swiss Alps (1931-99). *Int. J. Climatol.*, **23,** 733-750.

Laternser, M. C., 2002: Snow and avalanche climatology of Switzerland, PhD thesis No. 14493, Eidgenössisch Technische Hochschule (ETH), Zürich, 139 pp.

Latif, M., K. Arpe, and E. Roeckner, 2000a: Oceanic control of decadal North Atlantic sea level pressure variability in winter. *Geophys. Res. Lett.*, **27,** 727-730.

Latif, M., E. Roeckner, U. Mikolajewicz, and R. Voss, 2000b: Tropical stabilization of the thermohaline circulation in a greenhouse warming simulation. *J. Clim.*, **13,** 1809-1813.

Lejenäs, H. and H. Økland, 1983: Characteristics of Northern Hemisphere blocking as determined from a long time series of observational data. *Tellus*, **35A,** 350-362.

Lejenäs, H. and B. Döös, 1987: The behaviour of the stationary and travelling planetary-scale waves during blocking - A Northern Hemispheric data study. *J. Meteorol. Soc. Jpn*, **65,** 709-725.

Leuenberger, D., 2005: High-resolution Radar Rainfall Assimilation: Exploratory Studies with Latent Heat Nudging, PhD thesis No. 15884, Eidgenössisch Technische Hochschule (ETH), Zürich, 103 pp.

Lindzen, R. S., 1986: Stationary Planetary-Waves, Blocking, and Interannual Variability. *Adv Geophys*, **29,** 251-273.

Liu, Q., 1994: On the Definition and Persistence of Blocking. *Tellus*, **46A,** 286-298.

Lorenz, E. N., 1956: Empirical orthogonal functions and statistical weather prediction. M. I. T. Dept. of Meteorology, Sci. Rept. No. 1, Contract AF19(604)-1566, 49 pp.

Lupo, A. R. and P. J. Smith, 1995: Climatological Features of Blocking Anticyclones in the Northern-Hemisphere. *Tellus*, **47A,** 439-456.

Luterbacher, J., E. Xoplaki, D. Dietrich, R. Rickli, J. Jacobeit, C. Beck, D. Gyalistras, C. Schmutz, and H. Wanner, 2002: Reconstruction of sea level pressure fields over the Eastern North Atlantic and Europe back to 1500. *Clim. Dyn.*, **18,** 545-561.

Marshall, J., Y. Kushnir, D. Battisti, P. Chang, A. Czaja, R. Dickson, J. W. Hurrell, M. McCartney, R. Saravan, and M. Visbeck, 2001: North Atlantic Climate Variability: Phenomena, Impacts and Mechanisms. *Int. J. Climatol.*, **21,** 1863-1898.

Martin, E., E. Brun, and Y. Durand, 1994: Sensitivity of the French Alps Snow Cover to the Variation of Climatic Variables. *Ann. Geophys.*, **12,** 469-477.

Massacand, A. C. and H. C. Davies, 2001a: Interannual variability of European Winter Weather: The Potential Vorticity Insight. *Atmospheric Science Letters*, **2,** 52-60.

Massacand, A. C. and H. C. Davies, 2001b: Interannual variability of the extratropical northern hemisphere and the potential vorticity wave guide. *Atmospheric Science Letters*, **2,** 61-71.

McCabe, G. J. and M. D. Dettinger, 2002: Primary Modes and Predictability of Year-to-Year Snow-pack Variations in the Western United States from Teleconnections with Pacific Ocean Climate. *J. Hydromet.*, **3,** 13-25.

McWilliams, J. C., 1980: An Application of Equivalent Modons to Atmospheric Blocking. *Dynam. Atmos. Oceans*, **5,** 43-66.

Meehl, G. A., F. Zwiers, J. Evans, T. Knutson, L. Mearns, and P. Whetton, 2000: Trends in extreme weather and climate events: Issues related to modeling extremes in projections of future climate change. *Bull. Amer. Meteor. Soc.*, **81,** 427-436.

Meehl, G. A. and C. Tebaldi, 2004: More Intense, More Frequent, and Longer Lasting Heat Waves in the 21st Century. *Science*, **305,** 994-997.

Mindling, G. W., 1940: Do climatological averages serve adequately as normals? *Bull. Amer. Meteor. Soc.*, **21,** 3-6.

Moberg, A. and P. Jones, 2005: Trends in indices for extremes in daily temperature and precipitation in central and western Europe, 1901-99. *Int. J. Climatol.*, **25,** 1149-1171.

Monahan, A. H., 2000: Nonlinear principal component analysis by neural networks: Theory and application to the Lorenz system. *J. Clim.*, **13,** 821-835.

Mörikofer, W., 1948: The dependence on altitude of the snow cover in the Alps. *Proceedings Union Géodésique et Géophysique Internationale*, 19-28 August 1948, Oslo, 161-170.

Morinaga, Y., S. F. Tian, and M. Shinoda, 2003: Winter snow anomaly and atmospheric circulation in Mongolia. *Int. J. Climatol.*, **23,** 1627-1636.

Mosedale, T. J., D. B. Stephenson, M. Collins, and T. C. Mills, 2005: Granger Causality of Coupled Climate Processes: Ocean Feedback on the North Atlantic Oscillation. *J. Clim.*, accepted.

Mote, P. W., 2003: Trends in snow water equivalent in the Pacific Northwest and their climatic causes. *Geophys. Res. Lett.*, **30,** art. No.-1601.

Mote, P. W., A. F. Hamlet, M. P. Clark, and D. P. Lettenmaier, 2005: Declining mountain snowpack in western north America. *Bull. Amer. Meteor. Soc.*, **86,** 39-49.

Müller, W. A., C. Appenzeller, and C. Schär, 2005: Probabilistic seasonal prediction of the winter North Atlantic Oscillation and its impact on near surface temperature. *Clim. Dyn.*, **24,** 213-226.

North, G. R., T. L. Bell, R. F. Cahalan, and F. J. Moeng, 1982: Sampling Errors in the Estimation of Empirical Orthogonal Functions. *Mon. Wea. Rev.*, **110,** 699-706.

Obukhov, A. M., 1947: Statistically homogeneous fields on a sphere. *Usp. Mat. Nauk.*, **2,** 196-198.

Obukhov, A. M., 1960: The statistically orthogonal expansion of empirical functions (English Translation). *Bull. Acad. Sci. USSR Geophys. Ser.*, 288-191.

Ohmura, A., M. Wild, and L. Bengtsson, 1996: A possible change in mass balance of Greenland and Antarctic ice sheets in the coming century. *J. Clim.*, **9,** 2124-2135.

Ohmura, A., 2001: Physical basis for the temperature-based melt-index method. *J. Appl. Meteorol.*, **40,** 753-761.

Palmer, T. N., 1999: A nonlinear dynamical perspective on climate prediction. *J. Clim.*, **12,** 575-591.

Palmer, T. N., A. Alessandri, U. Andersen, P. Cantelaube, M. Davey, P. Delecluse, M. Deque, E. Diez, F. J. Doblas-Reyes, H. Feddersen, R. Graham, S. Gualdi, J. F. Gueremy, R. Hagedorn, M. Hoshen, N. Keenlyside, M. Latif, A. Lazar, E. Maisonnave, V. Marletto, A. P. Morse, B. Orfila, P. Rogel, J. M. Terres, and M. C. Thomson, 2004: Development of a European multimodel ensemble system for seasonal-to-interannual prediction (demeter). *Bull. Amer. Meteor. Soc.*, **85,** 853-872.

Parker, D. E., P. D. Jones, C. K. Folland, and A. Bevan, 1994: Interdecadal Changes of Surface-Temperature since the Late-19th-Century. *J. Geophys. Res.*, **99,** 14373-14399.

Pavan, V. and F. J. Doblas-Reyes, 2000: Multi-model seasonal hindcasts over the Euro-Atlantic: skill scores and dynamical features. *Clim. Dyn.*, **16,** 611-625.

Pavan, V., F. Molteni, and C. Brankovic, 2000a: Wintertime variability in the Euro-Atlantic region in observations and in ECMWF seasonal ensemble experiments. *Quart. J. Roy. Meteor. Soc.*, **126,** 2143-2173.

Pavan, V., S. Tibaldi, and C. Brankovic, 2000b: Seasonal prediction of blocking frequency: Results from winter ensemble experiments. *Quart. J. Roy. Meteor. Soc.*, **126,** 2125-2142.

Pearson, K., 1920: On the probable errors of frequency constants III. *Biometrika*, **13,** 113-132.

Peixoto, J. P. and A. H. Oort, 1992: Physics of Climate. American Institute of Physics, 520 pp.

Pelly, J. L. and B. J. Hoskins, 2003: A new perspective on blocking. *J. Atmos. Sci.*, **60,** 743-755.

Pepin, N. C. and D. J. Seidel, 2005: A global comparison of surface and free-air temperatures at high elevations. *J. Geophys. Res.*, **110,** D03104, doi:10.1029/2004JD005047.

Pfister, C., 1999: Wetternachhersage, 500 Jahre Klimavariationen und Naturkatastrophen (1496-1995). Verlag Paul Haupt, Bern, 304 pp.

Philipona, R., B. Dürr, C. Marty, A. Ohmura, and M. Wild, 2004: Radiative forcing - measured at Earth's surface - corroborate the increasing greenhouse effect. *Geophys. Res. Lett.*, **31,** L03202, doi:10.1029/2003GL018765.

Pichler, H. and R. Steinacker, 1987: On the Synoptics and Dynamics of Orographically Induced Cyclones in the Mediterranean. *Meteorol. Atmos. Phys.*, **36,** 108-117.

Preisendorfer, R. W., 1988: Principle Component Analysis in Meteorology and Oceanography. Vol. 17, Develop. Atm. Sci., Elsevier, Amsterdam, 425 pp.

Qian, B. D., J. Corte-Real, and H. Xu, 2000: Is the North Atlantic Oscillation the most important atmospheric pattern for precipitation in Europe? *J. Geophys. Res.*, **105,** 11901-11910.

Quadrelli, R., M. Lazzeri, C. Cacciamani, and S. Tibaldi, 2001a: Observed winter Alpine precipitation variability and links with large-scale circulation patterns. *Clim. Res.*, **17,** 275-284.

Quadrelli, R., V. Pavan, and F. Molteni, 2001b: Wintertime variability of Mediterranean precipitation and its links with large-scale circulation anomalies. *Clim. Dyn.*, **17,** 457-466.

R Core Team, 2005: R statistics programming language. Version 2.1.1, `http://www.r-project.org`.

Räisänen, J., 2002: CO2-induced changes in interannual temperature and precipitation variability in 19 CMIP2 experiments. *J. Clim.*, **15,** 2395-2411.

Rebetez, M., 1996: Public expectation as an element of human perception of climate change. *Climatic Change*, **32,** 495-509.

Rex, D. F., 1950: Blocking action in the middle troposphere and its effects upon regional climate. II. The climatology of blocking action. *Tellus*, **2,** 275-301.

Richman, M. B., 1986: Rotation of Principal Components. *J. Climatol.*, **6,** 293-335.

Robeson, S. M., 2004: Trends in time-varying percentiles of daily minimum and maximum temperature over North America. *Geophys. Res. Lett.*, **31,** art. No.-L04203.

Rodgers, J. C., 1990: Patterns of low-frequency monthly sea level pressure variability (1899-1989) and associated wave cyclone frequencies. *J. Clim.*, **3,** 1364-1379.

Rodriguez-Fonseca, B., I. Polo, E. Serrano, and M. Castro, 2006: Evaluation of the north atlantic SST forcing on the European and Northern African winter climate. *Int. J. Climatol.*, **26,** 179-191, doi: 10.1002/joc.1234.

Rodwell, M. J., D. P. Rowell, and C. K. Folland, 1999: Oceanic forcing of the wintertime North Atlantic Oscillation and European climate. *Nature*, **398,** 320-323.

Rohrer, M. B., 1989: Determination of transition air temperature from snow to rain and intensity of precipitation. *In: WMO IASH ETH International Workshop on Precipitation Measurement*, 475-582.

Rohrer, M. B., L. N. Braun, and H. Lang, 1994: Long-Term Records of Snow Cover Water Equivalent in the Swiss Alps. 1. Analysis. *Nord. Hydrol.*, **25,** 53-64.

Salvisberg, E., 1996: Wetterlagenklimatologie - Möglichkeiten und Grenzen ihres Beitrages zur Klimafolgenforschung im Alpenraum, Geographisches Institut, PhD thesis, Universität Bern, 187 pp.

Sardeshmukh, P. D., G. P. Compo, and C. Penland, 2000: Changes of probability associated with El Nino. *J. Clim.*, **13,** 4268-4286.

Sausen, R., W. König, and F. Sielmann, 1995: Analysis of blocking events from observations and ECHAM model simulations. *Tellus*, **47,** 421-438.

Schär, C., T. D. Davies, C. Frei, H. Wanner, M. Widmann, M. Wild, and H. C. Davies, 1998: Current Alpine Climate. In: Views from the Alps. Regional perspectives on Climate Change, P. Cebon, U. Dahinden, H. C. Davies, D. Imboden, and C. C. Jaeger, Eds., The MIT Press, Cambridge, Massachusetts, USA, 21-72.

Schär, C., 2002: Lee cyclogenesis. Encyclopedia of Atmospheric Sciences, J. R. Holton, J. Pyle, and J. A. Curry, Eds., Academic Press, 1602-1614.

Schär, C., P. L. Vidale, D. Lüthi, C. Frei, C. Häberli, M. A. Liniger, and C. Appenzeller, 2004: The role of increasing temperature variability in European summer heatwaves. *Nature*, **427,** 332-336.

Scherrer, S. C. and C. Appenzeller, 2003: Swiss Alpine snow variability and its links to large scale flow patterns. *Extended Abstract proceedings, ICAM/MAP Meeting 2003*, 567-570.

Scherrer, S. C., C. Appenzeller, P. Eckert, and D. Cattani, 2004a: Analysis of the Spread–Skill Relations Using the ECMWF Ensemble Prediction System over Europe. *Wea. Forecasting*, **19,** 552-565.

Scherrer, S. C., C. Appenzeller, and M. C. Laternser, 2004b: Trends in Swiss Alpine snow days - The role of local- and large-scale climate variability. *Geophys. Res. Lett.*, **31,** doi:10.1029/2004GL020255.

Scherrer, S. C., C. Appenzeller, M. A. Liniger, and C. Schär, 2005: European temperature distribution changes in observations and climate change scenarios. *Geophys. Res. Lett.*, **32,** L19705, doi:10.1029/2005GL024108.

Scherrer, S. C., C. Appenzeller, and M. A. Liniger, 2006a: Recent temperature trends in Switzerland and Europe: Implications for climate normals. *Int. J. Climatol.*, **26,** doi: 10.1002/joc.1270 (in press).

Scherrer, S. C., M. Croci-Maspoli, C. Schwierz, and C. Appenzeller, 2006b: Two dimensional indices of atmospheric blocking and their statistical relationship with winter climate patterns in the Euro-Atlantic region. *Int. J. Climatol.*, **26,** 233-249, doi:10.1002/joc.1250.

Schmidli, J., C. Frei, and C. Schär, 2001: Reconstruction of mesoscale precipitation fields from sparse observations in complex terrain. *J. Clim.*, **14,** 3289-3306.

Schmidli, J., C. Schmutz, C. Frei, H. Wanner, and C. Schär, 2002: Mesoscale precipitation variability in the region of the European Alps during the 20th century. *Int. J. Climatol.*, **22,** 1049-1074.

Schmidli, J. and C. Frei, 2005: Trends of heavy precipitation and wet and dry spells in Switzerland during the 20th century. *Int. J. Climatol.*, **25,** 753-771.

Schönwiese, C.-D. and J. Rapp, 1997: Climate trend atlas of Europe. Based on observations 1891–1990. Kluwer Academic Publishers, Amsterdam, 228 pp.

Schüepp, M., 1979: Witterungsklimatologie. *Beiheft zu den Annalen der Schweizerischen Meteorologischen Anstalt*, **20,** 93 pp.

Schüepp, M., G. Gensler, and M. Bouët, 1980: Schneedecke und Neuschnee, Klimatologie der Schweiz Heft 24/F, Beiheft zu den Annalen der Schweizerischen Meteorologischen Anstalt, 63 pp.

Schwierz, C., 2001: Interactions of Greenland-scale orography and extra-tropical synoptic-scale flow, PhD Thesis No. 14356, Eidgenössisch Technische Hochschule (ETH), Zürich, 155 pp.

Schwierz, C., M. Croci-Maspoli, and H. C. Davies, 2004: Perspicacious indicators of atmospheric blocking. *Geophys. Res. Lett.*, **31,** L06125, doi:10.1029/2003GL019341.

Schwierz, C., C. Appenzeller, H. Davies, M. Liniger, W. Müller, T. Stocker, and M. Yoshimori, 2005: Approaches and challenges posed by seasonal-to-decadal climate variability. In: Special issue of Climatic Change: "Climate variability, predictability and climate risk: A European perspective", M. Grosjean, R. Roethlisberger, and H. Wanner, Eds., accepted.

Seager, R., N. Harnik, Y. Kushnir, W. Robinson, and J. Miller, 2003: Mechanisms of hemispherically symmetric climate variability. *J. Clim.*, **16,** 2960-2978.

Shabbar, A., J. Huang, and K. Higuchi, 2001: The relationship between the wintertime North Atlantic Oscillation and blocking episodes in the Northern Atlantic. *Int. J. Climatol.*, **21,** 355-369.

Shapiro, S. and M. Wilk, 1965: An analysis of variance test for normality (complete samples). *Biometrika*, **52,** 591-611.

Shukla, J. and K. C. Mo, 1983: Seasonal and Geographical Variation of Blocking. *Mon. Wea. Rev.*, **111,** 388-402.

Simmons, A. J., P. D. Jones, V. da Costa Bechtold, A. C. M. Beljaars, P. W. Kållberg, S. Saarinen, S. M. Uppala, P. Viterbo, and N. Wedi, 2004: Comparison of trends and low-frequency variability in CRU, ERA-40, and NCEP/NCAR analyses of surface air temperature. *J. Geophys. Res.*, **109,** D24, D24115, doi:10.1029/2004JD005306.

Smith, R. B., 1984: A Theory of Lee Cyclogenesis. *J. Atmos. Sci.*, **41,** 1159-1168.

Spagnoli, B., S. Planton, M. Deque, O. Mestre, and J. M. Moisselin, 2002: Detecting climate change at a regional scale: The case of France. *Geophys. Res. Lett.*, **29,** doi:10.1029/2001GL014619.

Staudte, R. and S. Sheather, Eds., 1990: Robust estimation and testing. Wiley series in probability and mathematical statistics, John Wiley & Sons Inc., New York, 351 pp.

Stein, O., 2000: The variability of Atlantic-European blocking as derived from long SLP time series. *Tellus*, **52A,** 225-236.

Steinacker, R., 1983: Diagnose und Prognose der Schneefallgrenze. *Wetter und Leben*, **35,** 81-90.

Steinacker, R., 1987: Orographie und Fronten. *Wetter und Leben,* **39,** 65-70.

Stephenson, D. B., V. Pavan, and R. Bojariu, 2000: Is the North Atlantic Oscillation a random walk? *Int. J. Climatol.*, **20,** 1-18.

Stephenson, D. B., A. Hannachi, and A. O'Neill, 2004: On the existence of multiple climate regimes. *Quart. J. Roy. Meteor. Soc.*, **130,** 583-605.

Stott, P. A., S. F. B. Tett, G. S. Jones, M. R. Allen, W. J. Ingram, and J. F. B. Mitchell, 2001: Attribution of twentieth century temperature change to natural and anthropogenic causes. *Clim. Dyn.*, **17,** 1-21.

Studer, S., C. Appenzeller, and C. Defila, 2005: Inter-annual variability and decadal trends in Alpine spring phenology; A multivariate analysis approach. *Climatic Change*, **73,** 395–414.

Sutton, R. T. and D. L. R. Hodson, 2003: Influence of the ocean on North Atlantic climate variability 1871-1999. *J. Clim.*, **16,** 3296-3313.

Temperli, S., 2002: Mehr grüne als weisse Weihnachten. *Tages-Anzeiger von 21. Dezember 2002,* Seite 13.

Thompson, D. W. J. and J. M. Wallace, 2000: Annular modes in the extratropical circulation. Part I: Month-to-month variability. *J. Clim.*, **13,** 1000-1016.

Tibaldi, S. and F. Molteni, 1990: On the operational predictability of blocking. *Tellus*, **42A,** 343-365.

Tibaldi, S., E. Tosi, A. Navarra, and L. Pedulli, 1994: Northern and Southern-Hemisphere Seasonal Variability of Blocking Frequency and Predictability. *Mon. Wea. Rev.*, **122,** 1971-2003.

Tibaldi, S., F. D'Andrea, E. Tosi, and E. Roeckner, 1997: Climatology of Northern Hemisphere blocking in the ECHAM model. *Clim. Dyn.*, **13,** 649-666.

Trigo, R., I. Trigo, C. DaCamara, and T. J. Osborn, 2004: Climate impact of the European winter blocking episodes from the NCEP/NCAR Reanalyses. *Clim. Dyn.*, **23,** doi:10.1007/s00382-004-0410-4.

Uppala, S. M., P. W. Kallberg, A. J. Simmons, U. Andrae, V. da Costa Bechtold, M. Fiorino, J. K. Gibson, J. Haseler, A. Hernandez, G. A. Kelly, and X. Li, 2005: The ERA-40 Reanalysis. *Quart. J. Roy. Meteor. Soc.,* **131,** 2961-3012.

van Loon, H. and J. Rogers, 1978: The seesaw in winter temperatures between Greenland and Northern Europe, Part I: General description. *Mon. Wea. Rev.,* **106,** 296-310.

Vautard, R., 1990: Multiple Weather Regimes over the North Atlantic: Analysis of Precursors and Successors. *Mon. Wea. Rev.,* **118,** 2056-2081.

Venegas, S. A., L. A. Mysak, and D. N. Straub, 1997: Atmosphere-ocean coupled variability in the South Atlantic. *J. Clim.,* **10,** 2904-2920.

Verbunt, M., J. Gurtz, K. Jasper, H. Lang, P. Warmerdam, and M. Zappa, 2003: The hydrological role of snow and glaciers in alpine river basins and their distributed modeling. *J. Hydrol.,* **282,** 36-55.

Verkley, W. T. M., 1990: Modons with Uniform Absolute Vorticity. *J. Atmos. Sci.,* **47,** 727-745.

Vidale, P. L., D. Lüthi, R. Wegmann, and C. Schär, 2005: European climate variability in a heterogeneous multi-model ensemble. *Climatic Change*, accepted.

von Storch, H. and F. W. Zwiers, 1999: Statistical Analysis in Climate Research. Cambridge University Press, New York, 484 pp.

Walker, G. T., 1909: Correlation in seasonal variation of climate. *Mem. Ind. Met. Dept.,* **20,** 122.

Walker, G. T., 1924: Correlations in seasonal variations of weather. *IX. Mem. Ind. Meteor. Dept.,* **24,** 275-332.

Wallace, J. M. and D. F. Gutzler, 1981: Teleconnections in the geopotential height field during the Northern Hemisphere winter. *Mon. Wea. Rev.,* **109,** 784-812.

Walland, D. and I. Simmonds, 1997: Association Between Modes of Variability of January Northern Hemispheric Snow Cover and Circulation. *Theor. Appl. Climatol.,* **58,** 197-210.

Wanner, H. and M. Furger, 1990: The Bise - Climatology of a Regional Wind North of the Alps. *Meteorol. Atmos. Phys.,* **43,** 105-115.

Wanner, H., R. Rickli, E. Salvisberg, C. Schmutz, and M. Schuepp, 1997: Global climate change and variability and its influence on Alpine climate - Concepts and observations. *Theor. Appl. Climatol.,* **58,** 221-243.

Wanner, H., E. Salvisberg, R. Rickli, and M. Schuepp, 1998: 50 years of Alpine Weather Statistics (AWS). *Meteorol. Z.,* **7,** 99-111.

Wanner, H., D. Gyalistras, J. Luterbacher, R. Rickli, E. Salvisberg, and C. Schmutz, 2000: Klimawandel im Schweizer Alpenraum. vdf Hochschulverlag AG an der ETH Zürich, Zürich, 285 pp.

Wanner, H., S. Brönnimann, C. Casty, D. Gyalistras, J. Luterbacher, C. Schmutz, D. B. Stephenson, and E. Xoplaki, 2001: North Atlantic Oscillation - Concepts and studies. *Surv. Geophys.,* **22(4),** 321-382.

White, A. V., 1985: Perception. Climate impact assessment: Studies of the Interaction of Climate and Society, R. W. Kates, Ed., Chichester and New York, 403-436.

Widmann, M., 1996: Mesoscale variability and long-term trends of Alpine precipitation and their relation to the synoptic scale flow, PhD thesis No. 11769, Eidgenössisch Technische Hochschule (ETH), Zürich, 185 pp.

Widmann, M. and C. Schär, 1997: A principle component and long-term trend analysis of daily precipitation in Switzerland. *Int. J. Climatol.*, **17,** 1333-1356.

Widmann, M., 2005: One-dimensional CCA and SVD, and their relationship to regression maps. *J. Clim.*, **18,** 2785-2792.

Wielke, L.-M., L. Haimberger, and M. Hantel, 2004: Snow cover duration in Switzerland compared to Austria. *Meteorol. Z.*, **13,** 13-17.

Wild, M., P. Calanca, S. C. Scherrer, and A. Ohmura, 2003: Effects of polar ice sheets on global sea level in high-resolution greenhouse scenarios. *J. Geophys. Res.*, **108,** art. No.-4165.

Wilks, D. S., 1995: Statistical Methods in the Atmosphere. Vol. 59, International Geophysics Series, Academic Press, San Diego, 467 pp.

Wilks, D. S., 1997: Resampling hypothesis tests for autocorrelated fields. *J. Clim.*, **10,** 65-82.

Witmer, U., P. Filliger, S. Kunz, and P. Küng, 1986: Erfassung, Bearbeitung und Kartierung von Schneedaten in der Schweiz. *Geographica Bernensia*, **G25**.

WMO, 1959: Technical Regulations No. 49. Volume 1 (Bd. 2), 2nd edition. World Meteorological Organization, Geneva, Switzerland.

WMO, 1967: A note on climatological normals. Technical Note No. 84. World Meteorological Organization, Geneva, Switzerland, Geneva.

Yiou, P. and M. Nogaj, 2004: Extreme climatic events and weather regimes over the North Atlantic: When and where? *Geophys. Res. Lett.*, **31,** art. No.-L07202.

Zingg, T., 1951: Beziehung zwischen Temperatur und Schmelzwasser und ihre Bedeutung für Niederschlags-und Abflussfragen. *IAHS Publ.*, **32,** 266-269.

Zingg, T., 1954: Die Bestimmung der klimatischen Schneegrenze auf klimatologischer Grundlage. *Mitteilungen des Eidgenössischen Instituts für Schnee- und Lawinenforschung*, **12,** Weissfluhjoch-Davos.

Zwiers, F. W. and V. V. Kharin, 1998: Changes in the extremes of the climate simulated by CCC GCM2 under CO2 doubling. *J. Clim.*, **11,** 2200-2222.

Zwiers, F. W. and H. von Storch, 2004: On the role of statistics in climate research. *Int. J. Climatol.*, **24,** 665-680.

Acknowledgements

This thesis has only been possible because of the help and engagement of many people at *MeteoSwiss*, the Institute for Atmospheric and Climate Science IAC**ETH** Zürich and in my private environment. My special thanks go to the people and institutions listed below (whereby the list does not claim to be exhaustive!).

<div align="center">

Christof Appenzeller

Christoph Schär

David B. Stephenson

Mark A. Liniger

Wolfgang A. Müller

Heike Kunz

Sibylle Studer

Martin Laternser

Conny Schwierz

Mischa Croci-Maspoli

André Walser

Andreas Weigel

Christoph Frei

Hubert Mathis

my parents

Germano Bosco

</div>

The collaborators of climate services and the model group at *MeteoSwiss*

MeteoSwiss for financing this study through the "Legat Brunner"

Veröffentlichung

MeteoSchweiz

Veröffentlichungen der MeteoSchweiz

Kürzlich erschienen:

72 Mathis H: 2005, Impact of Realistic Greenhouse Gas Forcing on Seasonal Forecast Performance, 80pp, 75 Fr.

71 Leuenberger D: 2005, High-Resolution Radar Rainfall Assimilation: Exploratory Studies with Latent Heat Nudging, 103pp, 81 Fr.

70 Müller G und Viatte P: 2005, The Swiss Contribution to the Global Atmosphere Watch Programme – Achievements of the First Decade and Future Prospects, 112pp, 83 Fr.

69 Müller WA: 2004, Analysis and Prediction of the European Winter Climate, 115pp, 34Fr.

68 Bader S: 2004, Das Schweizer Klima im Trend: Temperatur- und Niederschlagsentwicklung seit 1864, 48pp, 18 Fr.

67 Begert M, Seiz G, Schlegel T, Musa M, Baudraz G und Moesch M: 2003, Homogenisierung von Klimamessreihen der Schweiz und Bestimmung der Normwerte 1961-1990, Schlussbericht des Projektes NORM90, 170pp, 40 Fr.

66 Schär Christoph, Binder Peter, Richner Hans (Eds.): 2003, International Conference on Alpine Meteorology and MAP Meeting 2003, Extended Abstracts volumes A and B, 580pp, 100 Fr.

65 Stübi R: 2002, SONDEX / OZEX campaigns of dual ozone sondes flights: Report on the data analysis, 78pp, 27 Fr.

64 Bolliger M: 2002, On the characteristics of heavy precipitation systems observed by Meteosat-6 during the MAP-SOP, 116pp, 36 Fr.

63 Favaro G, Jeannet P, Stübi R: 2002, Re-evaluation and trend analysis of the Payerne ozone sounding, 99pp, 33 Fr.

62 Bettems JM: 2001, EUCOS impact study using the limited-area non-hydrostatic NWP model in operational use at MeteoSwiss, 17pp, 12 Fr.

61 Richner H, et al.: 1999, Grundlagen aerologischer Messungen speziell mittels der Schweizer Sonde SRS 400, 140pp, 42 Fr.

60 Gisler O: 1999, Zu r Methodik einer Beschreibung der Entwicklung des linearen Trends der Lufttemperatur über der Schweiz im Zeitabschnitt von 1864 bis 1990, 125pp, 36 Fr.

59 Bettems J-M: 1999, The impact of hypothetical wind profiler networks on numerical weather prediction in the Alpine region, 65pp, 25 Fr.

58 Baudenbacher, M: 1997, Homogenisierung langer Klimareihen, dargelegt am Beispiel der Lufttemperatur, 181pp, 50 Fr.

57 Bosshard, W: 1996, Homogenisierung klimatologischer Zeitreihen, dargelegt am Beispiel der relativen Sonnenscheindauer, 136pp, 38 Fr.

56 Schraff, C: 1996, Data Assimilation and Mesoscale Weather Prediction: A Study with a Forecast Model for the Alpine Region, 138pp, 38 Fr.

55 Wolfensberger, H: 1994, Chronik der Totalisatoren, Handbuch zu den Niederschlags-Totalisatoren, 390pp, 78 Fr.

54 Fankhauser, GA: 1993, Einfluss der Witterung auf den Ertrag und die Qualität von Zuckerrübenkulturen, 116pp, 36 Fr.

53 de Montmollin A: 1993, Comparaisons de différentes méthodes de calcul de la température journalière dans leurs influences sur les longues séries d'observations, 144pp, 41 Fr.

> Frühere *Veröffentlichungen* und *Arbeitsberichte* finden sich unter
> www.meteoschweiz.ch

Veröffentlichung

MeteoSchweiz

Arbeitsberichte der MeteoSchweiz

Kürzlich erschienen:

210 Buss S, Jäger E and Schmutz C: 2005: Evaluation of turbulence forecasts with the aLMo, 58pp, 70 Fr.

209 Schmutz C, Schmuki D, Duding O, Rohling S: 2004, Aeronautical Climatological Information Sion LSGS, 77pp, 25 Fr.

208 Schmuki D, Schmutz C, Rohling S: 2004, Aeronautical Climatological Information Grenchen LSZG, 73pp, 24 Fr.

207 Moesch M, Zelenka A: 2004, Globalstrahlungsmessungen 1981-2000 im ANETZ, 83pp, 26 Fr.

206 Schmutz C, Schmuki D, Rohling S: 2004, Aeronautical Climatological Information St.Gallen LSZR, 78pp, 25 Fr.

205 Schmutz C, Schmuki D, Ambrosetti P, Gaia M, Rohling S: 2004, Aeronautical Climatological Information Lugano LSZA, 81pp, 26 Fr.

204 Schmuki D, Schmutz C, Rohling S: 2004, Aeronautical Climatological Information Bern LSZB, 80pp, 25 Fr.

203 Duding O, Schmuki D, Schmutz C, Rohling S: 2004, Aeronautical Climatological Information Geneva LSGG, 104pp, 31 Fr.

202 Bader S: 2004, Tropische Wirbelstürme – Hurricanes –Typhoons – Cyclones, 40pp, 16 Fr.

201 Schmutz C, Schmuki D, Rohling S: 2004, Aeronautical Climatological Information Zurich LSZH, 110pp, 34 Fr.

200 Bader S: 2004, Die extreme Sommerhitze im aussergewöhnlichen Witterungsjahr 2003, 25pp, 14 Fr.

199 Frei T, Dössegger R, Galli G, Ruffieux D: 2002, Konzept Messsysteme 2010 von MeteoSchweiz, 100pp, 32 Fr.

198 Kaufmann P: 2002, Swiss Model Simulations for Extreme Rainfall Events on the South Side of the Alps, 40pp, 20 Fr.

197 WRC Davos (Ed): 2001, IPC - IX, 25.9. - 13.10.2000, Davos, Switzerland, 100pp, 32 Fr.

196 Hächler P et al.: 1999, Der Föhnfall vom April 1993, 139pp , 40 Fr.

195 Urfer Ch, Vogt R, 1999, Die Niederschlagsverhältnisse in Basel 1964-1998, 43pp, 40 Fr.

194 Courvoisier HW: 1998, Statistik der 24-stündigen Starkniederschläge in der Schweiz 1901 – 1996, 20pp, 11 Fr.

193 Defila C, Vonderach G: 1998, Todesfälle und Wetterlagen in Schaffhausen, 72pp, 25 Fr.

192 Maurer H: 1997, Frostprognose in der Schweiz: neue Methode mit automatischen Stationen, 38pp, 16 Fr.

191 Schönbächler M: 1996, Objektive Kontrolle der Textprognose SMA OPKO, 31pp, 14 Fr.

190 Brändli J: 1996, Statistische Auswertungen von täglichen und monatlichen Verdunstungswerten an 22 Standorten der Schweiz, 52pp, 19 Fr.

189 Schneiter D: 1994, SMI contribution to ETEX project in 1994, 24 Fr.

188 Fröhlich C: 1996, Internationaler Pyrheliometervergleich Comparison IPC VIII 25 September - 13 October 1995 Results and Symposium, 35 Fr.

187 Calame F: 1996, Evolution de la température de l'air et de la phénologie d'espèces végétales entre 1952 et 1992 dans la région genevoise et sur le Plateau Suisse, 19pp, 11 Fr.

Frühere *Veröffentlichungen* und *Arbeitsberichte* finden sich unter
www.meteoschweiz.ch